DIRECT MEASUREMENT OF SKIN FRICTION IN COMPLEX SUPERSONIC FLOWS

By

Michael George Bernard Novean

A DISSERTATION SUBMITTED TO THE FACULTY OF
VIRGINIA POLYTECHNIC INSTITUTE AND STATE UNIVERSITY
IN PARTIAL FULFILLMENT OF THE REQUIREMENTS FOR THE DEGREE OF
DOCTOR OF PHILOSOPHY
IN
AEROSPACE ENGINEERING

Joseph A. Schetz, Chairman

Bernard Grossman

Robert W. Walters

Roger L. Simpson

Rodney D. W. Bowersox

March 1996

Blacksburg, Virginia

Keywords: Skin Friction, Aerodynamics, Supersonic Flow, Scramjet

Abstract

DIRECT MEASUREMENT OF SKIN FRICTION
IN COMPLEX SUPERSONIC FLOWS

by

Michael George Bernard Novean

Committee Chairman: Joseph A. Schetz
Aerospace Engineering

(Abstract)

An instrument for the direct measurement of skin friction in complex supersonic and hypersonic flows was developed. The flows were complex because they were of very short duration, with high temperature and shocks and often injection, mixing, and combustion. A wall-mounted, miniature cantilevered beam device measured the small tangential shear force on the non-intrusive floating element. Semiconductor strain gages mounted at the beam's base measure the small strains that are generated. By modifying the geometry of the sensing unit, this design can be adapted for a variety of test flows. The use of engineering plastics and short beam length provide high frequency response and make the beam stiff so that the floating head's deflection due to the shear is negligible, allowing for a non-nulling design. Measurements were made in scramjet models at the NASA Ames 16-inch Shock Tunnel and the General Applied Science Laboratory HYPULSE facility. Test flow conditions were harsh with the facilities simulating Mach 14 enthalpy conditions (320 atm and 10000

R total temperatures) for 0.3-2 milliseconds. The use of engineering plastics reduces heat transfer, so that measurements can be made in these very hot impulsive flows without thermal contamination of the data. Skin friction data in agreement with other correlations and measurements were obtained at both facilities. Mach 2.4 cold flow tests were also performed in the Virginia Tech Supersonic Tunnel. These helped verify the concept and to establish pressure gradient sensitivity in the case of a shock wave impacting directly on the sensing head. Analysis of the measurement uncertainty in the cold supersonic flow tests showed that an uncertainty of approximately 10 percent is achievable. An uncertainty of 15-20% is estimated for the most severe hot cases. An assortment of variations were applied to the gage to extend gage life. The most significant was the replacement of the oil in the sensing gap with a silicon rubber, eliminating service requirements. Tests at all of the facilities confirmed that the rubber-filled gages provided approximately the same level of accuracy as was achieved with the original oil-filled gage design, except when shocks impacted the gage head.

Acknowledgements

First and foremost, I'd like to thank Dr. Joseph Schetz for the great opportunity which he provided me and the faith to entrust me with such responsibility. I was fortunate to travel to some unique testing facilities, and without Dr. Schetz to open the doors for me, that never would have occurred.

Special thanks go out to Dr. Rodney Bowersox and Dr. Ken Chadwick for their assistance when I was just starting out, and to Raymond Fuller and Wade Pulliam for their help fixing the problems that arose and their support throughout. Thanks to everyone in the "Sun Room" for their help and friendship.

Also, thanks to the Aerospace Engineering machine shop and staff– Bruce Stanger, Frank Shelor, Kent Morris, Greg Dudding, and Gary Stafford. I'd also like to thank the employees at the NASA Ames 16 inch Shock Tunnel and GASL.

Last, I'd like to thank my parents and grandparents for the love and support they've given me throughout my life. And, of course, to Cathy, for making the bad times bearable and the good times even better.

Nomenclature

A	Area
c_p	Specific heat at constant pressure
C_f	Skin friction coefficient
d	Diameter
e	Voltage rise, electric charge
E	Modulus of Elasticity
E_{ex}	Excitation Voltage
f	Frequency
h	Enthalpy
i	Current
I	Moment of Inertia
K	Bulk Modulus
L	Beam length
m	Mass
M	Mach number
N_i	Number of charge carriers
P	Applied load
Pr	Prandtl Number
q	Dynamic pressure
q_w	Wall heat transfer rate
r	Radius
R	Resistance
Re_x	Reynolds number based on x

St	Stanton Number
t	Time
T_w	Temperature at the wall
T_{aw}	Adiabatic temperature at the wall
U	Reynolds averaged steady state velocity
U_B	Bridge voltage
u^*	Friction velocity
X	Axial distance
y	Normal distance to wall
Y	Young's Modulus
δ_t	Boundary layer thickness
Δ_y	Beam deflection distance
ε	Strain
θ	Momentum thickness
μ	Viscosity
μ_{ave}	Average mobility of N_i
ν	Kinematic viscosity, $\frac{\mu}{\rho}$
π_L	Longitudinal piezoresistive coefficient
ρ	Density
ρ	Resistivity
σ	Applied stress
τ	Resonant period
τ	Shear stress

Subscripts

B	Bridge
e	Condition at edge of boundary layer
eff	Effective
ex	Excitation
h	Height
L	Longitudinal

o	Stagnation condition
w	Condition at wall
∞	Free stream condition upstream of shock

Contents

List of Figures

Chapter 1

Introduction

1.1 Background

A knowledge of the drag resulting from skin friction is important for several reasons, both scientific and practical. From a practical perspective, skin friction is important to the performance of virtually all fluid machinery systems and components. For example, skin friction plays a key role in drag, and hence the thrust available, in a scramjet combustor. The determination of thrust or drag in a hypersonic vehicle can be thought of as a summation of several large numbers, such as thrust from the nozzle and fuel momentum addition and drag from such things as wave drag and skin friction drag, which result in a small net difference. Thus, as engineers one must be careful in estimating a value for C_f, since the difference in a skin friction value of .002 and .003 may be the difference in a scramjet producing thrust for a hypersonic vehicle or causing it to be a drag body. Scientifically, the skin friction is a key component in determining the *friction velocity*,

$$u^* = \sqrt{\frac{\tau_w}{\rho_w}} \tag{1}$$

that is used as the scaling velocity in the correlation of turbulent boundary layer profiles. Hence, accurate skin friction values are required to generate good turbulence models.

The measurement of skin friction is not a new science. Skin friction has been

successfully measured for years using indirect and direct methods. Most laminar flow situations have reliable skin friction measurements available, and a host of prediction methods are available for simple flows over a flat plate. However, it will be shown that there is a need for a simple, successful technique for measuring skin friction in a supersonic, chemically-reacting, high-enthalpy flow environment especially in short, duration tests.

The measurement of skin friction can be classified into two categories of techniques– indirect or direct methods. Indirect methods involve measurement of the boundary layer velocity gradient or heat transfer along with some assumptions so that the skin friction can be inferred. Reference [1] presents a thorough review of many of these methods and their strategies. Reference [2] presents in tabular form a list of advantages and disadvantages of several types of experimental skin friction measurements. These are reproduced in Table 1 below. Wooden and Hull treat Reynolds Analogy measurements, as a separate method as they consider the physical quantity being measured (i.e., force, total pressure, and heat transfer) as their dividing criterion. In this discussion, however, Reynolds Analogy will be considered a subset of indirect methods.

Among the indirect methods are the Preston tube, as shown in Figure 1. The Preston tube [1] operates by resting a small tube on the wall surface in order to measure the Pitot pressure. The tube's size allows the probe to sense the viscous sublayer, the logarithmic portion, and the so-called "buffer layer" between them of the wall region of the turbulent boundary layer, meaning that the complete law of the wall must be supposed when utilizing this technique. The relation between the wall shear and measured dynamic pressure in the probe is usually represented by an empirical calibration curve which is a fit through a logarithmic law. The problem with such an arrangement is that direct relationship between the law of the wall and the calibration method indicate that measurement of skin friction by a Preston tube technique will break down in situations that lead to a deviation from the law of the wall. Thus, the Preston tube will fail in such flows as a transition region or separating and reattaching flows as the law of the wall breaks down. Furthermore, it will be of very limited use in a three-dimensional flow regime.

Table 1: Advantages and Disadvantages of Experimental C_f Measurements[from Wooden and Hull, Ref. [2]]

Method	Advantages	Disadvantages
Direct Measurement (Force)	- Most believable - High precision measurement - High precision calibration - Direction sensitive	- Tare sensitive - Small force - High cost - Large size (inside model) - Direction sensitive
Indirect Measurement (Laminar Sublayer total pressure)	- Simple - Low cost (after calibration) - High precision measurement	- Flow calibration required - Medium precision curve fit - Minimum B.L. thickness limited - Direction sensitive
Reynolds Analogy (Thermal measurement)	- Dual purpose sensor - Low cost - Not direction sensitive	- Calibration not available - Low precision measurement - B.L. edge conditions required - Not direction sensitive

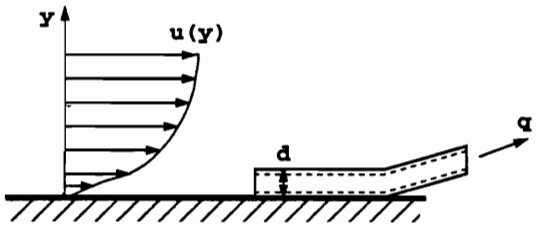

Figure 1: Preston Tube Technique

Similar in principle to the Preston tube, a Stanton tube [3] consists of a Pitot tube with a rectangular opening. A Stanton tube can easily be fabricated by placing a piece of razor blade over a static pressure hole. This makes it simpler to get readings close to the surface compared to the Preston Tube. A schematic of a Stanton tube is shown in Figure 2. While being very similar, there are some important differences between Stanton and Preston tubes. Unlike the Preston tube, the Stantion tube does not respond to Bernoulli-type pressures (pressures resulting due to the deceleration of fluid in front of the tube), therefore it can respond more quickly to local shear stress fluctuations. Also, the numerous phyisical parameters such as width and overall height of the device and the flow entrance opening all contribute to the calibration of the Stanton tube and make calculation of the wall shear levels much more tedious than those of the Preston Tube [3]. However, the operation principle behind the Stanton tube is similar to that of the Preston tube– the pressure (and its variations) in the near wall region is measured and the wall shear is calculated through empirical relations using the law of the wall to fix a velocity profile. Likewise, the Stanton tube must be compensated as well when utilized in three-dimensional flows or flows with pressure gradient, since the velocity profile will be changed.

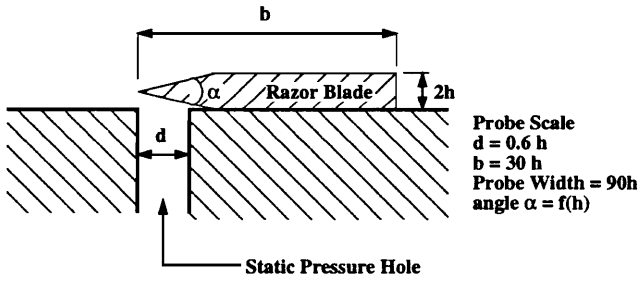

Figure 2: Stanton Tube Technique

In addition, a hot-wire at a fixed distance above the wall can be utilized in the logarithmic region to determine the velocity u_h at a distance above the wall. However, although this method is less sensitive to changed wall laws, it still has the same restrictions as the Preston tube method.

Another technique involves the use of heated wires or films along the wall in order to measure heat transfer. In 1874, Osborne Reynolds suggested that the mechanism

between the heat transfer and momentum transfer in a turbulent boundary layer are similar. This conclusion leads to the Reynolds Analogy– a relationship between the skin friction coefficient and the heat transfer coefficient. The Reynolds Analogy can be expressed as [4]

$$St\ Pr^{\frac{2}{3}} = \frac{C_f}{2} \tag{2}$$

or simply as

$$\frac{St}{(\frac{C_f}{2})} = 1 \tag{3}$$

in the case of Prandtl number of unity. His theory has been modified by various researchers as given in Wooden[2] which follows from Rubesin[5]. These empirical modifications and corrections refine the calibrations for given types of flows. Only the basic Reynolds Analogy technique for a surface hot film sensor will be discussed here.

The surface hot-film technique is based upon the concept that the convective losses of a small electrically heated sensor mounted in the wall and maintained at a constant temperature can be correlated to the wall shear stress through calibration. The convective loss is generally assumed to be proportional to the electric power input to the sensor. The empirical calibration formula is commonly of the form:

$$U_B^2 = A + B\tau_w^n \tag{4}$$

with U_B representing the bridge voltage and n commonly between 0.25 and 0.3. Such a surface hot film sensor can be seen in Figure 3 from [1]. Several researchers have measured skin friction with such a technique [6], [7], [8]. The technique does well in cases where Reynolds' Analogy may be applied. However, in those flow cases where there is mixing and combustion, it is a very large assumption to conclude that an accurate and reliable, simple relation between momentum and heat transfer exists. In addition, Bellhouse and Schultz [9], raise concerns for use of a heated film. Equation (2) can only be applied in the case of a wall-heated sensor with no unheated starting length; otherwise, τ_w is proportional to h^3 for an unheated starting length. The hot-film technique is also not useful for measuring the shear direction in three-dimensional flows.

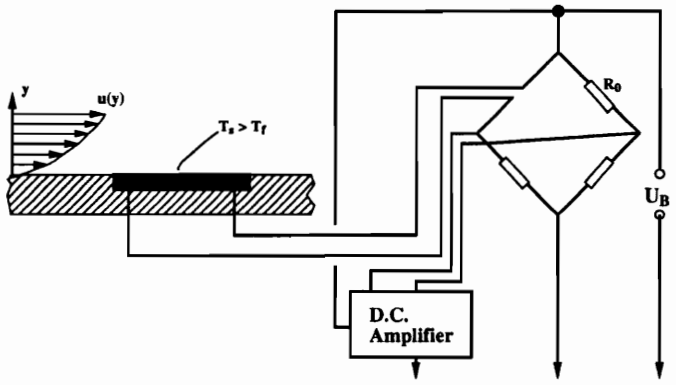

Figure 3: Hot Film Sensor Technique

A final indirect technique involves the use of liquid crystals to qualitatively and quantitatively measure skin friction [10]. Liquid crystals are optically active mixtures which have the ability to reflect light of a particular wavelength which changes in response to a given physical stimuli. By making the crystals sensitive to shear stress, a calibration curve can be generated which relates the shear stress to reflected wavelength. However, the output from liquid crystals is much more qualitative than quantitative– the crystals can indicate areas of high shear and low shear well but do a poor job of, say, indicating a region of a 1000 Pa wall shear compared to a region of 900 Pa wall shear. For this reason, liquid crystals are still much more suited to indicating transition location than reporting skin friction measurements.

Figure 4 shows a simple scramjet schematic and also illustrates the problems involved with utilizing an indirect measurement technique. The oncoming flow is slowed and compressed through the inlet. It then passes through the isolator to the combustor where fuel is added and burned at supersonic speeds. The combusted mixture is then expanded through the nozzle and back into the atmosphere. Several potential

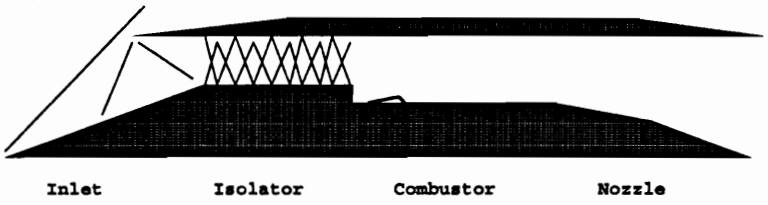

Figure 4: Scramjet Schematic

problems with the indirect methods can be seen in the combustor. First, the flow encounters a rearward facing step as it enters the combustor and also possibly behind the injectors if a ramp injection scheme is used. This results in a separated and reattaching flow and violates many assumptions in the usual indirect measurement techniques. In addition, there will be combustion in the flow– leading to high heat fluxes, potential local hot-spots, and chemically reacting with a changing mass composition. For these reasons, a direct measurement method is preferable to an indirect one, because it is doubtful that the required assumptions for indirect methods can be made. In addition, the direct method has an advantage for application in the various flows encountered since it will work in laminar, turbulent, or transitional flows and requires no prior knowledge of the flow type.

However, before going into a discussion of the direct methods, a brief survey of what will be called semi-direct or quasi-direct methods will be made. Among these would be the use of a thin liquid film [11] which is placed on the surface of the body and deformed by the gas flow over it. Hence, the term "semi-direct method" as the film is placed on the body rather than in the body as a floating-element gage would be. The concept behind a thin oil film technique is that the surface shear stress can be deduced from the rate of deformation of the thin oil film based upon lubrication theory. The shear stress can be assumed to be the primary force on the film if the film is thin relative to its length, there is little surface curvature, and the flow is unaffected by the film's presence. If one has the ability to measure the deformation of the thin oil film over time, then it is possible to accurately determine the skin friction based upon a characteristic film profile.

For the case of the Seto and Hornung's [12] experiment, the characteristic film profile for constant shear stress, zero pressure gradient two-dimensional flow was

$$y = \frac{\mu x}{\tau t} \tag{5}$$

where y is the film thickness, μ the viscosity, x is the distance from the leading edge of the film, τ is the shear stress and t is the time. A schematic of such a profile can be seen in Figure 5. The linear profile above occurs in the limiting case of increasing time and decreasing film thickness. So for a very thin film case, the influence of

the film on the flow is negligible and equation (5) gives a direct relation between the shear stress and the film thickness and deformation. Several researchers have different

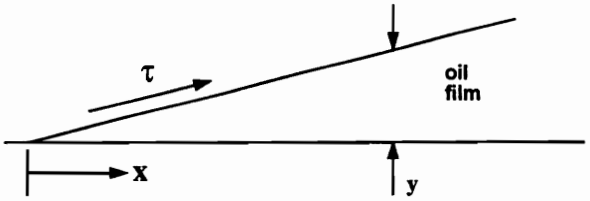

Figure 5: Oil Film Profile

methods for measuring the deformation of the oil. Tanner and Blows [13] used laser inferometric thickness measurements of the oil thickness. A non-intrusive double laser beam inferometer system was developed as an advancement to Tanner's arrangement [14]. These methods were further improved by O'Brien and Christiansen [15] who placed microspheres on the surface of the film and imaged their motion through a microscope beneath the flow. Other researchers utilize other techniques for visualizing the oil deformation [12]. These techniques are all very successful at measuring skin friction on a flat plate in a non-intrusive manner. However, their utility in very hot, high-speed testing will be limited. Also, time response is a problem in short duration testing. In addition, it is likely that the model may be in motion on the test stand as it is subjected to large aerodynamic loads from both the oncoming flow and the exhausted combustion gases and the optical access to the test stand might be limited due to the high temperatures and enthalpies encountered in hypersonic flows.

Winter [16] presents a history of early direct measurement designs. Direct force measurement techniques generally include two types of force balances– nulling and non-nulling. In the nulling design, the sensing element, a small movable portion of the wall, is acted upon by the shearing force but it is not deflected (see Figure 6. Instead, it is held fixed in its initial position by a restoring force that is equal to the shear force. In the non-nulling design, the sensing element is allowed to deflect under the shearing load. This type of design is much simpler than a self-nulling design, however it introduces some concern as the deflection allows the sensing head to tilt and protrude into the flow and it permits the sensor geometry to vary.

Many of the nulling gages are mechanically complex, using some parallel linkage

arrangement to sense the force on the floating element. That is, the sensing element does not move but instead transfers the force through the parallel linkage which measures the amount of compensating force required to keep the element stationary. A schematic of such a design from Allen [17] can be seen in Figure 6. Vakili [18] suggested a moving belt technique called a Belt Skin Friction Balance (BSFB). As shown in Figure 7, this gage functions by having a flexible belt wrapped tightly around two cylinders with parallel axes. As the flow goes over the belt, the shear force applied to the belt forces the cylinders to rotate a very small amount. Strain gages installed on the flexure measure the strain which is proportional to the belt's deflection.

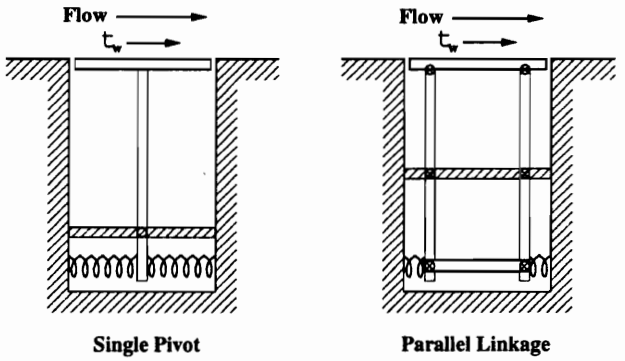

Figure 6: Nulling Gage Schematic

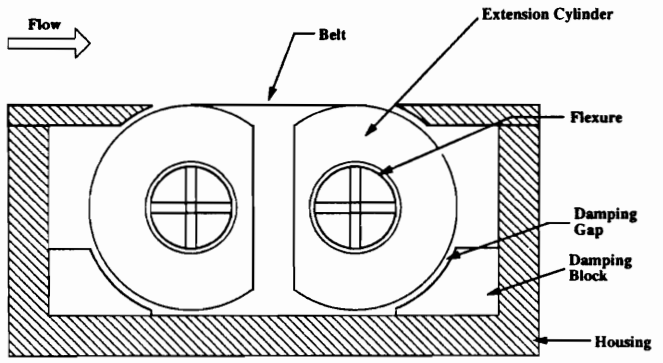

Figure 7: Belt Skin Friction Balance Schematic

A nulling device is attractive for many reasons since it is a direct measurement with no assumptions regarding the properties of the flow and the balance remains

fixed and will not alter the flow. Many nulling designs exist for measuring skin friction. However, there are some drawbacks to the nulling design. First, these designs have been primarily subjected to supersonic flows with moderate total temperatures. Second, the mechanical complexity can present a problem with fabrication, reliability and susceptibility to error. Third, they are of limited use for three-dimensional flows. Last, and very importantly for these short duration tests, a nulling design has a much slower time response.

Thus, we come to the non-nulling direct measurement method for a skin friction balance in the hopes that this configuration will be successful for the applications of interest here. The non-nulling device allows the cantilevered floating element to move a very small distance, and the bending at the base of the beam can be measured. This is mechanically much simpler than the nulling design, and by using a stiff beam, the tilting of the head can be made so small that errors due to misalignment are minimal. Chadwick[19] and DeTurris [20] present data using a non-nulling cantilevered arrangement measured in scramjet combustors over several test programs. However, all of these tests are of a long duration variety where the key is preventing thermal contamination of the test signal. The development of such a device for impulsive facilities has seen few attempts.

One skin friction balance for measurements in impulsive facilities has been developed by researchers at Calspan [21] [22] [23]. These gages use lead zirconium titanate piezoelectric ceramics as energy sources and field effect transistors (FET) as power amplifiers. This device functions by having a pair of crystal sensing elements that will produce output under deflection. The first floating element is exposed to the flow and will deflect under the wall shear. Since the sensing beam is also susceptible to acceleration loads, the gage contains a second piezoelectric ceramic and a mass equivalent to the metric diaphragm for acceleration compensation. This second element is not exposed to the flow but instead only responds to the acceleration. By taking the difference of the two outputs, the wall shear can be found. The unit is complex and only limited success has been achieved.

Researchers at the University of Queensland in Australia [24] have also developed a non-nulling skin friction balance for use in impulse facilities. A schematic of this

skin friction balance can been seen in Figure 8. The Queensland gage functions as follows. The sensing element consists of a 0.4 mm thin metal disk acting as a thermal cover which is bonded to a stack of two piezoelectric transducer elements (each 7x7 mm by 1.5 mm thick) made of piezoceramic PZT-7A. The thermal cover was made of Invar and is designed to protect the piezoresistives from heating. Invar has a very low coefficient of thermal expansion and was chosen to prevent expansion into the flow or straining of the transducer elements due to thermal expansion of the disk. Also an assortment of rubber vibration isolation techniques were used to prevent vibration induced acceleration of the gage. Based on sensor geometries and density, gage natural frequencies are above 300 kHz.

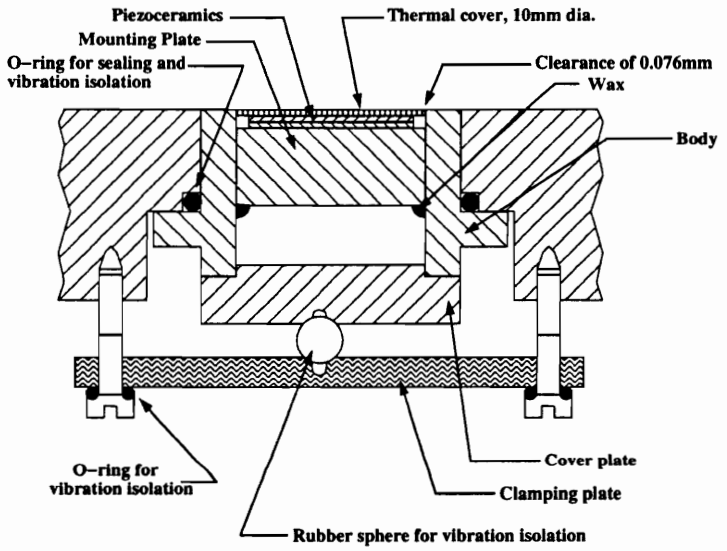

Figure 8: University of Queensland Gage Schematic

In theory, such a gage with the elements properly aligned should only respond to the wall shear force, but in practice it was found to be sensitive to normal pressure force as well. For this reason, the pair of piezoresistive elements was used with one inverted relative to the other. One element would provide an output e_1 proportional to the sum of the wall shear and pressure applied to the disk while the other would provide an output e_2 proportional to the difference. Although the theory behind the gage appears sound and its time response is extremely fast on the order of 20 μsec, no successful measurements in a test flow have ever been published. Currently, this

Queensland gage remains in a prototype stage– a clever idea which has yet to be successfully implemented.

The baseline gage used for the development of the current gage design (to be discussed in detail in the next chapter) was a design first developed by Dr. Rodney Bowersox [25]. It consists of an axisymmetric floating element beam which is exposed to the wall shear. The beam will deflect a miniscule amount (the deflection is so small the change in geometry is non-intrusive to the flow) under the shear force. Strain gages are mounted at the base of the beam in a half-bridge configuration of a Wheatstone bridge; one strain gage will go in tension and the other in compression under the shear force. The resulting resistance change in the strain gages will result in a linear output of voltage versus shear force. The sensing head is made larger than the sensing beam for an increased shear force sensitivity. This beam rests upon a foundation which is used to feed lead wires through to the strain gages on the beam. The beam and foundation are then pinned inside an axisymmetric surrounding housing although the housing could be constructed to be of any shape. The gap between the sensing beam and housing is filled with a silicon oil which acts to minimize errors due to pressure gradients on the head and vibrations and to thermally isolate the strain gages at the base of the beam.

This basic gage design is extended here to meet some testing goals. First, the range of application was extended to facilities with shorter test times and also for testing in more harsh and severe conditions. Second, the gage design was further refined. This involves experimentation with additional surface coatings and materials as well as use of a silicon rubber in the gap around the sensing head to extend the survivability and reduce the time needed to maintain the gages. Third, an investigation of the effect of a sharp pressure gradient on the sensing head on gage operation was conducted.

There are many differences between the Queensland gage and the general gage design employed here. First is the use of strain gages mounted to the sensing beam instead of making the gages out of piezoelectric elements. This leads to a situation where signal contamination by normal pressure sensitivity is much less of a problem. Also the use of strain gages in a Wheatstone bridge means that calibration is much simpler as data can be taken under a steady load rather than trying to measure output

due to a transient load. There are drawbacks such as lower natural frequency and slower time response due to the beam geometry and inertia, but the time response can still be made sufficiently fast for the shortest test facilities in current use. Obviously, there is a clear tradeoff between each design and it is felt that the current design provides both the time response needed for impulsive testing and the confidence level that the results are not being contaminated by other system variables. A description of the current gage design begins in the next chapter.

1.2 Scope of the Investigation

The skin friction gages were further developed and analyzed and tested in two scramjet testing programs as well as in the Virginia Tech supersonic tunnel. The flows at the scramjet tests were supersonic to hypersonic, simulating true Mach 14 enthalpy conditions. These were fully functional scramjet models which were burning hydrogen in high enthalpy air over short testing times on the order of a millisecond to several milliseconds. The approximately 6-second cold flow tests in both a clean two-dimensional flow and in a shock/boundary layer interaction at Virginia Tech proved the design concept and repeatability and were also used to aid in the uncertainty analysis. Further, a careful study of the effects of shock impingement directly on the floating head was undertaken.

The scramjet model tests occurred at the NASA Ames 16 inch shock tunnel and at the General Applied Science Laboratory (GASL) Hypulse facility. Several series of runs were made at NASA Ames over a seven month testing period in which three model configurations were tested. The models were fabricated by GASL personnel. Several skin friction gage designs with different shear sensitivities and response times were constructed for these tests. Measurements were made in both the model inlet and combustor with the majority of the tests being made in the combustor. Test times were approximately 2 milliseconds.

The tests at GASL were made in two different test series which were over a year apart. Those scramjet models were also built by GASL personnel. Again multiple gage designs were tested at this facility. For these tests, all the gage ports were located

in the combustor. Test times in this facility were approximately 0.3 milliseconds. In addition some tests were made at the Instrumentation Shock Tube (IST) at GASL to verify the time response of the skin friction gages.

The tests at VPI were primarily used to generate results for cold flow correlations to verify the gage design and to study gage sensitivity to various parameters that could cause uncertainty such as a pressure gradient impacting nearby or on the gage head. A pair of gage designs were tested in the VPI tunnel as well. The first was a 10 kHz baseline gage used at the scramjet tests and the second was a slower time response gage with increased shear sensitivity designed for the lower shear of the supersonic tunnel. The tests were all made in the tunnel floor which is essentially a flat plate with two-dimensional flow. Unlike the scramjet tests, these tests could be considered long duration with run times on the order of five to ten seconds.

The following chapters will present the process for designing a small skin friction balance for impulsive flow testing. In Chapter 2, a description of the ideas and principles behind the cantilevered beam skin friction gage will be discussed as well as the principles of strain gage theory. In Chapter 3, the variations to the baseline gage will be covered, especially the use of a silicon rubber compound in the gage annulus instead of silicon oil. Chapter 4 contains a description of the NASA Ames test facility as well as the results from those tests. Chapter 5 presents the description of the test facilities at GASL and the results of the tests. The facilities and procedure used at the Virginia Tech Supersonic Tunnel are presented in Chapter 6, as are the cold flow correlations and results from a shock impingement test in the region of the skin friction gages. Conclusions and recommendations for what should be done in future balance designs are given in Chapter 7. The Appendices include listings of the programs used in gage design as well as additional data traces which were obtained.

Chapter 2

Gage Description

2.1 Principles of Operation

Figure 9 illustrates the basic gage concept employed here– a plastic floating head which is mounted upon a cantilevered beam sensing element. This beam is then pinned within an axisymmetric surrounding housing. The principle for sensing is that the wall shear force from a passing flow will deflect the sensing head in a non-intrusive manner so that strain gages at the base of the cantilevered beam will measure this shear force of the undisturbed flow. The sensor head is made larger than the beam in order to provide greater shear force sensitivity. This basic scheme was first developed at Virginia Tech [26]. Here, the approach is refined and extended and put on a more solid basis by further testing and analysis. First, the range of application in impulsive testing is extended to allow use in a shorter test time facility and also in harsher conditions. A second goal is refinement of the design to make it more rugged and reduce maintenance demands. Third, the effect of a sharp $\frac{dp}{dx}$ on the sensing head is investigated to quantitatively ascertain the effect of a pressure gradient on the gage.

Before proceeding into the gage design further, it is illustrative to point out some factors complicating direct measurement of skin friction and the elements of the present skin friction balance which are designed to mitigate them. Factors complicating direct measurement of skin friction are from Winter Ref. [16].

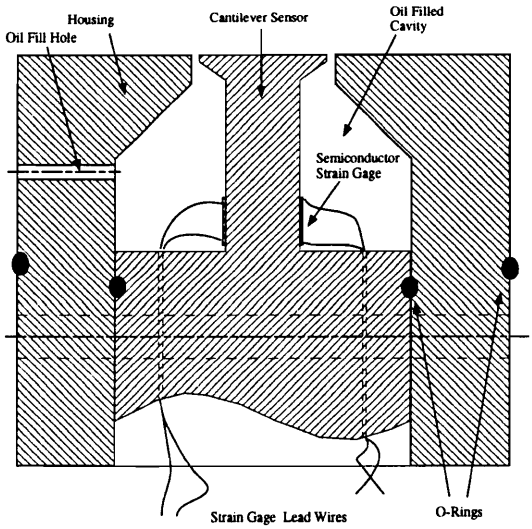

Figure 9: Basic Gage Concept

"*1. Provision of a transducer for measuring small forces or deflections, and compromise between requirement to measure local properties and necessity of having an element of sufficient size that the force on it can be measured accurately*"

Use of semiconductor strain gages (Micro Gage Inc. Model 919 to be further discussed in section 2.5) allows for the ability to measure very small forces on the sensor. The gage sensing head has been enlarged from the beam diameter but its nominal 0.460 cm diameter still allows for measurement of local wall shear. The effects of head protrusion are minimal as will be discussed later.

"*2. Effect of necessary gaps around the floating element*"

The gaps can be sized to minimize any spurious effects according to Allen [17]. Use of an oil or room-temperature vulcanizing (RTV) rubber in the annulus also helps to make the gap appear as a solid surface to the oncoming flow.

"*3. Effects of misalignment on the floating element*"

The construction technique should virtually eliminate misalignment. The use of a stiff beam reduces errors due to head tilting to a negligible level. The primary misalignment error is due to not getting the sensing axis to coincide directly with the flow axis. However, for 5 degree misalignment, the error is less than 0.4 percent (i.e. $\cos 5° = 0.996$) and for 10 degrees the error is only around 1.5 percent.

"*4. Forces arising from pressure gradients*"

The pressure gradient effect is investigated in detail in some wind tunnel tests in the Virginia Tech Supersonic Tunnel. These are discussed in section 6.3 on page 92.

"*5. Effects of gravity or acceleration if balance is to be used in a moving vehicle*"

The use of the plastics ULTEM [27] and Victrex Polyethersulfone (PES) [28] with their low densities reduces "accelerometer" tendencies of the gage. Also, a gage with high natural frequency should damp out disturbances due to accelerations prior to the beginning of the test window.

"*6. Effects of temperature changes* and *7. Effects of heat transfer*"

Temperature effects are indeed large and can be catastrophic for semi-conductor strain gages. There are many compensation methods that have been developed in an attempt to minimize the effect of temperature change [29]. The simplest solution, however, is to insure heat does not affect the strain gages. In other designs [19] [20], active cooling is employed to keep the strain gages at fixed temperature. However, due to the impulsive nature of the test environment of primary intent in this work, the solution employed here was much less complicated. The low thermal conductivity of the engineering plastics allowed for the development of a design where the thermal effects would not reach the strain gages until well after the run was over. For example, based on a 1-D, transient, heat transfer analysis, a temperature gradient of about 5700K (i.e. free stream total temperature of 6000K and 300K starting wall temperature) and a wall heat flux, q_w, of 3.0 kW/cm^2 would imply that the temperature 2 mm below the surface would increase only 1°C in approximately 1000 msec [25]. In addition, the strain gages were mounted in resistance matched pairs. This meant that both strain gages would have a resistance of say 347.0 ohms at 25°C and 347.2 ohms at 50°C. By having an equivalent resistance change per degree, each strain gage cancels the effect of the other when exposed to a temperature change. This meant that gage output and calibration should not vary if the gage was calibrated at a given facility at one temperature and then tested in another temperature. This could be the case if the gage was calibrated in a climate controlled lab room but then tested in a wind tunnel where the test section may not have heating and air-conditioning.

"*8. Use with boundary layer injection or suction*"

This is not a concern for the test environment involved here. The basic gage design could be extended to such cases.

"*9. Effect of leaks*"

A series of o-rings were installed in the gap and around the gage to eliminate leakage. The lead wire holes and backside of the gage were also coated with 5-minute epoxy.

"*10. Protection of the measuring system against transient normal forces during starting and stopping if the balance is to be used in a supersonic tunnel*"

The gage design is very rugged. The cantilever beam is very resistant to normal forces. Once assembled, there is little potential for breakage. The alignment pin prevents recession due to normal pressure and the housing prevents a large deflection which could damage the beam or strain gages.

Having already said what was done to minimize the complications of a direct measurement technique, the following criteria were used to guide the gage design: 1) high frequency response, 2) high wall shear force sensitivity, 3) low weight, and 4) low thermal and normal pressure sensitivities. The miniature cantilever sensors constructed out of the engineering plastics ULTEM [27] and Victrex PES (polyethersulfone) [28] met all of the above criteria. The plastics provide the further benefits of being easy to machine and inexpensive.

The gap between the sensing element and housing is filled with silicon oil (Dow Corning 200 Fluid) of various viscosities ranging from 200 to 10000 centistoke. The oil fill port on the side of the gage assists in filling the gap with oil, especially when working with the more viscous oils. The oil serves three purposes. First, the oil is incompressible and acts to minimize errors due to pressure gradients along the head (i.e., the gage behaves as a solid wall). Second, the oil thermally isolates the temperature sensitive semiconductor strain gages (the thermal conductivity was about 0.15 W/mK). Third, the damping from the oil, coupled with the low specific inertia of the cantilever sensor, helps to reduce sensor vibrations due to the initial shock.

The gage's high stiffness mitigates any protrusion effects due to tilting of the head. For example, a nominal 1000 Pa wall shear will displace the 10 kHz baseline gage head about 0.2μm which produces 20 microstrain. The intrusion of the head into

the flow associated with this miniscule tilting is essentially non-existent with the head lip protruding approximately 0.07μm [25]. This means that the protrusion distance normalized by the head diameter is 1.52E-7. With the gage geometry of a lip to diameter ratio of .01 to .181, Allen [17], for the given c/D of 0.055, predicts that the balance will be virtually insensitive to this protrusion if the boundary layer thickness is greater than .004 cm (.0016 in). So, with its high stiffness and small deflection, the skin friction gage should be insensitive to protrusion. A further discussion of beam geometry issues begins below.

Finally, it is important to note that the basic gage design can be extended to three-dimensional flows with two, orthogonal components of the wall shear by using two sets of opposing strain gages at the base of the cantilever support arm.

2.2 Beam Element Design and Analysis

The beam material and geometry are key design parameters in determining the strain obtained for a given shear force. For the purpose of the tests carried out, it was desired to have both a high gage sensitivity as well as a high natural frequency.

The high sensitivity is required in order to measure the small shear force with strain gages. As a general rule, at least 10 microstrain should be produced at the beam base for a realistic chance to measure it with strain gages. For the gage designs utilized, all had a sensitivity of 10 microstrain per 1000 Pa except for the 20 kHz design which had a sensitivity of approximately 9 microstrain/1000 Pa. However, the tests that these gages were used in experienced an average shear of around 1800 Pa so the gages were still above the 10 microstrain rule of thumb. Experience from previous tests gave an indication of the order of magnitude of the shearing force expected, and, from that, gages could be custom designed for different sensitivities.

The low density plastic serves to reduce the mass of the sensing beam and, therefore, the acceleration induced load from the starting of a facility. This was a concern in the shock tunnel facilities as the startup accelerations were on the order of 100 g's in the NASA Ames 16-inch Shock Tunnel. A simple analysis for a baseline gage for the Ames shock tunnel with a nominal 2000 Pa wall shear and 100 g acceleration was

carried out. The acceleration load of 100 g was imposed upon the combined mass of the sensing head and sensing beam to find the acceleration force. The shear force was simply found by taking the wall shear pressure and multiplying by the area of the sensing head. This simple analysis shows that the force induced by the wall shear is nearly two orders of magnitude greater than the force under the acceleration load.

With a known expected shear force, a simple parametric study can be undertaken to determine the cantilever beam geometry. This design is also dependent upon the beam material which as discussed earlier was either ULTEM or Victrex PES (polyethersulfone). The study was based upon the following simple mechanics of materials equations.

The normal strain in a cantilever beam is given as [30]:

$$\varepsilon = \frac{\sigma}{E} \tag{6}$$

where E is the modulus of elasticity of the beam material and σ is the applied stress. The stress can be computed from the following:

$$\sigma = \frac{PLd}{2I} \tag{7}$$

with P being the applied load at the beam end, L being the beam length, and d the beam outer diameter. I is given as

$$I = \frac{\pi}{4}({r_{inner}}^4 - {r_{outer}}^4) \tag{8}$$

so the resulting strain at the base of the beam is:

$$\varepsilon = \frac{PLd}{2EI} \tag{9}$$

with a deflection at the beam end given as

$$\Delta y = \frac{PL^3}{3EI} \tag{10}$$

The use of the engineering plastics resulted in a stiff beam which kept the resultant deflection small to prevent protrusion of the sensing head into the flow but allowed for sufficient strain at the base such that it could be accurately measured.

The high natural frequency is desired in avoiding resonance effects as well damping of vibrational effects while providing adequate time response for short duration tests (0.3-3 milliseconds). The natural frequency is determined by simply modelling the cantilever sensor as a beam with a mass on the end. Obviously, the larger the mass, the lower the natural frequency. However, this mass also represents the size of the sensing head, so a large mass is desired from a shear sensing standpoint. This tradeoff will be discussed in more detail later. The governing equations for the natural frequency analysis are as follows

$$\tau = \frac{2\pi l^{\frac{3}{2}} \sqrt{\frac{1}{EI}(m_{beam} + 4m_{end})}}{3.5} \tag{11}$$

$$f = \frac{1}{\tau} \tag{12}$$

where l is the length of the beam, and $m_{beam} = \rho l A$ or the beam volume multiplied by its density with the area defined as

$$A = \frac{\pi}{4}(d_{outer}^2 - d_{inner}^2) \tag{13}$$

The mass at the beam end is computed by $m_{end} = \rho a_{eff} \bar{t}$ where $\bar{t}$ is the average of the root and tip thicknesses. The effective area $a_{eff} = a_h - \frac{\pi}{4}d^2$ with the head area similar as in the area equation above, eqn (13), using the head diameter instead of the cantilever outer diameter and fixing the inner diameter to zero since the head cannot be hollow.

Figure 10 more clearly shows each of these dimensions and what they correspond to on the gage's geometry.

A listing of the skin friction gage design program can be found in Appendix section A.1 on page 118. This program is based upon one originally developed by Rodney Bowersox at Virginia Tech. It was later modified to allow the user to iterate over given geometric parameters in case parametric studies are desired. The program allows the user to enter the gage material and its properties as well as the sensor geometry and the expected value of wall shear. The program then outputs the gage natural frequency as well as the expected tip deflection and strain due to the applied shear force. If an iterative study is carried out, a table of results will be output.

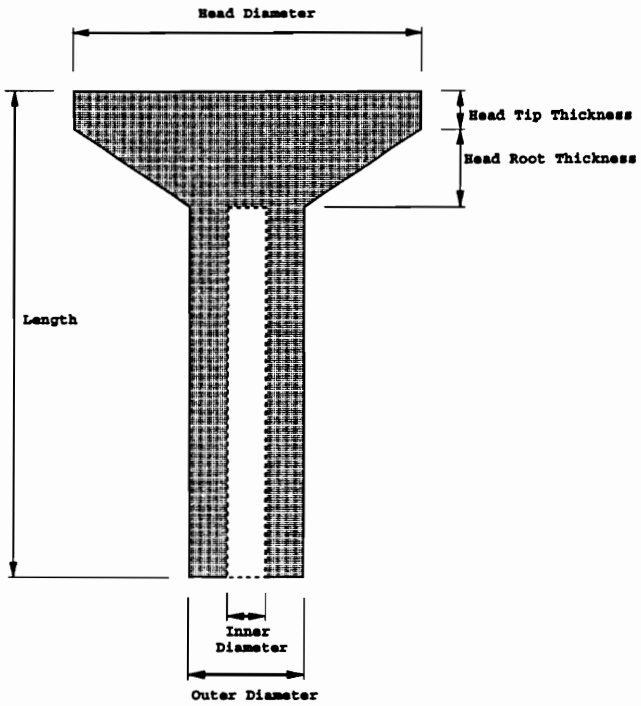

Figure 10: Sensor Geometry Dimension

2.3 Tradeoff: Sensitivity versus Natural Frequency

As noted before, a high natural frequency is desired for several reasons. Among them is the fact that in any test, the gage will exhibit a "ringing" at a value near the natural frequency. This trait can be seen in almost any of the traces obtained such as in Figure 11. Thus, a high natural frequency will diminish this significance of the ringing in the tests and allow for more accurate data to be acquired.

The resonance phenomena, which is the presence of large output from small input, will occur at the the undamped natural frequency of the system which is often referred to as the resonant frequency. For the undamped second order model of the gage, the undamped natural frequency of the gage, ω_f, is defined as [31]

$$\omega_f = \sqrt{\frac{k}{m}} \tag{14}$$

Excitation of the gage at the resonant frequency will lead to the situation where the gage vibrates indefinitely at its natural frequency with no loss of energy ideally

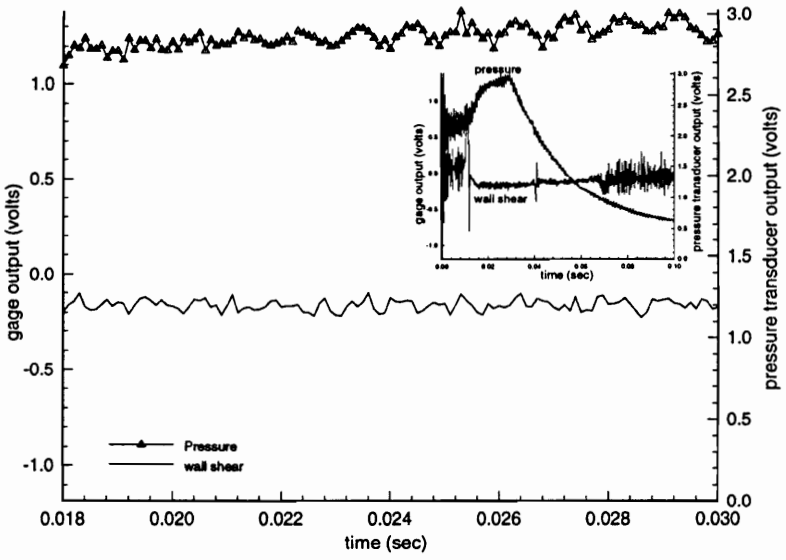

Figure 11: Trace showing ringing in Gage Signal

for no damping. If more energy is input to the gage at the resonant frequency, the magnitude of the output will grow as

$$\frac{E_{out}}{E_{in}} > 1 \tag{15}$$

The design of the high natural frequency is desirable to prevent the resonance phenomena such as if the gage were to be excited by the vibrating test model and to insure that any "ringing" in the signal due to resonance can be distinguished from the signal due to wall shear. For the beam geometry defined above, the natural frequency of the gage, f, is

$$f = \frac{1}{2\pi l^{\frac{3}{2}}} \sqrt{\frac{12EI}{m_{beam} + 4m_{end}}} \tag{16}$$

Once the gage is constructed, the natural frequency can be experimentally determined in a number of ways. A common method of determining the resonant frequencies of a mechanical system is to put it on a shaker table and to randomly excite it. This was done on a gage as shown in Figure 12 below. The shaker table is a small platform which is vibrationally driven by a power amplifier which is controlled

via computer. The gage is mounted in a holder and then fastened to this platform. The shaker table functions by driving a random signal through a specified range into the gage. Here the range used was from 0 to 12 kHz. Then, the output of the gage is examined and transferred into the frequency domain using a fast Fourier transform (FFT). This process is repeated 50 times to get a good nominal value. As can be seen in the graph below, the first harmonic of natural frequency for the gage is around 4.1 kHz. This can be seen in both the peak in the magnitude (on the bottom part of the graph) and the phase angle change (on the top of the graph).

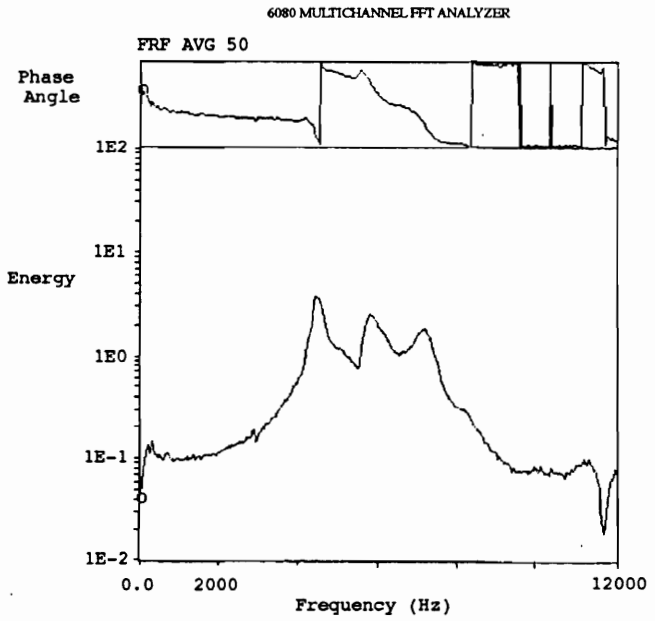

Figure 12: Shaker Table Resonant Analysis– Phase Angle and Power versus Frequency

Although testing in a shaker table is a relatively simple, straightforward, and quick procedure, the facilities necessary for such tests were not always readily available. Combining that with the fact that there were several dozen skin friction gages constructed, a need for a simpler solution to the problem of experimentally verifying a gage's natural frequency became apparent. As mentioned above, the presence of a "ringing" signal at the gage's natural frequency had been noticed in previous experiments. What was a small detriment to the measurements could now be exploited.

By applying an impulsive load to the gage (such as by a brisk hit with a hammer), these oscillations at the gage's natural frequency could be generated. This will produce a damped ringing signal as seen in Figure 13. A FFT of this data and spectral analysis will show the frequencies at which the gage shows the most energy. Using the same gage as was tested on the shaker table, a 2048-point FFT was performed on the data to determine the gage's natural frequency. The data shown in Figure 13 were obtained by sampling on a LeCroy 8013A consisting of a LeCroy 8310 waveform recorder which was hooked to an IBM 486/DX2 66 MhZ PC. The data were sampled at 1 megahertz for over 4 milliseconds. In Figure 13, approximately 300 microseconds of pre-trigger samples have been removed. This high sampling rate would allow for measuring a frequency spectrum of up to 500 kHz after aliasing. All of this range wasn't required as the natural frequency was much lower.

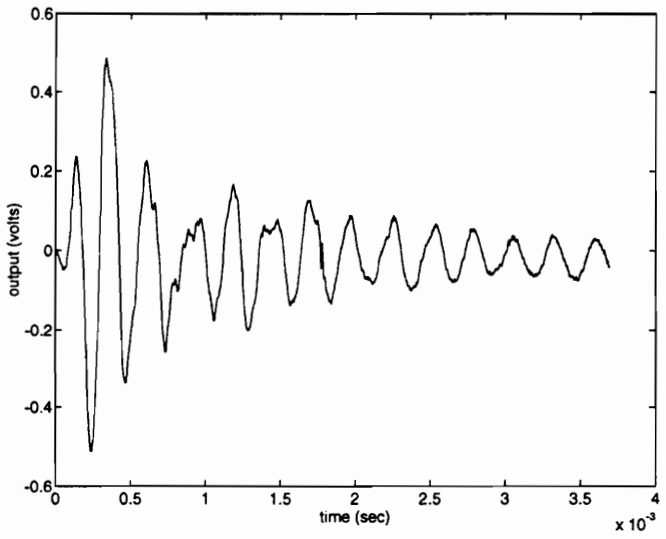

Figure 13: Impulsive Load Ringing Signal

This can be seen in Figure 14. The frequency spectrum is only shown up to 10 kHz since the higher frequencies show little energy. This trace verified the 4kHz frequency obtained from the shaker table test. To get better confidence, the average of several traces after 1024-point FFTs were taken as shown in Figure 15. This shows a nominal 4 kHz value for the first harmonic as was obtained before when the gage

was tested on the shaker table. Thus, this method allows for a very simple process to experimentally verify a gage's natural frequency and is in very good agreement with the results obtained from the shaker table test.

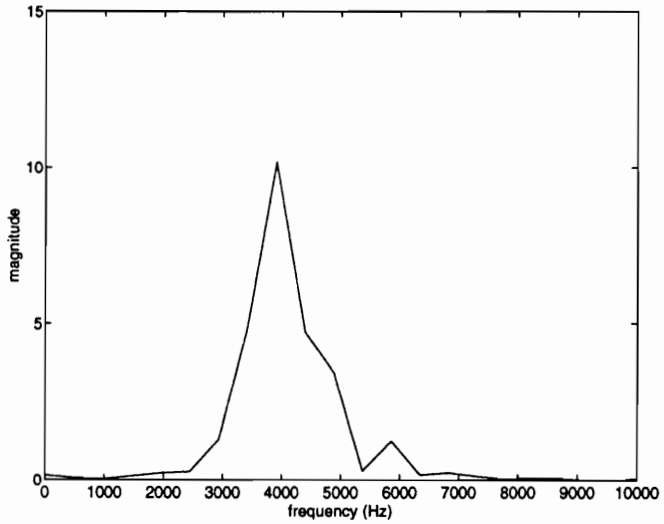

Figure 14: Impulsive Load Resonant Frequency Analysis

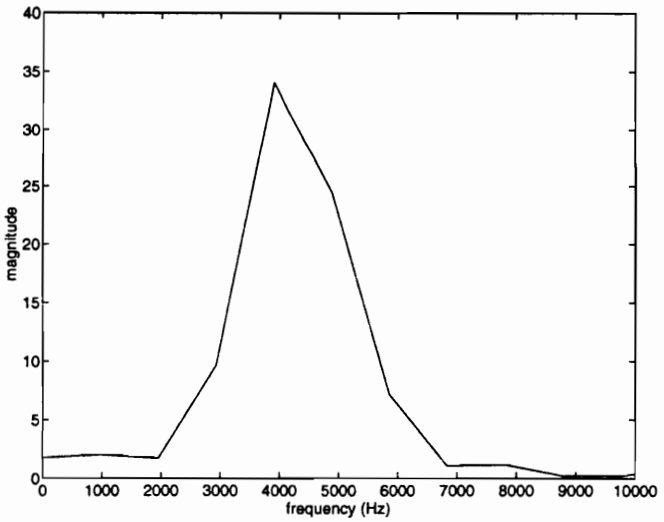

Figure 15: Averaged FFT Resonant Frequency Plot

The time response properties of the baseline gage were discussed in Bowersox et al [25]. These tests involved some gage evaluation studies in a Ludwig Tube and

shock tunnel. A comparison of a local Pitot pressure trace (with a 330 kHz pressure transducer) and a skin friction gage trace showed that there was no measurable lag in the skin friction gage response. This confirmed theoretical estimates.

The time response of the gage can also be approximated by looking at its natural frequency. For the second order system approximation of the gage, for small values of ζ, the expected time response can be approximated as roughly three times the natural period [31]. For the 9.2 kHz to 20 kHz gages used at NASA Ames, this would mean an expected time response of 0.32 milliseconds and 0.15 milliseconds, respectively. These gages are responding much faster than the test period. For the 11 kHz design used at GASL, the time response is approximately 0.27 milliseconds. This is very close to the nominal 350 μsec test time for the facility. However, there is also 400 μsec of pretest flow as the acceleration gas passes through the test cell, so there is still adequate test time for the gages to respond. For the tests in the Virginia Tech Supersonic Tunnel, the 3.6 kHz gage's time response of approximately 1 millisecond is well below the nominal 6 second testing time.

Experimental verification of the mechanics of materials analysis of the strain generated in the base of the beam was somewhat more difficult. There are several more variables that can affect the resultant strain measured by the strain gages including variations in gage fabrication, misalignment effects during strain gage mounting, and other errors generated during the mounting of the strain gages. Ideally, the strain gages should be mounted exactly at the base of the cantilevered beam but such precision during manufacturing was impossible to achieve. The strain gages were all mounted within 0.25 mm of the base of the beam. Nonetheless, even with variations in fabrication most calibrations for a given gage design were within +/- 10 percent of a nominal average value, and relative variations between gages proved to be as expected. That is, the change in the slopes of calibration curves behaved as expected. As seen in the Figure 16 for the NASA Ames tests, the 20kHz gages had a sensitivity of approximately 9 microstrain per 1000 Pascals, so the 14kHz gages with around 12 microstrain per Pascal should experience a calibration with $\frac{4}{3}$ as high slope and the 9.2kHz gages with a sensitivity of approximately 20 microstrain per 1000 Pascal should have a calibration output over twice as large. As shown later in the gage

calibration section, this was indeed the case as seen in Figure 20 on page 36.

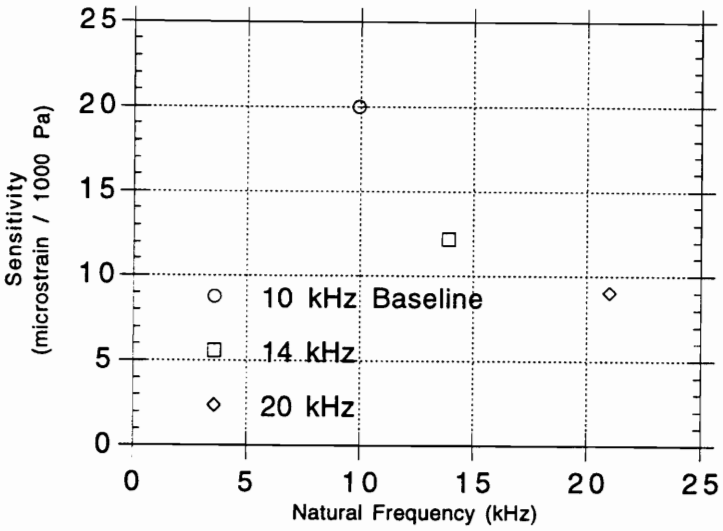

Figure 16: Design Space for Ames Tests

Presented in Figure 16 is evidence that there is always going to be a tradeoff between response time and sensitivity. This relation falls out immediately from the equations and is intuitively obvious. That is, in order to increase the strain at the base of the beam, one would like to reduce the outer diameter of the beam. However, this also acts to reduce the amount of mass in the beam and increase the ratio of head mass to beam mass for the frequency analysis, thus driving down the natural frequency. Likewise, it can be shown for lengthening the beam that the strain goes up, but the natural frequency goes down.

Thus, judgement had to be used when designing for a test facility to design a gage with adequate response characteristics to the expected shear and testing time period. Experience from previous tests helped make these decisions easier. In addition, multiple gage designs were often applied to tests to see which performed best– for the NASA Ames tests, gages with a frequency response from 9.2 to 20 kHz were tested.

Listed in Table 2 below are the dimensions and characteristics of the gage designs tested. All dimensions are listed in millimeters, and the natural frequency is in kilohertz. The material for all test cases was assumed to be Victrex polyethersulfone which has a modulus, E, of 2.67 GPa and a density of 1370.0 kg/m^3. These drawings

also can be seen in Appendix section C.

Table 2: Gage Designs Statistics

Gage Type	20 kHz	14 kHz Ames	11 kHz GASL	10 kHz baseline	3 kHz SST
Outer Diam (mm)	3.30	3.13	3.00	2.54	2.30
Inner Diam (mm)	0.00	0.00	0.00	0.00	0.00
Length (mm)	5.00	6.00	6.70	6.40	9.40
Head Diam (mm)	4.55	4.55	4.60	4.60	5.40
Head Tip (mm)	0.25	0.25	0.25	0.25	0.25
Head Root (mm)	1.02	1.02	0.76	0.76	0.76
Microstrain per 1000 Pa	8.641	12.183	15.792	24.854	67.501
Nat freq (kHz)	21.217	13.909	10.922	9.165	3.601

2.4 Strain Gage Theory

Dilatational strain is defined as, $\varepsilon = \frac{\Delta L}{L}$, or the ratio of change in length of a specimen to initially unstressed reference length. A strain gage is an element which senses this variation in strain and converts it to a change in electrical output. This occurs for several reasons. Considering a conductor of uniform cross-sectional area and length with a resistivity, ρ, the resistance, R, of such a conductor is given by

$$R = \frac{\rho L}{A} \tag{17}$$

If this conductor is stretched or compressed, its resistance will change because of dimensional changes in the cross-sectional area and length and because of the piezoresistance property of materials. Piezoresistance refers to a dependence of resistivity ρ on the mechanical strain [32]. By measuring the strain gage output with applied strain, measurement of the wall shear can be made.

For the skin friction gage, this works as follows. The strain gage was cemented to the base of the cantilevered beam. As the beam is acted upon by shear force, one side goes into tension while the other goes into compression. These strains are

then transmitted directly to the strain gages as each of them undergoes tension or compression. When a strain gage is stretched or compressed, it experiences a change in its electrical resistance since its cross-sectional area is changed. This strain is related to resistance change by:

$$\varepsilon = \frac{\Delta R}{R_0(GF)} \tag{18}$$

where GF is the gage factor of the strain gage. The strain gages are commonly arranged in a Wheatstone bridge circuit as shown in Figure 17 in order to record the change in resistance.

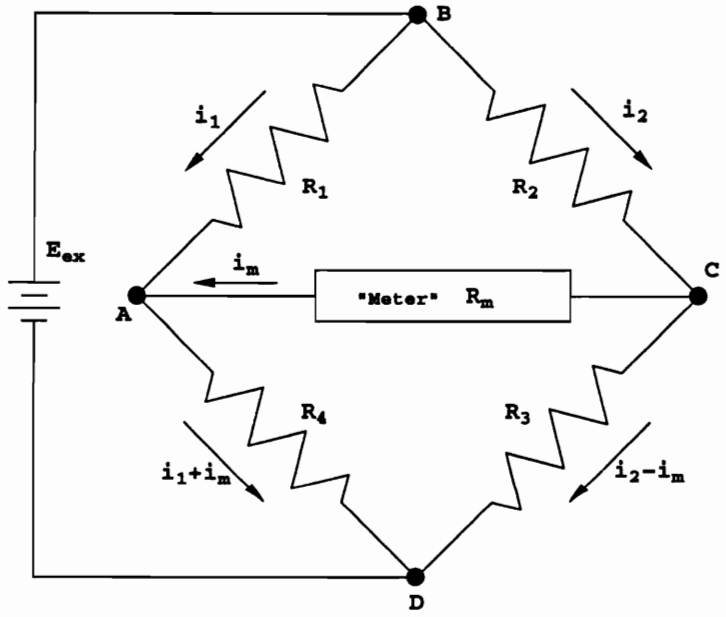

Figure 17: Wheatstone Bridge Arrangement

A Wheatstone bridge may be arranged so that 1, 2, or 4 elements are active sensors; these are called quarter- , half-, and full-bridge arrangements, respectively. An active sensor is one where a strain gage is utilized on that leg of the bridge. An inactive leg will utilize a dummy resistor in order to complete the bridge balance. A Wheatstone Bridge is usually arranged so that the "meter" has a very high internal resistance such that the current flow along CA, represented as i_m, is negligible. Then,

we will have the following expressions for the resistances in the other legs.

$$i_1 = \frac{E_{ex}}{R_1 + R_4} \tag{19}$$

$$i_2 = \frac{E_{ex}}{R_2 + R_3} \tag{20}$$

using Ohm's law, $V = IR$, we can claim that the voltage rise from A to B, e_{AB}, is

$$e_{AB} = i_1 R_1 = \frac{R_1}{R_1 + R_4} E_{ex} \tag{21}$$

likewise,

$$e_{CB} = i_2 R_2 = \frac{R_2}{R_2 + R_3} E_{ex} \tag{22}$$

which yields

$$e_{AC} = e_{AB} + e_{BC} = e_{AB} - e_{CB} = \left(\frac{R_1}{R_1 + R_4} - \frac{R_2}{R_2 + R_3} \right) E_{ex} \tag{23}$$

This equation tells several things about a Wheatstone bridge. First, the bridge will be in a null state when $R_1 R_3 = R_2 R_4$. Second, we can see that the output voltage e_{AC} is linearly related to the bridge excitation E_{ex} but nonlinearly related to the resistances of the bridge arms. However, in the case of small ΔR compared to R, the bridge response is very nearly linear. This is commonly the case in strain gages, as the variation in resistance from the nominal value rarely exceeds 1 percent.

For the experimental setup for the skin friction gages, R_1 and R_4 were active strain gages and R_2 and R_3 were provided by the Measurements Group 2310 Signal Conditioning unit. That is, 2 of the legs were active strain gages and 2 were dummy completion resistors from the 2310 unit and a half-bridge circuit was utilized. The governing equation for a full Wheatstone Bridge is:

$$e_{AC} = \left(\frac{(R_1 + \Delta R_1)}{(R_1 + \Delta R_1) + (R_4 + \Delta R_4)} - \frac{(R_2 + \Delta R_2)}{(R_2 + \Delta R_2) + (R_3 + \Delta R_3)} \right) E_{ex} \tag{24}$$

Considering the two active gages, numbers 1 and 4, will undergo equal and opposite strains (i.e. $+\Delta R_1 = -\Delta R_4$), that the resistances in the dummy gages are fixed

($\Delta R_2 = \Delta R_3 = 0$), and assuming the nominal resistances are equal, then equation (24) reduces to

$$e_{AC} = \frac{\Delta R_1}{2R_0} E_{ex} \tag{25}$$

Substituting in from equation (18) to relate the resistance change to strain and equation (9) to relate the beam base strain to mechanical variables, then the final expression for output voltage of a half-bridge circuit for our beam sensor is:

$$E_{output} = \frac{(GF)}{2} \frac{PLd}{2EI} E_{excit} \tag{26}$$

2.5 Semi-Conductor Strain Gages

The gages chosen for this design were Model 919 strain sensors from Micro Gage Inc. These gages are narrow enough to be mounted on the slender beam and also had a short length so that they could be positioned at the beam base. They also had the required large gage factor to measure the small strains generated at the beam base. Rather than solder tabs, they have small gold leadwires at each end of the strain gage; these wires can be easily wrapped around and soldered to the leadwires which feed up through the base of the skin friction gage. In addition, these gages are easily bonded to the beam and are inexpensive.

The gages have an overall length of .203 cm (.08 in) and an overall width of 0.0229 cm (0.009 in). The Model 919 sensors come in resistance increments of 350, 500, and 1000 ohms with gage factors of 135, 140, and 145, respectively. Gages of the 350 ohm variety were used for almost all of the tests; 500 ohm gages were used during a short period when the 350 ohm variety was unavailable from the vendor. The resistance has negligible effect on the performance of the gage as long as the active gage pair has a matched resistance.

The strain gages were cemented onto the base of the sensing beam with Micro Measurements M-Bond 200, a standard strain gage adhesive, at 180° to each other. Commonly the sensing axis of the strain gages was made to the coincide with the alignment pin. This was done to aid in alignment during installation of the gages

into a model or facility. The gold lead wires from the strain gages are then wrapped around and soldered to the lead wires that are fed through the holes in the gage base.

Semiconductor strain gages were chosen for use rather than foil gages because of their much high sensitivity– almost 2 orders of magnitude with gage factors of 135-140 here versus gage factors of 2 for foil type strain gages. Gage factor is the term used to define the functional change in resistance of a gage with applied strain and will be discussed in further detail later. The principle employed in these gages is the piezoresistance effect, which is defined as the change in electrical resistivity with applied stress [29]. This resistance change occurs in all conditions of static and dynamic strain. All materials exhibit the effect to some degree, but in certain semiconductors the effect is very large and an appreciable change in resistivity occurs with applied stress. For a semiconductor:

$$\rho = \frac{1}{eN_i\mu_{ave}} \tag{27}$$

where ρ is resistivity, e is electronic charge, N_i is the number of charge carriers, and μ_{ave} is the average mobility of N_i.

When stress is applied to a semiconductor, both N_i and μ_{ave} will change; the magnitude and sign of the change depend upon the specific semiconductor, its carrier concentration and orientation with respect to the applied stress. Thus gages can be designed with positive or negative gage factors. For a simple tension or compression, the relative change in resistivity is given by

$$\frac{\Delta\rho}{\rho_0} = \pi_L\sigma \tag{28}$$

where π_L is the longitudinal piezoresistive coefficient and, of course, σ is the applied stress. The gage factor is then

$$GF = \frac{\Delta R}{R_0\varepsilon} = 1 + 2\nu + \pi_L y \tag{29}$$

The first two terms represent the change in resistance due to dimensional changes while the last term represents change in resistivity with strain. See Ref. [29] for a complete discussion of semiconductor strain gage theory including doping, resistivity, and hysteresis effects.

2.6 Gage Calibration

A skin friction gage is calibrated by directly applying a force along the gage's measurement axis. This is commonly done by placing the unit in a horizontal position so that the desired calibration axis is vertical. This is shown in greater detail in Figure 18. Known mass standards (i.e. 1 gram, 2 grams, 5 grams) are attached to the center of the floating head via a thin line and allowed to hang vertical, insuring that the force is applied in the desired direction. The balance electronics are turned on, and the balance output can be recorded either by the PC-based data acquisition system or manually with a digital voltmeter.

Care must be taken in applying the load so that a small pendulum action is not induced in the line. This would diminish the output of volts per gram as the load vector would be off of the measurement axis. Commonly, the voltmeter is used to acquire the data, because it is simpler and the calibrations sampled on the PC, at 100 Hz for 2 sec and then averaged, showed no difference. After calibration, the gage is rotated 180° and recalibrated to insure no sensitivity in the load application direction. Sample calibrations for skin friction balances can be seen in Figures 19 and 20.

The gages will exhibit a linear response of

$$\tau_w = a\ \Delta V \tag{30}$$

where τ_w is the wall shear stress, a is a calibration constant, and ΔV is the change in output voltage. A least-squares regression is performed on the calibration data to obtain the linear calibration curves in units of volts per gram. These curves are highly linear with a variance on the order of 10^{-4}.

So now a linear gage calibration is available in the units of volts per gram of mass applied. However, it is desired to get the calibration in terms of volts per Pascal of shear force. This is done by multiplying the mass by gravity to get the units of Newtons and then dividing by the area of the sensing head. This yields the desired output in Pascals. For example, a gage with a 0.01m diameter sensing head and a 100 mV/gram calibration would result in a calibration of 0.801 mV/Pa. Thus, a given output corresponds to a given wall shear which can be normalized by the dynamic

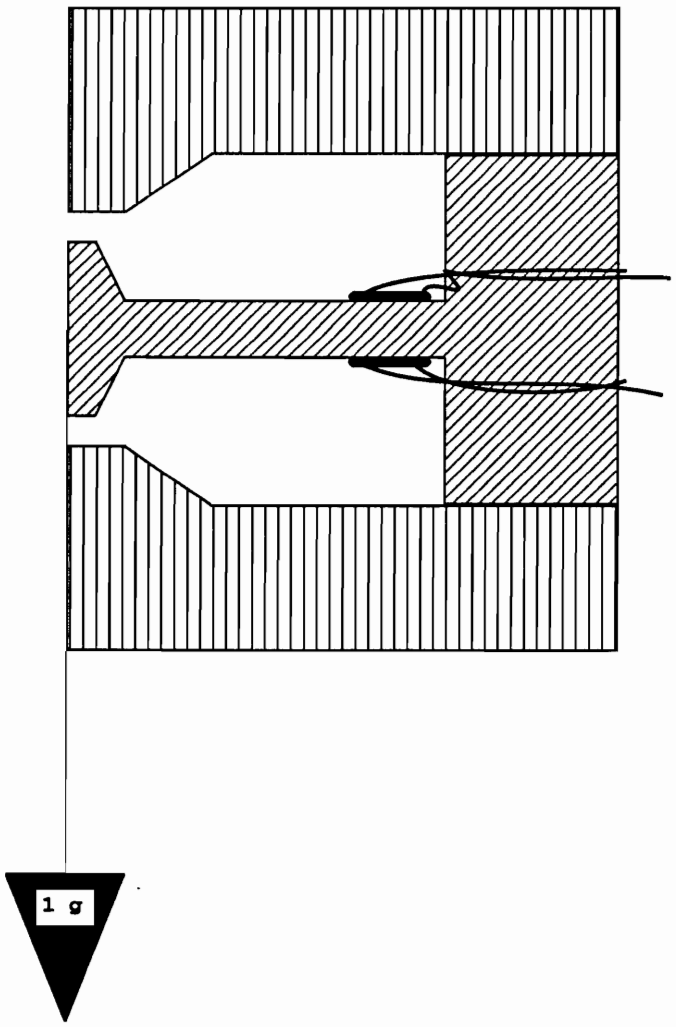

Figure 18: Gage Calibration Technique

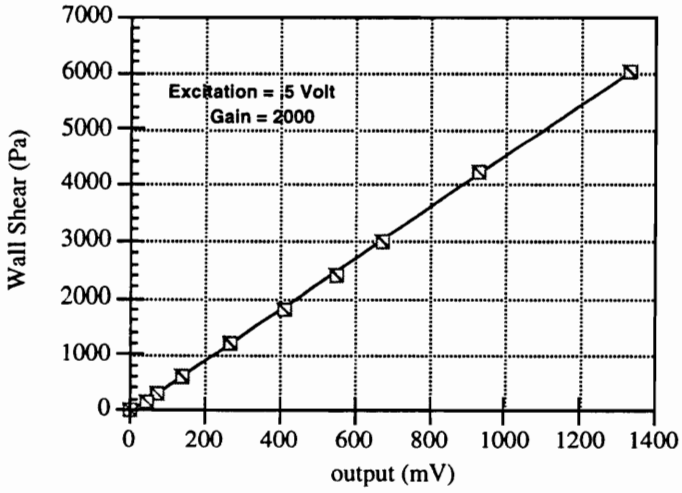

Figure 19: Sample Gage Calibration

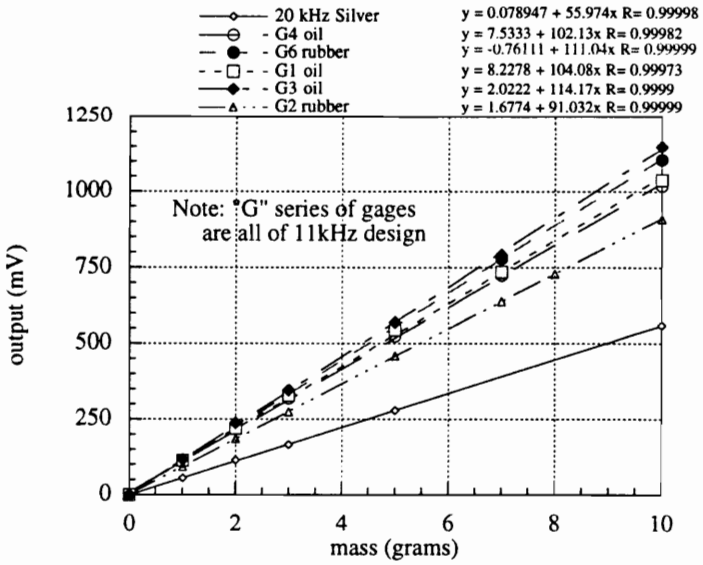

Figure 20: Another Sample Gage Calibration

pressure at some point in the flow in order to yield the skin friction coefficient.

2.7 Oil Fill Procedure

The procedure for filling the gage annulus is straightforward and simple. It is required to get oil into the annulus while removing all of the air bubbles. This is done by placing the skin friction gage into a beaker filled with the oil and then placing the beaker in a vacuum chamber. This is shown in Figure 21.

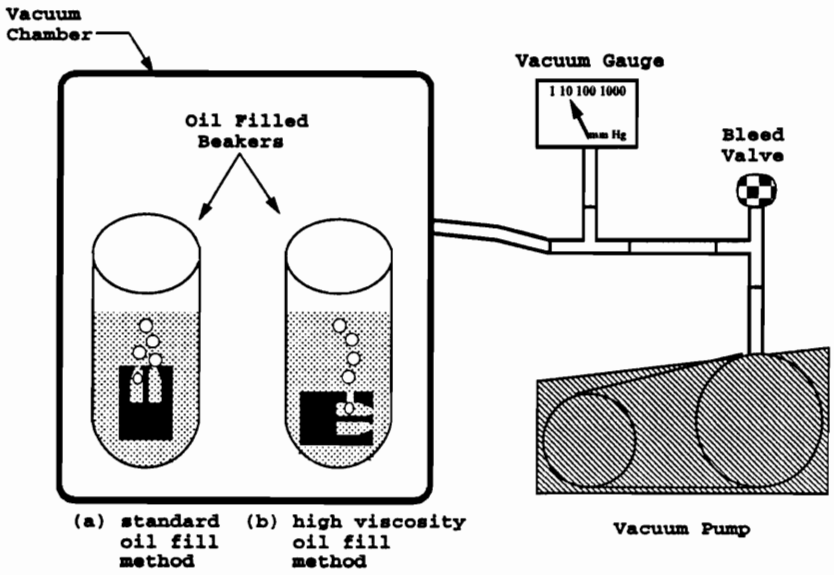

Figure 21: Gage Oil Fill Procedure

The figure shows the air bubbles coming out from the annulus. It also shows the use of the oil fill port on the side of the gage and how it is used to set up a channel so that oil enters through the gap and air exits through the fill hole. However, for most lower viscosity oils (500 centistokes or lower) it was found that simply putting the gage in an upright position with the gap facing upward was adequate for getting all of the air out. It is imperative to get all of the air bubbles out of the annulus as shown in the exaggerated cartoon in Figure 22. As pressure decreases, as is often the case in supersonic tests, the air bubble increases in volume. It also begins to exert an outward force on both the gage housing and the cantilevered beam. The extraneous

force exerted on the beam then contaminates the wall shear results. The chamber should be pulled down to as close to vacuum as possible or at least to a pressure lower than that in the test section. Using a good chamber, achieving a good vacuum should not be a problem, and the outgassing of air will be dramatic with a bubbling foam forming at the air/oil interface. In order to remove any air bubbles that may attempt to adhere to the side of the beam or housing, it is recommended that the beaker be vibrated slightly during the vacuum process if possible and also that the vacuum process is cycled several times by pulling down to the near vacuum condition for several minutes, then releasing to near-atmospheric pressure, back to near vacuum for a few minutes again, and then repeating. Experience has shown this does a better job than simply pulling to vacuum and holding there for an hour or several hours.

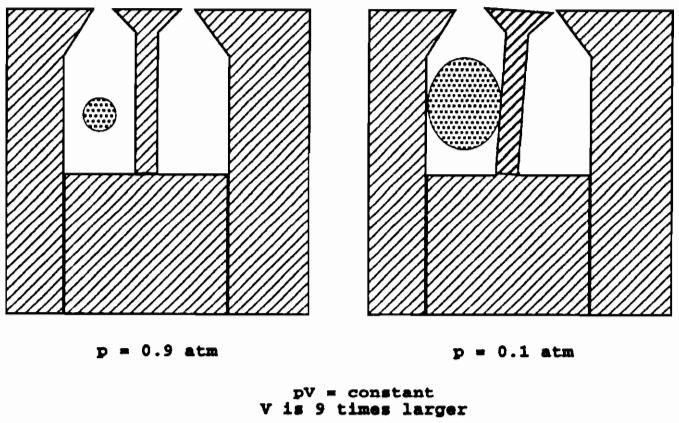

Figure 22: Error Caused by Air Bubble

Chapter 3

Design Variations to the Baseline Gage

3.1 Variations to the Gage Surface

Sputtered Surface

One of the simplest and most beneficial modifications to the skin friction gages was the use of the sputtered surface as suggested in Ref. [26] . This refers to the electronic depositing of an oxide or other substance onto the gage head and housing head. During the NASA Ames testing series, the gages were coated with several different materials including titanium, iridium, chromium, yttrium-oxide, chromium-oxide, and titanium-oxide. The 0.2 micrometer coatings were electronically deposited onto the sensing head– the gages are placed in a containment chamber and the substance is taken from a target and "sprayed" onto the gage head. Generally speaking, the skin friction gages are so small and the spraying area is so big that there is no difference in cost between sputtering one gage or a dozen gages. These coatings then provide for a smooth and much more durable surface while not affecting the gage's response characteristics.

The need for the more durable sputtered surface was clearly seen during the tests at NASA Ames. The sensing surfaces of the skin friction gages were suffering from erosion and scarring due to a combination of thermal effects on the gage surface and

impacts from microparticles travelling down the shock tunnel at hypersonic speeds. The sputtered gage surface was much more rugged than the plain plastic surface and increased the lifetime of a skin friction gage. There is an increase in manufacturing cost and time, but it is more than offset by the increased hardiness of the gage surface and the fact that the gage response is unaltered from an unsputtered model.

Ceramic Head

Another modification to the skin friction gage's sensing head and housing was the attachment of a machinable ceramic head to the tip of the cantilever and the sensing end of the housing as shown in Figure 23. As can be seen in the figure, the ceramic head lacks the head taper of the plastic heads, since this taper was difficult to fabricate. The benefits for the ceramic head gage are similar to the ones for the sputtered gage surface. The ceramic will be less likely to scar than the plastic and will also have a very low heat transfer down the beam towards the strain gages.

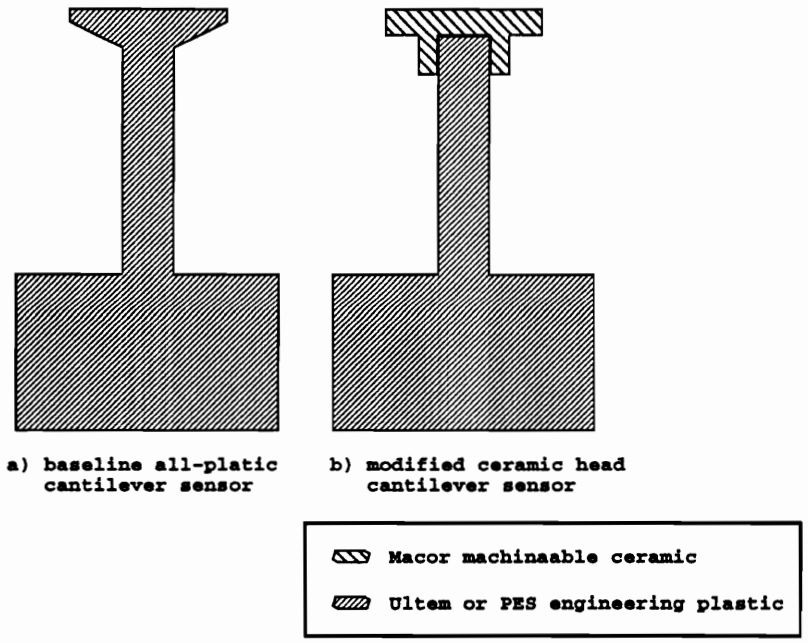

Figure 23: Ceramic Head Skin Friction Gage

The drawbacks to such a scheme are as follows. First, there was always a difficulty in keeping the ceramic head attached to the plastic cantilever. Standard epoxies or cements would not work due to the high testing temperatures that were encountered.

In addition, many high temperature adhesives are not designed for joining ceramics and plastics. A specialized adhesive (Master Bond Polymer Adhesive EP30HT) was finally found, and the ceramic head pieces were cemented on.

In addition, the ceramic used was Macor machinable glass ceramic [33]. This ceramic is approximately twice as dense as Ultem or Victrex PES with a density of 2520 $\frac{kg}{m^3}$ versus 1370 $\frac{kg}{m^3}$ for Victrex. The density change places more mass at the end of the beam, driving down its natural frequency. Thus, for identical geometries, the skin friction gage with the ceramic head will have poorer time response properties.

Other problems experienced with the Macor head gage were brittleness and a difficulty in placing the ceramic tip onto the end of the cantilever beam without misalignment. The "sleeve" only fits a short distance over the beam and it is filled with epoxy. Care must be taken to insure that the tip is placed on so that there is not protrusion at one end of the sensing head and recession from the housing at another. In addition, the ceramic is brittle so it was found to chip if stressed too hard during fabrication or during testing. A ceramic head gage was successfully built and tested in the Virginia Tech Mach 3 Shock Tunnel, however the difficulties involved with such a gage led to the abandonment of such a design.

Stainless Steel Housing

Another variation to the gage surface involved the use of a skin friction gage where the surrounding housing was made out of stainless steel rather than an engineering plastic. This was done for two reasons. First, it was feared that the plastic housings may have been buckling during the firing of the shock tunnel and causing a water-hammer effect in the skin friction gage which squirted the oil out. Second, the steel would provide a very durable surface that would be much more difficult to scar during testing. The drawbacks to a stainless steel housing include an increased manufacturing time and concerns about the increased heat transfer rate through the steel leading to a possible thermal contamination of the results.

Fears about the increased heat transfer were never realized, as the gages with steel housings showed no thermal contamination of the test signal. Experimental testing also showed that the stainless steel housing did not provide any noticeable benefits in the retention of silicon oil in the gage cavity. It did, however, provide a much more

rugged surface than a plastic housing, however not much more so than one which had been sputtered. Unfortunately , the plastic sensing head was still susceptible to damage and would have to be sputtered. As mentioned before, there is really no cost difference in sputtering a coating onto a single sensing head or a head and housing so the toughness benefits of the stainless steel housing are diminished since both can simply be sputtered at the same time (as a matter of fact, one stainless steel housing was coated with an oxide covering). It is overkill to make the entire housing out of metal when sputtering a thin coating onto a plastic housing surface provides the same benefits.

3.2 Modifications to the Gap

Two-part Silicon Rubber

Probably the most significant modification was the replacement of silicon oil in the gap with a 2-part RTV Silicon Rubber, GE Silicones RTV615. This was done to try and extend a gage's testing life between servicing. Checking and maintaining the oil filling of the gage makes it a relatively "high maintenance" device. It is often necessary to remove the unit from the test article to check the oil and refill it if needed. It was desired to have a rubber substance with a low modulus relative to the beam plastic so that the output would not be impacted very much, a low viscosity so that the gap could be easily filled, a low thermal conductivity to prevent thermal effects, and a room temperature cure. The RTV615 met all of these requirements. Therefore, was selected for trial use.

During common testing, the silicon oil must be replaced fairly often (approximately every 3 to 5 runs) to prevent thermal contamination. This can sometimes present a problem since once the model and test section are sealed, they may not be reopened for an extended period of time. To combat this problem, the rubber-filled gage idea was utilized. The primary benefits of the rubber-filled gage are the reduced maintenance requirements and the fact that the rubber is a good thermal insulator as well. Drawbacks include changed gage response, such as diminished shear sensitivity, due to the rubber.

The gap is filled by first mixing the rubber to the 10:1 by mass ratio as specified by the manufacturer. Next, it is cycled under vacuum to get air bubbles out (deaeration). It is then poured into the gap. The mixed liquid is clear and colorless and is relatively easily poured with a nominal viscosity of 4000 cps. Once the gap is filled, the rubber-filled gage is cycled under vacuum yet again to get out air bubbles. The rubber will expand, crest, and recede to about the original level as the bubbles break. During this time, additional rubber may have to be added as the surface level may go down as entrapped air is removed. The cycling process is repeated until all air bubbles are gone. RTV615 has a four hour work time, so there is time to accomplish this task. Once the gap is filled, the gage is allowed to sit until the 24-hour cure time is reached. After that, a delicate slicing along the top with a razor blade is done to remove excess rubber. The gage is then calibrated and ready for testing.

A theoretical model was developed with the aid of Dr. Rakesh Kapania [34] to try and determine the diminished shear sensitivity and provide a gage design tool. This was accomplished by modeling the beam as a 2-part beam resting on an infinite spring base as seen in Figure 24. The spring stiffness, k, was determined by modelling the rubber with a one-term Ritz method solution. The computer programs to model this can been found in Appendix section A.2. Since the beam is modeled as two parts with constant diameter, the taper section of the actual beam was modeled as half of the small beam diameter and half of the large head diameter.

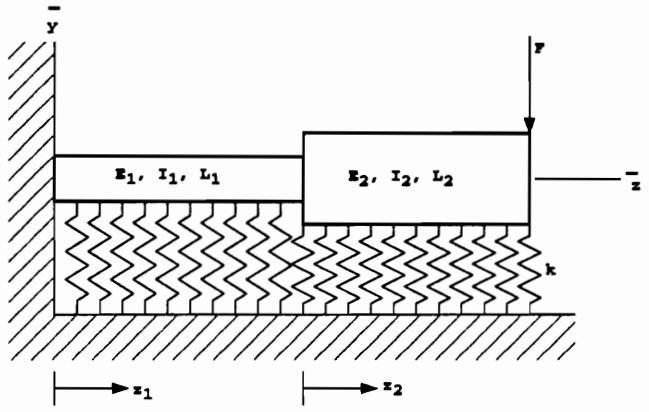

Figure 24: Rubber Model Concept

The spring stiffness of the rubber, k, is computed by using the principle of minimum total potential energy. A linear displacement model is used with the maximum displacement, u, being on the gage head and the minimum being zero where the rubber touches the housing.

Once a value of the rubber spring stiffness is acquired, a second problem is solved. For the problem in Figure 24, the governing equation is

$$EI\frac{d^4\bar{y}}{d\bar{z}^4} + k\bar{y} = 0 \tag{31}$$

where $\bar{y}$ is the displacement in the y direction and $\bar{z}$ is the displacement in the z direction. Letting $\beta^2 = \sqrt{\frac{k}{4EI}}$, this reduces to

$$\frac{d^4\bar{y}}{d\bar{z}^4} + 4\beta^4\bar{y} = 0 \tag{32}$$

Each of the displacements is non-dimensionalized using $\gamma_1 = \beta_1 L_1$, $\gamma_2 = \beta_2 L_2$, $y_1 = \beta_1\bar{y}_1$, $y_2 = \beta_2\bar{y}_2$, $z_1 = \frac{\bar{z}_1}{L_1}$, and $z_2 = \frac{\bar{z}_2}{L_2}$

This results in a general, non-dimensionalized solution to the differential equation of the form.

$$\frac{y_1}{\beta_1} = e^{\gamma_1 z_1}(c_1 sin(\gamma_1 z_1) + c_2 cos(\gamma_1 z_1)) + e^{-\gamma_1 z_1}(c_3 sin(\gamma_1 z_1) + c_4 cos(\gamma_1 z_1)) \tag{33}$$

$$\frac{y_2}{\beta_2} = e^{\gamma_2 z_2}(c_5 sin(\gamma_2 z_2) + c_6 cos(\gamma_2 z_2)) + e^{-\gamma_2 z_2}(c_7 sin(\gamma_2 z_2) + c_8 cos(\gamma_2 z_2)) \tag{34}$$

Next, eight boundary conditions are applied to the system. They are the two at the fixed wall that displacement and rotation are zero, four matching the displacement, rotation, shear, and moment where the 2 beam sections meet, and two governing the shear and moment at the free end. Applying the boundary conditions and solving results in a closed form solution of 8 equations for 8 unknowns. One of the solutions is trivial ($c_2 = -c_4$), so the actual system to be solved is 7 equations for 7 unknowns. These equations are then solved for the coefficients, c, using Gaussian Elimination. After determining c, the displacement of the free end of the beam as well as the shear at the beam base can be calculated as seen in the program.

These new rubber values for the strain and deflection can be substituted for the output from the sfgd.f program (of section A.1). So the theoretical solution for a

potential rubber gage design was an iterative process– first solve for natural frequency and strain produced with the regular beam model and then solve and apply the "rubber model correction".

The change in natural frequency was determined by a side-by-side experimental comparison of two identical gages, one with an oil-filled gap and the other with a rubber-filled gap. For this experiment, both were placed on the shaker table with 50 random excitations being applied, transformed via FFT into the frequency domain, and then averaged. It can be seen that the silicon rubber had a negligible effect on the gage's natural frequency in Figure 25.

The primary design criteria for the rubber-filled gage was to create a situation where the rubber-filled gap exerted a minimum amount of spring stiffness onto the beam. This would insure that the output from the beam would see the smallest decrease. Not surprisingly, the output from the gelim program showed that an anulus with the largest outer diameter would result in the smallest decrease in the amount of microstrain generated in the beam. So a large gap was utilized with the maximum gap size constrained by the size of the hole drilled through for the sensing piece to fit into the housing. This size is equivalent to the diameter of the base that the beam rests upon.

An additional effect caused by these large rubber gaps was that there was a large increase in the measured wall shear. It was found that the large gap size resulted in a new effective sensing head size as the wall shear was acting on and deflecting the rubber which in turn exerted a force on the sensing beam. In some cases, the rubber-filled gap had an outer diameter of 0.375 inches compared to the sensing head diameter of 0.181 inches. This doubled diameter resulted in a four-fold increase in sensing area and indeed increases in the wall shear of three to four times were seen.

Fortunately, this increase was found to be constant independent of flow conditions. For a side-by-side comparison of an oil-filled and rubber-filled gage, the increase remained the same no matter what the upstream conditions were. Thus, a correction factor could be applied to the rubber-filled gage output to make it correlate to that of the oil-filled gage. The scaling factor between the rubber and oil-filled gages was also found to be essentially constant for gages of a given geometric family. That is, the

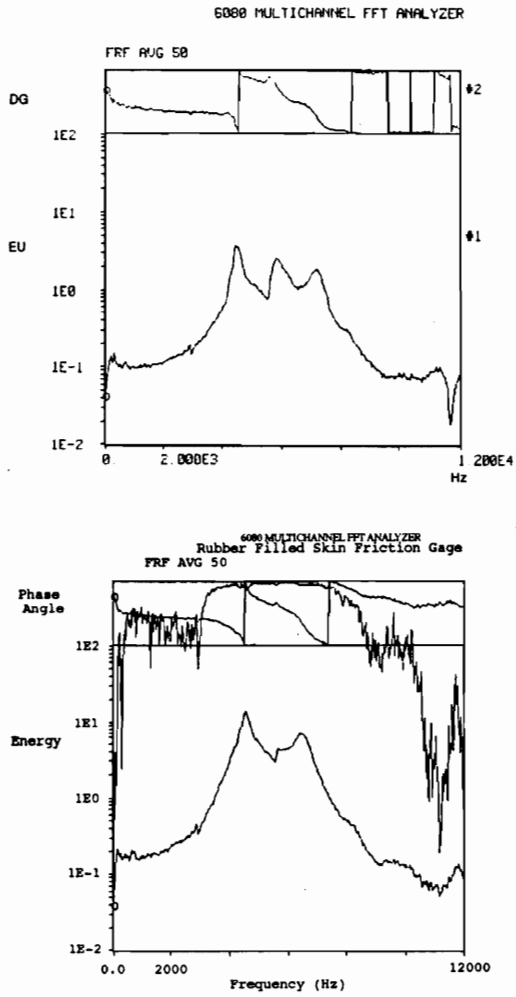

Figure 25: Natural Frequency Comparison– Phase Angle and Power vs. Frequency

factor showed essentially no variation between gages if their geometry was the same.

This "effective sensing head factor" was determined by a dynamic calibration method. This involved placing a rubber-filled and an oil-filled gage side-by-side for comparative testing. A few runs would be made in the Virginia Tech supersonic tunnel at a very low pressure condition to see the ratio of rubber to oil-filled gage output. Then, runs would be made at a high pressure condition and the ratio checked again. Last, runs would be made at a moderate pressure condition and the ratio calculated once more. It was found that this ratio of rubber to oil-filled gage output remained constant, independent of pressure. Since the wall shear predicted by the oil-filled gage was known to be correct through the application of skin friction correlations, the rubber-filled gage output could be divided by this ratio to generate results which agreed with predictions and other experimental testing. The fact that the ratio between the rubber and oil-filled gages remains constant in a variety of flow conditions increases confidence in its accuracy.

In addition, the factor was dependent upon geometrical parameters that one would naturally expect to be significant. There was a very strong relation between the area of the sensing head and the area of the sensing head plus rubber. In addition, there was a weaker relation between the gage stiffness and the increase due to the increased area due to the rubber. The stiffer, higher frequency gages were less impacted by the rubber. These effects intuitively make sense. A gage with a doubling of surface area will see roughly twice the force. By making the beam stiffer, the spring stiffness of the rubber seems less significant compared to the stiffness of the beam.

Some typical results for this factor are as follows: for the 3.6 kHz design of Figure 96, the value was 3.05+/-0.05 which is close to the 3.22 area ratio of the 9.53 mm foundation diameter and the 5.40 mm diameter of the Victrex sensing head. For the 10kHz design of Figure 95, the ratio was 3.96+/-0.07, which again is slightly less than the 4.29 area ratio of the sensing head to the foundation. For the 11kHz GASL tested gages of Figure 94, this "effective sensing head factor" was found to be approximately 2.0 which is less than the 2.74 area ratio and shows the diminishment of the factor as the sensing beam becomes more stiff.

Reduced Gap Size

Due to oil leakage problems, a second modification to the gap was utilized. The gap size was reduced from a diameter .010 inches larger than the sensing head to only .003 inches larger. This would lead to a situation where the capillary forces retaining the oil would be much stronger. Indeed this was seen as the use of the oil fill port on the side of the gage was required in order to fill the anulus with oil.

The expected benefit of this modification would be an increased servicing time between runs. This could not be ascertained as the second test series at GASL only consisted of four runs. However, in additional tests where the HYPULSE facility was run but skin friction data was not taken, the reduced gap skin friction gage outlasted the regular oil-filled gage. However, it cannot be determined whether the gage failure was due to oil depletion or other effects.

The potential drawback to such a gage design is that any sort of misalignment can lead to a binding of the gage onto the housing. In addition, thermal expansion and scarring can also lead do a situation where the gage head binds to the side of the housing. Nonetheless, this concept is worthy of further study.

3.3 Modifications to the Cantilever

Hollow Beam

The hollow beam modification consists of drilling out the interior of the sensing cantilever, so that it is now a tube rather than a rod. This serves several purposes. First, the reduced mass decreases the shock response of the beam. Second, as shown in the Table 3 below hollowing can increase both the sensed strain and natural frequency of the gage by around 5%. As a general rule, the optimum point is generally where the hollowed out diameter is about half of the outer diameter. After that, the natural frequency of the gage will decrease as the mass of the sensing head becomes increasingly large relative to the mass of the beam. The sensed microstrain increases rapidly as well. The table shows the variation of microstrain and natural frequency for a baseline PES gage with the geometry of a 2.54 mm outer diameter, a 6.40 mm length, a 4.60 mm head diameter, 0.254 mm head tip thickness, and a 0.762 head root thickness.

Table 3: Hollow Beam Optimization Results

Inner Diameter (mm)	microstrain per 1000 Pa	Natural Frequency (kHz)
0.000	24.8544	9.1650
0.250	24.8567	9.1905
0.500	24.8918	9.2629
0.750	25.0448	9.3702
1.000	25.4662	9.4910
1.250	26.4030	9.5914
1.500	28.2959	9.6174
1.750	32.0838	9.4762
2.000	40.3743	8.9863

The primary drawback to such a modification is the potential for induced error if the hollowing hole is not concentric with the beam. Since the static pressure in the test section drops, the cantilever may see low pressure on the test side of the cantilever and atmospheric pressure on the back side and through the hollowed out hole. If the hollowing hole is off-center, this pressure imbalance may result in spurious output caused by pressure difference coming through the hole and exerting a force onto the beam. With the hole being off-center, one of the strain gages will sense more strain than the other resulting in an error.

The hollow beam design is a very worthwhile modification as it can increase both the natural frequency and strain sensitivity. However, for the tests in question, the primary emphasis was on reducing possible sources of uncertainty. The potential for false strain readings induced by a pressure differential between the test side and rear side of the skin friction gage led to the decision to sacrifice the 5% improvement in natural frequency and sensitivity for the time being.

Thermocouple Holes in Housing

An additional modification involved the implementation of thermocouple holes drilled into the base of the cantilever next to the feed-through holes. This was done so that thermocouples could be installed into the gage to take temperature data next to the strain gages as shown in Figure 26. A small 0.0625 inch hole was drilled in the base and a Type K thermocouple was then inserted through the base so that the

thermocouple was located at the same axial location on the cantilever as the center of a strain gage. The thermocouple was then secured and the hole sealed with epoxy applied to the backside of the gage base.

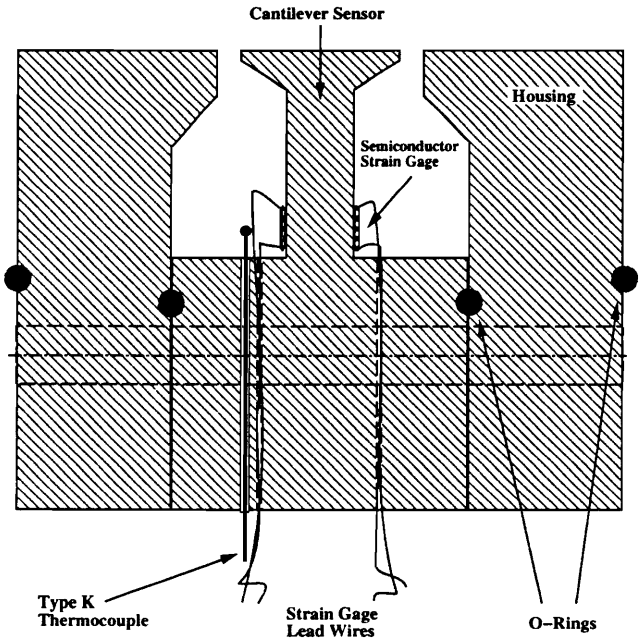

Figure 26: Thermocouple Hole Modification

This temperature data was required to determine the test window for the tests in the Virginia Tech Supersonic Tunnel. Considering the tunnel run time was on the order of 5 to 10 seconds, the assumption that the temperature near the strain gages remained constant could break down. By acquiring the thermocouple data, the end of the test window could be determined by noting when the local temperature next to the strain gages changed significantly. This temperature information is useful in all tests to insure that there is no heating of the strain gages leading to thermal drift.

Chapter 4

Skin Friction Tests at NASA Ames

A series of tests over several months were conducted at the NASA Ames 16 Inch Shock Tunnel. A variety of different inlet flow conditions and injector schemes were tested during the test series. A total of four gage locations were available for instrumentation– 2 in the inlet and 2 in the combustor. Data were acquired in each location, although much more data was acquired in the combustor due to greater interest in flow conditions there and also due to maintenance and support limitations.

4.1 Description of Facility and Test Procedure

The facility is described in Ref. [35]. It is configured in a semi-free jet ground test configuration. Thus, the scramjet model is pitched downward, so that the flow from the facility nozzle simulates the flow behind the leading edge body shock. This means that the model will experience the influence of the cowl and cowl shock and experience a thin body-side boundary layer. However, leading edge bluntness effects, boundary layer transition and thickness, and shock-on-cowl interaction are not simulated in this test configuration. These would be simulated in the free-jet configuration, however current ground test capability does not exist to test this configuration.

Figure 27 below shows the 4 types of test facilities. The first is the free jet, in which

the model would be placed into the tunnel and the data taken as is commonly done in subsonic and supersonic experiments. However, no such facility currently exists for air-breathing hypersonic vehicle ground testing. The semi-free jet configuration has been discussed above, where the model is pitched so that the incoming flow simulates that behind the shock off the vehicle nose. The semi-direct-connect configuration eliminates the cowl and the oncoming flow is turned by the shock shown in the figure to produce one-dimensional flow conditions at the combustor entrance. A segment of the one-sided nozzle may be included at the combustor exit. The direct connect configuration also neglects the cowl and provides one-dimensional flow conditions at the combustor entrance directly from the facility nozzle.

The tests carried out at the 16 Inch Shock Tunnel facility simulated true Mach 12-14 enthalpy conditions with reservoir $P_t = 32.4$ MPa and $T_t = 10000$ R and local Mach numbers on the order of 6. The testing time was reported by NASA Ames personnel, and an averaging period of 2-3 milliseconds was commonly used. The facility is said to have a nominal test time from 5-10 msec, a slug length of 25m, a core flow of 70 cm, and it can simulate flight Mach numbers of 10 to 17 [35].

The skin friction gages were placed into the cowl side of the model such that the sensing head was facing upward. A total of four gage ports were available: two in the inlet and another pair in the combustor. The inlet ports were in line with each other with one gage in front of the other, while the combustor ports were at the same axial location with one gage on the combustor centerline and the other port off to the side.

The data acquisition was completely provided by NASA Ames personnel as were the mean flow conditions. The sampling rates were originally 100 kHZ, but this was determined to be excessive based upon the test time, the gage's natural frequency, and also the size of the data files. After a few runs, the sampling rate was halved to 50 kHz.

The common test scenario was as follows. First, gages were installed and the wiring and connections were checked for continuity. The model was then sealed. The next morning, the gage bridges were excited and balanced and the shock tubes were drawn down to vacuum as necessary for testing. After the proper conditions were reached and held, the tunnel was fired. Pre-trigger samples were taken on all gage

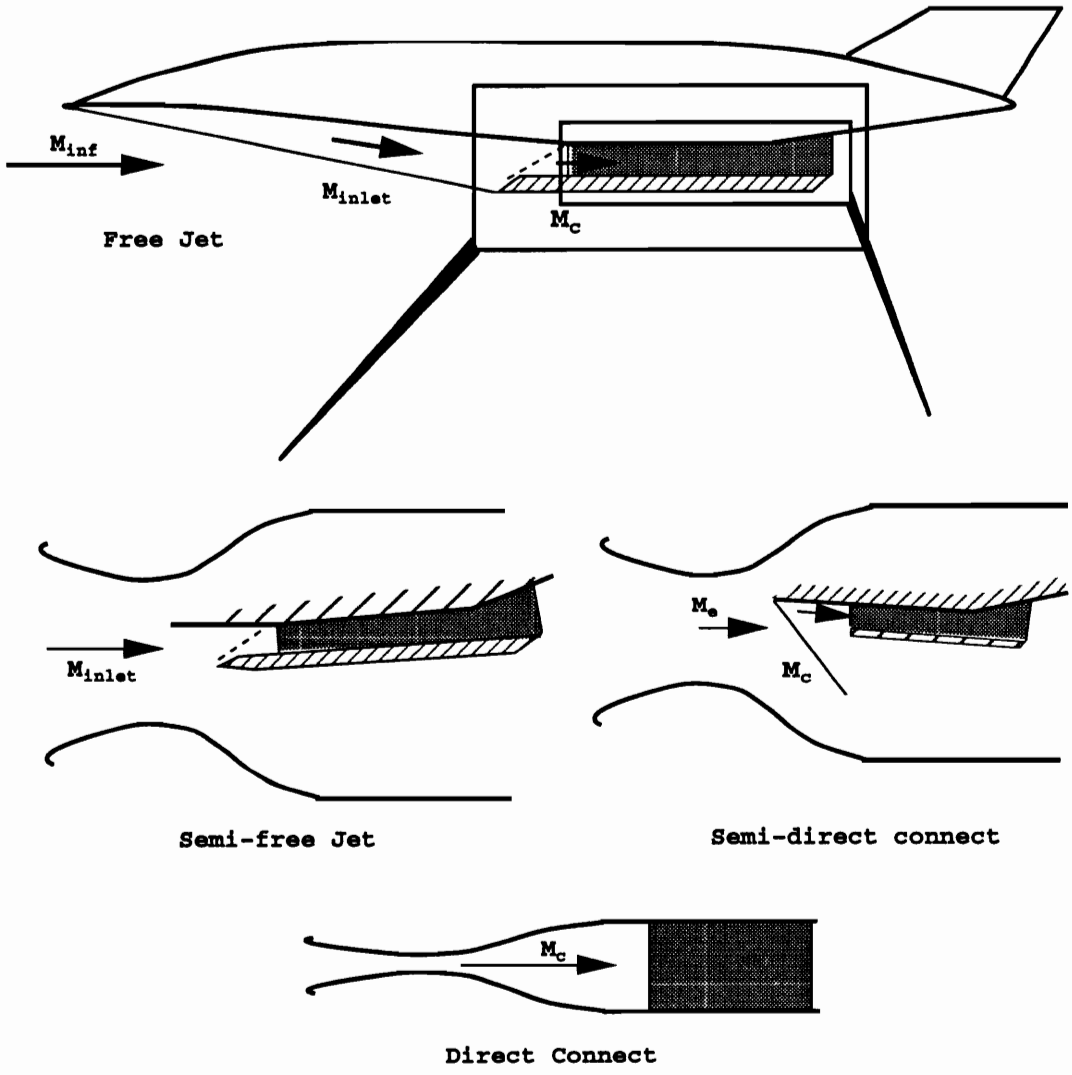

Figure 27: Ground Test Configurations

signals, so a baseline reading was always available if the gages drifted during the interim from when they were balanced.

The skin friction gages were hooked up to Measurements Group Model 2310 signal conditioning amplifiers. The excitation was 0.5 volts for all of the gages, but the gain varied from 1000 to 2000. The 10 kHz gages had a gain of 1000 while the gages with a lower sensitivity, the 14 kHz and 20 kHz, models had a gain of 2000. This served to balance out the sensitivities in Pascals per Volt of all of the gages, therefore the same voltage range could be specified for all of the skin friction gage channels on the data acquisition system. The Model 2310 units were provided by the facility, but cabling was different from that usually used with the skin friction gages. Male quick-disconnect connectors were soldered to the ends of the gage wires, and they were attached to female mates located inside the model. These wires were then sent down through a wiring bundle to a patch panel near the data acquisition room. From there, the Model 2310 was patched in using specially modified wires with BNC connector terminations on the 15-pin Bendix input on the rear of the 2310 unit. After conditioning, the output signal from the 2310 unit was connected via the patch panel to a different line and sent to the data acquisition room for sampling.

Although this arrangement added some difficulty, overall it was very successful and had some strong merits. First, some of the lines going into the patch panel were found to be noisy, so the skin friction gages were easily rerouted on other lines. Second, this arrangement allows for easy checks of bridge arm resistance, and it was also very easy to plug a shunt resistor into if necessary. Since the scramjet model was often sealed for multiple runs at a time, this arrangement allowed for a variety of external diagnostic checks to be run on the skin friction gage.

4.2 Experimental Results

Over 30 runs were made over a testing period that lasted more than half a year. During this testing time, three scramjet models were tested with different injector setups and geometries.

As mentioned before, this facility could simulate true Mach 12-14 enthalpy conditions with reservoir P_t and T_t of 32,405 kPa and 10000 R, respectively. The local combustor inlet Mach number was on the order of 5 or 6. Combustor inlet properties, which are not trivial to obtain for tests like these, were available for some of the runs conducted. However, in addition to being difficult to obtain, these numbers also require some sensitivity in their distribution. Therefore, wall shear values will be given for the runs rather than expressing the values in terms of the skin friction coefficient. It will be reported that for the inlet gage in Run 2066, the wall shear value of 1200 Pa corresponds to a inlet wall shear of 0.174 psi which produces a skin friction value of 0.0021.

Figure 28 presents a trace of wall shear versus time for a baseline gage mounted in the model inlet. The 2 millisecond averaging period beginning at 0.042 sec was reported by NASA Ames. The average measured wall shear during the averaging period was 1200 Pa. Since the scramjet inlet is essentially a flat plate, several skin friction correlations may be applied to this data. These will be further discussed in the next section. It should be noted that although the wall shear is not constant through the averaging period, the total pressure shows the same variation with time. This close tracking between $\tau_w(t)$ and $p_t(t)$ was seen in prior gage evaluation tests in a Ludwig tube [25] and throughout the testing series.

Figures 29-35 show combustor wall shear traces. The traces exhibit a lot of common traits. After the diaphragm is broken, there is approximately a 3 msec delay until the test gas reaches the model. After that, the test gas goes through for the next 2 msec. The averaging period for the tests was determined by measuring the flow with other transducers and was determined by NASA Ames personnel. The flow continues after the test gas passes through as the driver gases travel down the tunnel as well.

Figures 29 and 31 are measurements made using the 10 kHZ baseline gage as is Figure 30. It can be seen that the shear values vary during the test time. Considering the complex nature of the flow– a combusting gas with possible localized hot spots, injected gases, and flow going over rearward facing steps as it enters the combustor and injectors– it is not surprising that the shear values are not flat throughout the

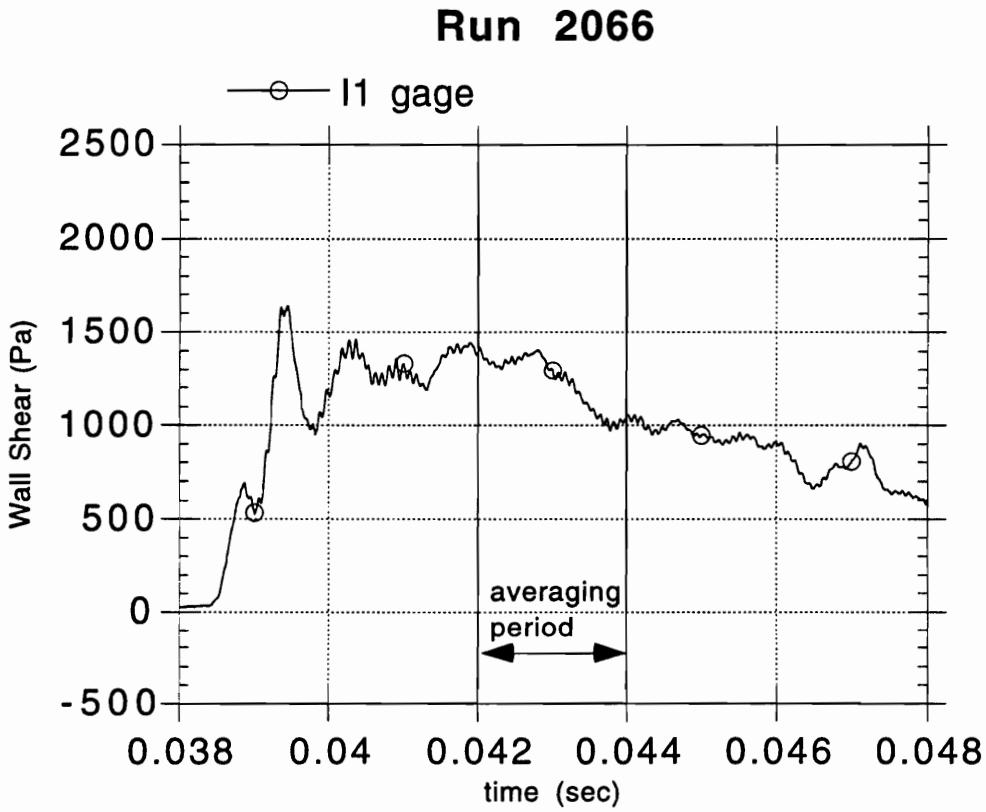

Figure 28: Inlet Gage Wall Shear versus Time- Run 2066 baseline gage

averaging period. Figure 32 used a 14 kHz gage in port 1 and a baseline gage in port 2. The close agreement between the two gages is evident in Figure 32; exact agreement should not be expected due to the complex nature of the flow and because one gage is on the centerline of the combustor and the other is off-center. A pair of baseline gages were run in the combustor in Figure 33. In this trace there is a larger difference between the two shear traces but this may be a real property of the flow. The C1 gage lies on the centerline of the combustor and may be seeing a higher shear value due to combusting flow, while the C2 gage, which lies off of the centerline, may see less of an increase in skin friction. Previous skin friction experiments [20] had shown large increases in measured values of skin friction in combustion experiments. Figure 34 also used a baseline gage, while Run 2091 (Figure 35) used a 14 kHz RTV-filled gage.

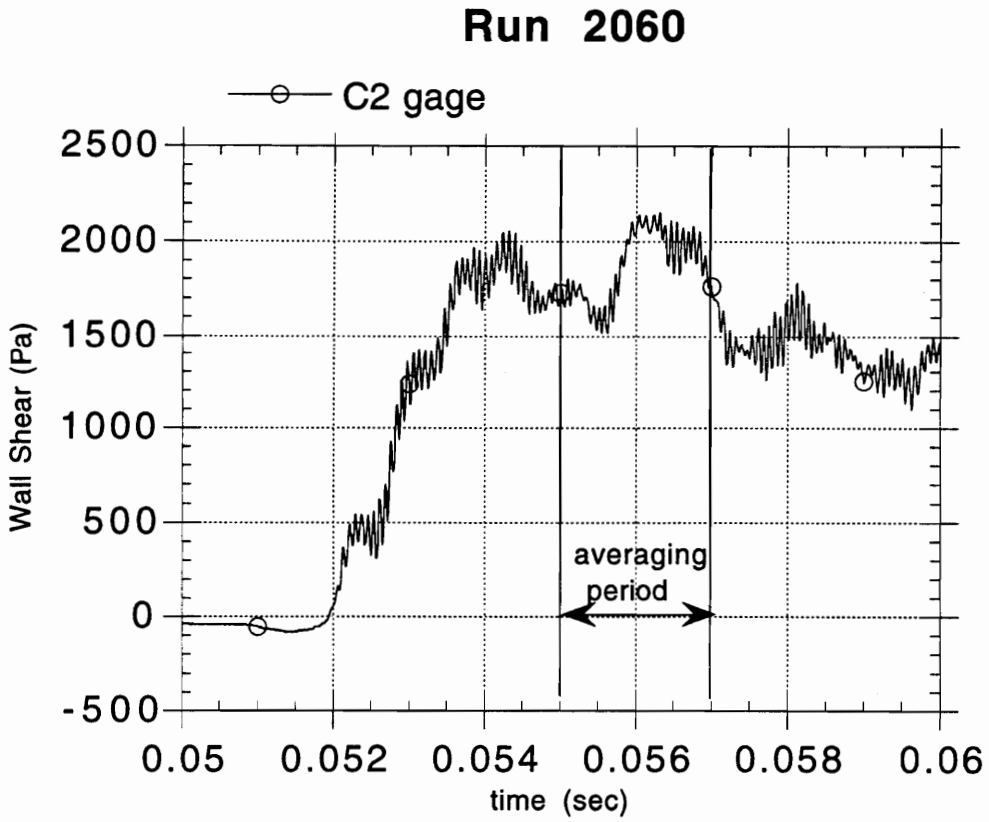

Figure 29: Combustor Gage Wall Shear versus Time- Run 2060 baseline gage

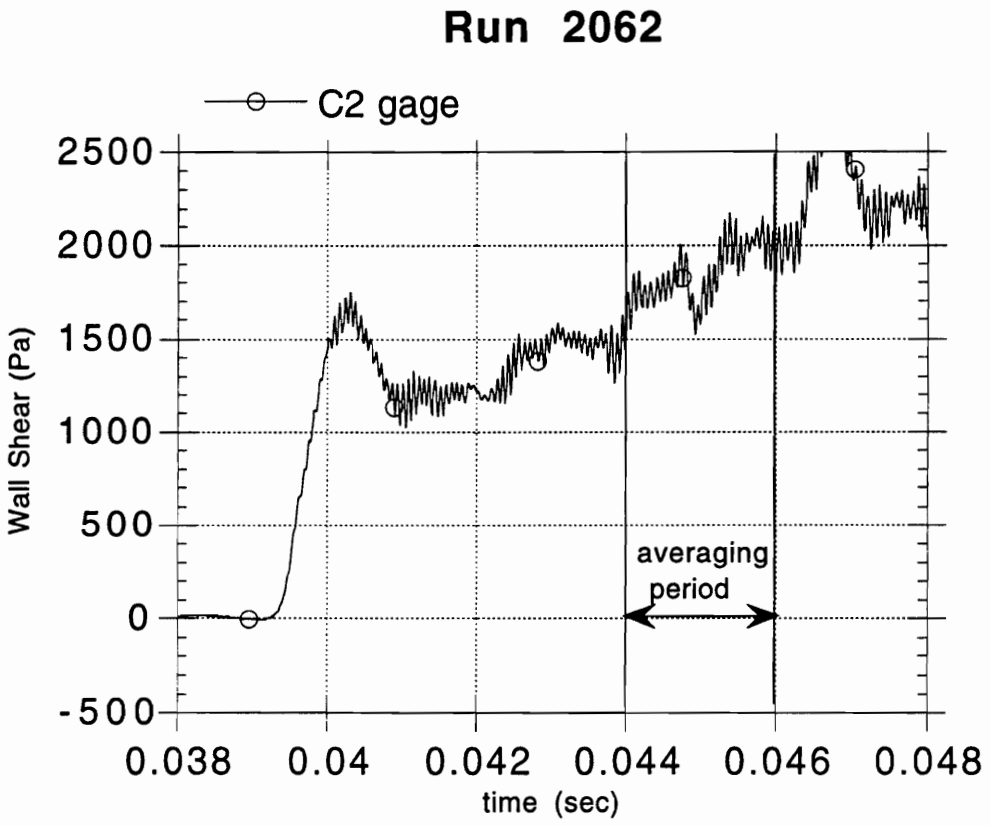

Figure 30: Combustor Gage Wall Shear versus Time- Run 2062 baseline gage

Table 4 summarizes the wall shear measurements gathered during the test series. The reported wall shear values are the averages over the 2 millisecond averaging period. The tests were run at various freestream conditions, and some tests used varying degrees of combustor film cooling. Due to the time and effort required to maintain the skin friction gages, most of the gages were placed in the combustor, where the flow is more complicated and not as well understood as in the inlet. The wall shear values reported in Table 4 represent only the longitudinal component of the wall shear, since these gages only have one set of strain gages. In cases for which the wall shear may have also had a transverse component, the values shown in Table 4 understate the magnitude of the total wall shear. Traces for runs not discussed above can be seen in Appendix section B.1 starting on page 129.

The baseline 10 kHz gage design performed very well throughout all of the tests.

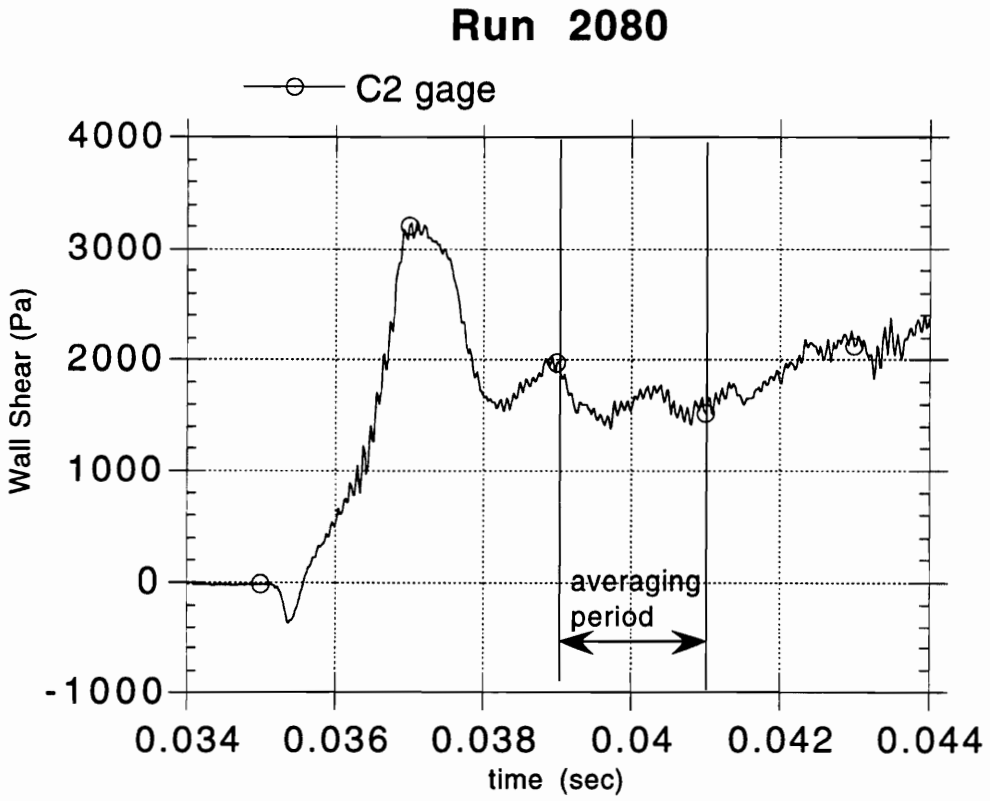

Figure 31: Combustor Gage Wall Shear versus Time- Run 2080 baseline gage

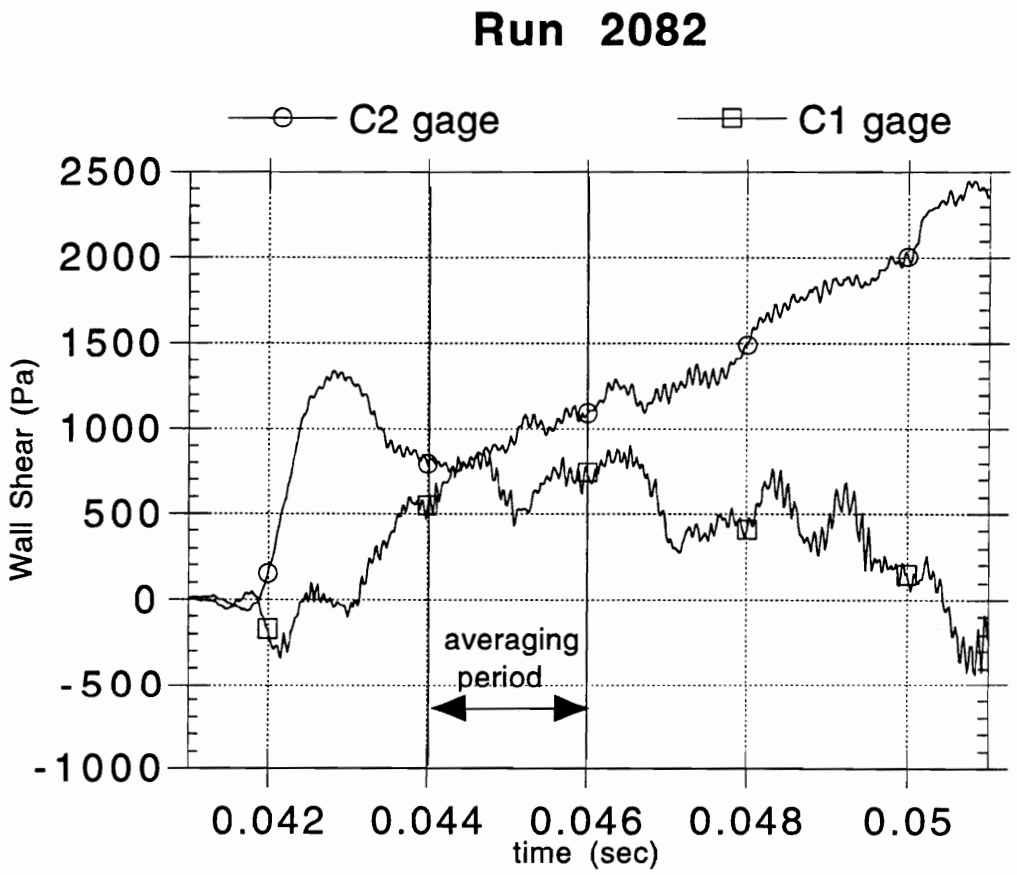

Figure 32: Combustor Gage Wall Shear versus Time- Run 2082 baseline and 14kHz gages

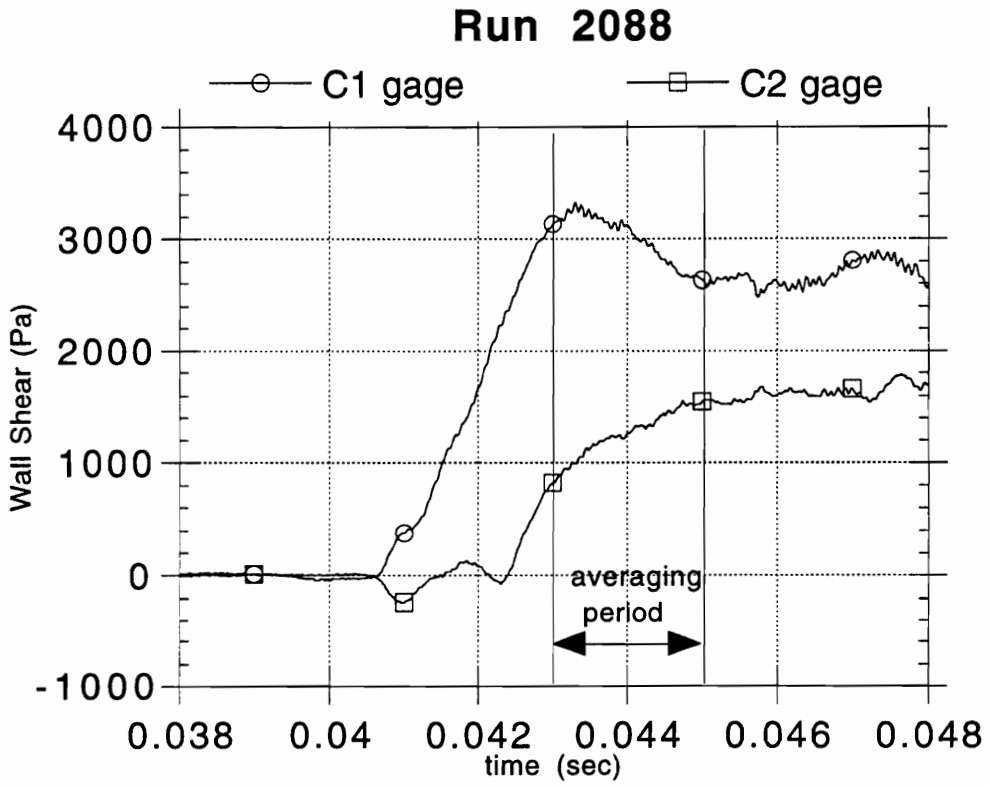

Figure 33: Combustor Gage Wall Shear versus Time- Run 2088 baseline gages

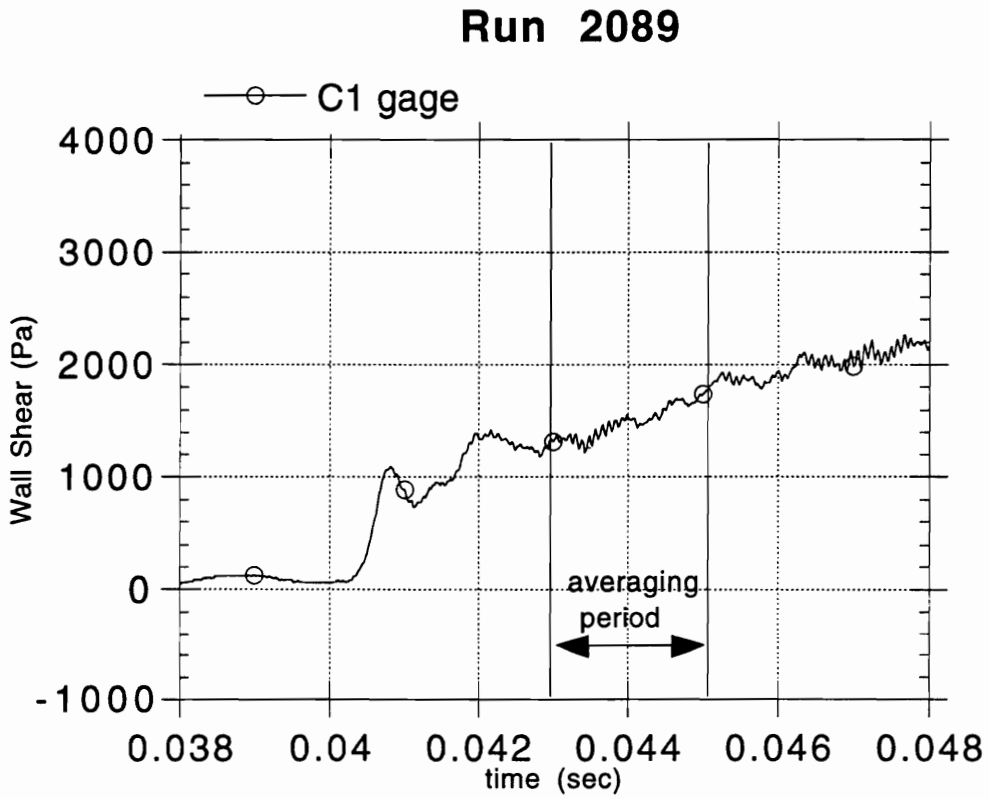

Figure 34: Combustor Gage Wall Shear versus Time- Run 2089 baseline gage

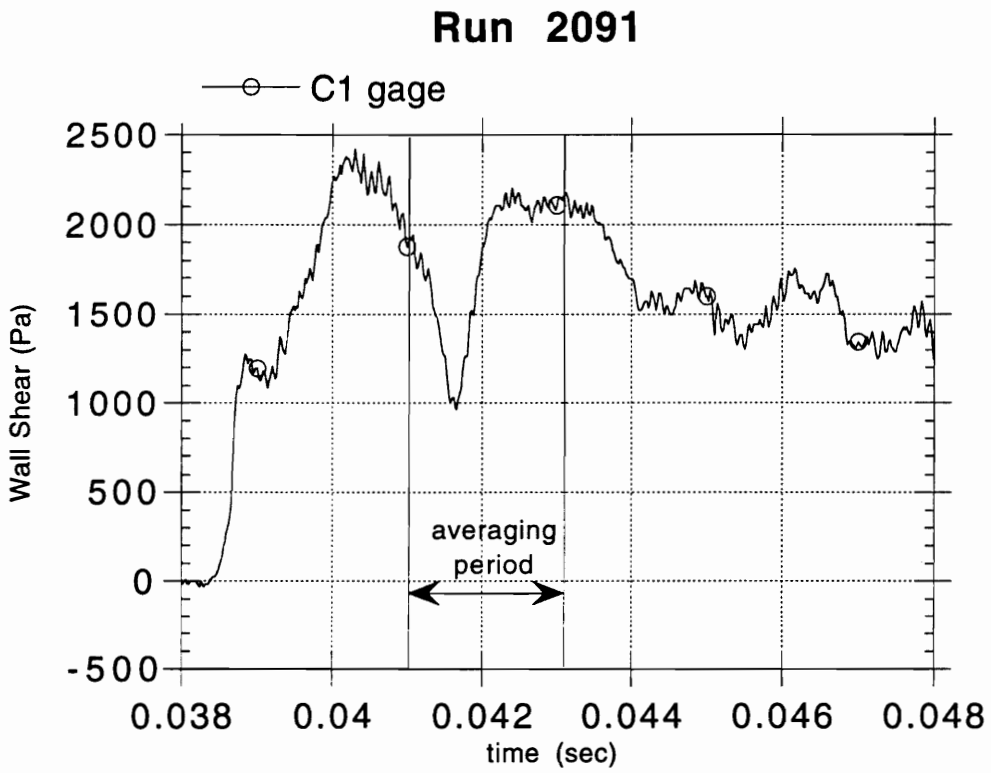

Figure 35: Combustor Gage Wall Shear versus Time- Run 2091 14kHz RTV gage

Table 4: Ames Wall Shear Results

Run Number and Gage Port	Wall Shear (Pa)	Standard Deviation
Run 2060 C2	1872	183
Run 2060 I2	1910	532
Run 2061 C2	1692	222
Run 2062 C2	1908	150
Run 2066 I1	1200	141
Run 2079 C2	2671	375
Run 2080 C2	1613	119
Run 2082 C1	688	103
Run 2082 C2	912	118
Run 2083 C2	1292	316
Run 2087 C1	205	195
Run 2088 C1	3036	316
Run 2088 C2	1694	199
Run 2089 C1	1423	138
Run 2089 C2	292	139
Run 2090 C1	2527	669
Run 2091 C1	1803	342
Run 2092 C1	372	102

Its time response was more than adequate for capturing data in the period of interest. Likewise, the 14 kHz gages yielded good data as well, but the silicon rubber in the annulus appeared to slow the time response somewhat. The 20 kHz gages appeared to be more questionable. Their shortened cantilever length made them more susceptible to thermal contamination and maintaining oil in the gage cavity became of paramount importance. Maintenance concerns as well as the decreased sensitivity of the 20 kHz gages combined with the excellent time response of the other gages, led to an abandonment of this design.

The most common gage failure was caused by thermal effects resulting from oil depletion. In this type of failure, both strain gages are exposed to circulating hot air in the oil cavity. The strain gage on the leading edge of the sensor heats more rapidly than the strain gage on the trailing edge, which causes a drastic increase in the voltage output. Repeated exposure to high temperatures results in either thermal setting of the strain gages or melting or other damage to the very thin lead wires.

The implementation of the sputtered coatings onto the gage and housing heads was very beneficial in lengthening gage life. Several gage surfaces were badly scarred and eroded by microparticles travelling down the tunnel at hypersonic velocities and also from the, although momentary, very high temperatures. These smooth coatings protected the gage heads from the harsh environment of the inlet ramp and combustor and had no impact on the gage response or sensitivity. It is the opinion of the author that an oxide coating should be used on any gage exposed to a harsh testing environment. It is rare that a modification results in benefits without drawbacks, but this is the apparent case with the sputtered coatings.

The use of silicon rubber compound in the gage cavity was not introduced until late into the testing series. The modification had mixed effects. The rubber had both low thermal conductivity and a high heat capacity so it too eliminated thermal effects. In addition, it was very rugged and survived many runs without an effect on its surface. However, it did decrease the gage sensitivity by about 30 percent. This was essentially mitigated by the increased sensing area of the rubber and plastic combination. Also, from the trace in Run 2091, the rubber may have slowed the gage response judging from the negative spike in the shear early in the averaging period.

However, this simply may have been a shock or other flow disturbance passing over the gage head. It was desired to have a 10 kHz RTV-filled gage to increase the sensitivity but there was not enough time to design, fabricate, and test such a unit.

4.3 Analysis and Correlation of Results

The inlet can be treated as a flat plate, and several skin friction correlations may be applied to the data. Correlations were applied to the inlet wall shear data of run 2066 by David Hazelton at the Air Force Institute of Technology [36] . The average measured wall shear for this run was 1200 Pa. Using the reported inlet freestream conditions for this run, the Van Driest II correlation [37] predicts a wall shear of 1606 Pa, the White and Cristoph method [38] predicts 1496 Pa, and the reference enthalpy method [39] predicts 1710 Pa. These results would appear to challenge the accuracy of the skin friction gage, however, as noted by Hopkins and Inouye [40] most skin friction correlations overestimate the wall shear for very cold walls as is the case here. The Spalding and Chi skin friction correlation [41], which has been shown to be more accurate for cold walls, provides and estimated skin friction of 1174 Pa for the Run 2066 conditions, which corresponds very favorably to the measured 1200 Pa.

After it was determined that the cantilever skin friction gage was providing reasonable results, an analysis of several potential sources of error was carried out to insure the results were not serendipitous. Among potential sources of error were: error due to normal pressure force on gage head due to decrease in p_{static} in the test section, error due to temperature mismatch between gage and model wall, and error due to a pressure gradient on the sensor head.

Normal pressure sensitivity as shown in Figure 36 was evaluated as a source of potential error [36]. The cantilever skin friction gage is designed to be insensitive to normal pressure. Insensitivity to normal pressure is desirable, because the magnitude of the force imposed by normal pressure is much greater than the force imposed by the wall shear. Provided that there is no pressure gradient across the surface of the sensor head, the normal pressure is hydrostatic in nature and is approximately the same all around the cantilever. For a solid core sensor, the strain imparted by this

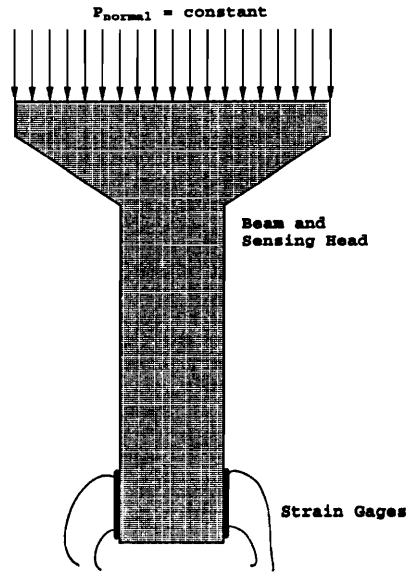

Figure 36: Normal Pressure on Gage Head

pressure is given by

$$\epsilon_{11} = \epsilon_{22} = \epsilon_{33} = -\frac{p}{3K} \tag{35}$$

where ϵ denotes the elements of the strain tensor, p is the pressure, and K is the bulk modulus [42]. The shear strains are zero. Thus, for a solid core cantilever, the strain is the same at all points on the cantilever, and whatever strain is imparted to one strain gage should be imparted to the other. Since the strain gages are used in a Wheatstone bridge arrangement, equal changes in resistance cancel, and any strain caused by normal pressure should not affect the voltage signal from the skin friction gage, even if the strain gages are misaligned.

For a hollow core cantilever, the interior and exterior pressure may differ, so shear strain may result from normal pressure. However, if the strain gages are properly aligned and the hole is concentric, the response to normal pressure is symmetric, so the change in resistance should be the same in both strain gages.

In order to verify the theoretically predicted normal pressure insensitivity, tests were conducted on both the solid and hollow core gages. A suction device was placed over the top of the skin friction gage. The pressure was reduced to near zero while the gage output was monitored. There was no discernable change in the voltage reading.

A valve was thrown, returning this pressure back to atmospheric, and again no change in voltage was noticed other than a brief and small (less than 50 Pa in magnitude) spike that was likely due to vibrations and/or the flow path as air returned into the vacuum chamber. Thus, normal pressure should not present a source of error as the gage output was shown both theoretically and experimentally to be unaffected by normal forces on the gage head.

The potential error due to a thermal mismatch on the sensing head was analyzed by David Hazelton [36] at the Air Force Institute of Technology. With a plastic sensor, the heat transferred from the flow is concentrated near the surface rather than being conducted into the interior of the material, as is the case with a metal model wall. This heat concentration near the surface of the sensor causes the sensor surface to increase in temperature more rapidly than the surrounding metal. This temperature mismatch between the gage and model causes the measured skin friction to differ from what it would otherwise be. The analysis predicted that the higher temperature of the sensor can potentially result in overestimation of the wall shear by 3.6 %.

Another potential source of error is error due to a pressure gradient on the sensor head. As shown in Figure 37, this would impart a bending moment to the cantilever and cause an imbalance in pressure on the sides of the beam, both of which would cause an apparent deflection of the beam toward the low pressure side. Since the head is small, it is not expected that the differences in pressure across the head of the gage would be significant, however a study was undertaken during the tests in the VPI Supersonic Tunnel to quantify the possible error caused by a pressure gradient. This will be further discussed in Section 6.3 on page 92.

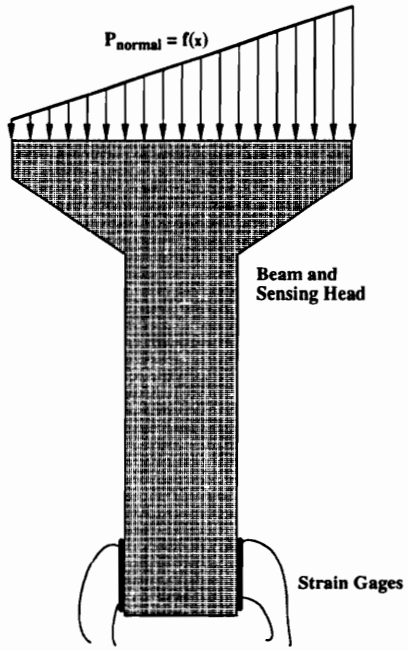

Figure 37: Pressure Gradient on Gage Head

Chapter 5

Skin Friction Tests at GASL

5.1 Description of Facility and Test Procedure

The HYPULSE facility is a 6 in. diameter, 115 ft. long expansion tube originally built by the NASA Langley Research Center in 1960 [43]. NASA Langley operated this facility from the 1960's until it was decomissioned in the 1983. NASA established, using air as a test gas, a 350 μsec steady flow testing condition at a total enthalpy which approximates a 5180 m/sec velocity about a stationary model. In 1987, GASL was awarded contracts to reactivate the facility and conduct supersonic mixing and combustion experiments. In March 1989, the first test was made and the facility is still active today.

The HYPULSE facility is an expansion tube,, and its performance is most easily described by the distance-time (x-t) diagram shown in the figure below. An expansion tube is physically similar to a shock tube with the addition of an acceleration tube onto the drive section which is separated from the other driven section, called the intermediate tube, by a secondary diaphragm. The driver is filled to high pressure, the intermediate tube is filled with the desired test gas to a generally subatmospheric pressure, and the acceleration tube is filled to an even lower pressure. The utilization of the expansion tube yields an increase in the flow enthalpy due to the shock heating (as in a reflected shock tube) and due to the unsteady expansion from states 2 to 5.

The flow is initiated by bursting the primary diaphragm which causes the primary

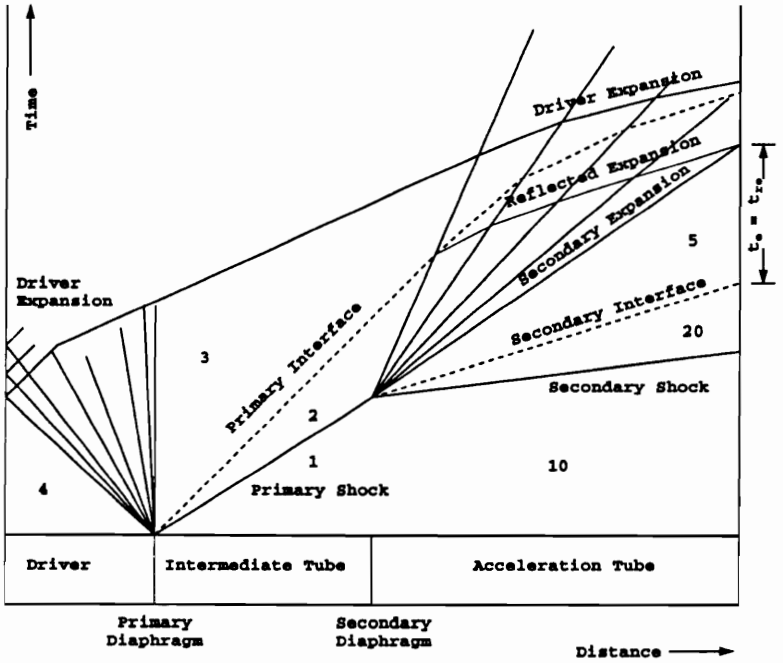

Figure 38: Expansion Tube x-t Diagram

shock wave to propagate down the intermediate tube yielding the flow in region 2. Upon striking and rupturing the secondary diaphragm, the primary shock acquires a higher Mach number as it enters the acceleration tube leading to the flow in region 20. To equilibrate the pressure and velocity from region 2 to 20, a system of unsteady expansion waves propagates into region 10 and accelerates the flow to the high velocity in region 5. The test section, which receives the test gas, is located at the exit of the acceleration tube. The test time is given by the period between the arrival of the acceleration gas/test gas interface and the first wave which interrupts the uniform test flow such as the secondary or reflected expansions. Ideally, both these expansions arrive at the same time as in the figure. The time is also potentially limited by the first reflection of the primary expansion off the driver end, however, in practice, this occurs later than t_e or t_{re}.

A perspective view of HYPULSE is given in Figure 39 [44]. The driver section is rated at 1360 atm, with an internal diameter of 16.5 cm and is 2.44 m long. The intermediate section has a rating of 680 atm for the first 2.5 m from the driver and

340 atm for the remainder. It has a 15.2 cm inner diameter and a total length of 7.44 m. The acceleration tube is similarly rated at 340 atm and is 14.14 m long However, the lengths of the intermediate and acceleration tubes are based upon the secondary diaphragm location which can be moved to any tube joint. The test section/dumptank has a maximum pressure rating of 10 atm, an inner diameter of 120 cm and is 10.5 m long. All tube sections are stainless steel forgings with a highly polished bore. The facility characteristics are further described in References [43] and [44].

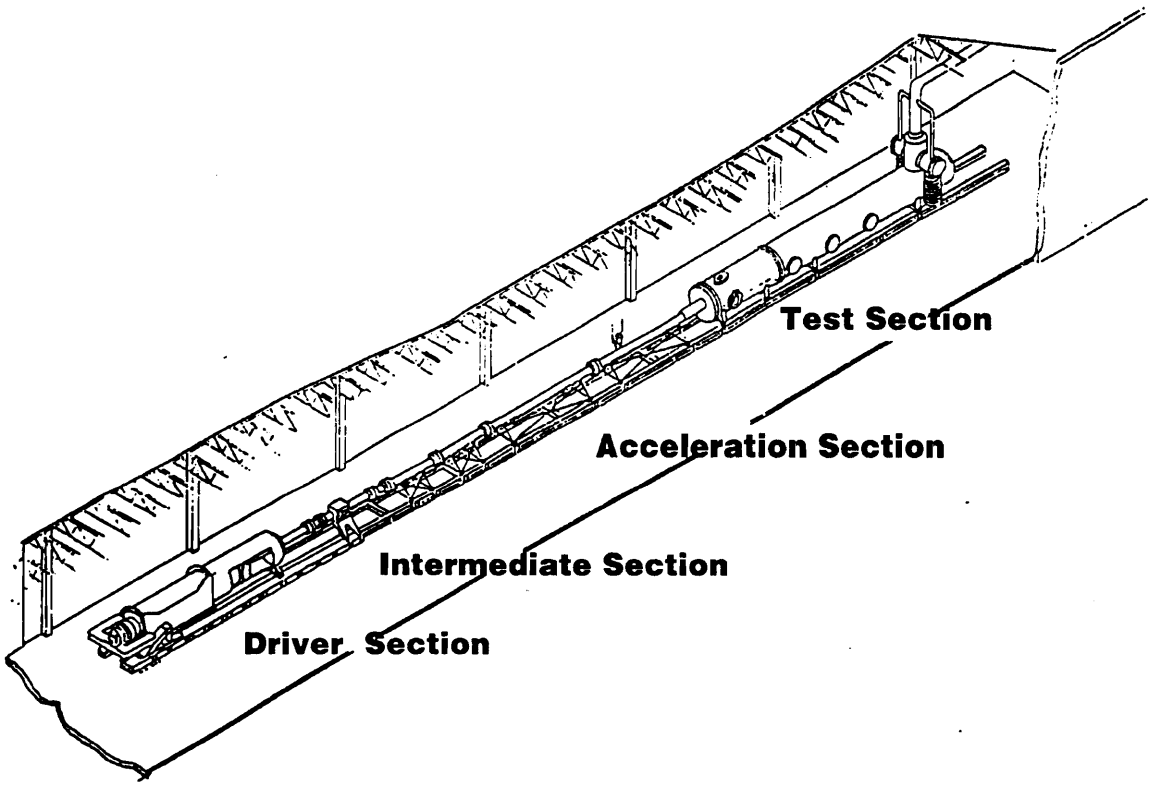

Figure 39: Perspective View of HYPULSE facility

The tunnel control system was designed by GASL. It consists of a system of manually and remotely-controlled interlocks for filling each of the tube sections with

the proper test gas. Facility and test flow data was acquired using 20 LeCroy 6810 4-channel transient wave form digitizers. Each channel can be sampled at up to 1 MHz, however data was taken at a rate of 500 kHz. Up to 512k samples can be taken per channel with 12-bit vertical resolution. Power for the digitizers is supplied by two LeCroy model 8025 high-power CAMAC crates. The system is controlled by an IBM-PC compatible, and data is taken using vendor supplied software ("Waveform CATALYST version 2.6"). For the second test series, the data acquisition system had been expanded to sample over 150 channels of data.

The test gas slug is on the order of 2 m in length and 10 cm in diameter. Accurate timing of the fuel injector system in the model is accomplished by use of a Ludwieg tube as the fuel supply. A fast acting valve, based on passage of the incident shock through the intermediate tube, controls the flow from the Ludwieg tube. By varying the test gas and pressures, a variety of facility operating points are available for testing [45].

5.2 First Test Entry Results and Analysis

The first testing phase occurred during August 1994. Two skin friction gages, one oil filled and one rubber filled, were brought to GASL in hopes of acquiring scramjet combustor wall shear data at the HYPULSE facility. As mentioned in the facility description, HYPULSE only has a test window of 350 μsec, so the response time of the gages was of critical importance. Therefore, prior to testing in HYPULSE, a series of checkout tests were carried out in the Mach 2 Instrumentation Shock Tube (IST) at GASL to verify the gages' high-frequency characteristics and calibration sensitivity.

The gages were both hooked up to Measurements Group Model 2310 Signal Conditioning Amplifiers which were then patched into the LeCroy data acquisition system. The gages were excited at 5 volts, and a gain of 800 was employed. Commonly, a 0.5 volt excitation is used to minimize thermal drift, but there were concerns about the low shear value to be measured in the IST, so the higher excitation was used. The decision was made to continue these excitation levels for testing in the HYPULSE rather than change the excitation and, therefore, possibly change the uncertainty in

the calibrations.

The IST tests confirmed the gages' 20 kHZ natural frequency (as shown by a FFT of the data) and ability to take data under the short test window, so the decision was made to test a pair of skin friction gages in the HYPULSE scramjet model during an upcoming test– one VPI skin friction gage and one University of Queensland piezoceramic gage as described in Chapter 1. The gages were located in the aft portion of the combustor, but still upstream relative to a laser flow imaging system, so the decision was made to go with a rubber-filled gage to prevent possible contamination of the flow by oil leakage.

Support personnel for either gage were not present during the testing phase so although several runs were made, often the skin friction data was not captured. However, data for both gages was obtained on HYPULSE run 850. The reported flow conditions for this run are tabulated below. The tunnel was operated at what is referred to as the M14HP (Mach 14, high pressure) condition for this test.

Table 5: GASL Run 850 Flow Conditions

Run Number	850
Test Gas	Air
Fuel Type	Cold
Test Window	7.08 to 7.48 msec
Equivalence Ratio	1.12
Pressure p_s	51.35 kPa
Velocity (m/sec)	3798

The wall shear trace for Run 850 can be seen in Figure 40 below. For this run, the measured wall shear stress over the averaging period was 6.05 kPa. The reported measured heat-transfer rate to the wall in the vicinity of the gage was 5.762 MW/m^2, the static pressure was roughly 138 kPa and the flow velocity was approximately 3800 m/sec. Assuming that the H_2 + air reaction goes to completion (i.e. η_c = 100 percent) for the equivalence ratio of 1.12, the following equilibrium properties were calculated: T = 2880 K and ρ = 0.1282 kg/m^3. Using a simple Reynolds Analogy, the computed C_f is .00251. From the skin friction gage wall shear measurement C_f is .00643. The GASL reported CFD solution [46] gives a C_f value of .0050 at

this location. While these numbers didn't match, the measured values certainly were judged reasonable, and the decision was made to conduct further scramjet skin friction tests at HYPULSE. Note, that skin friction values measured in long duration scramjet combustor tests have always come out higher than CFD or simple correlation predictions [19] [20].

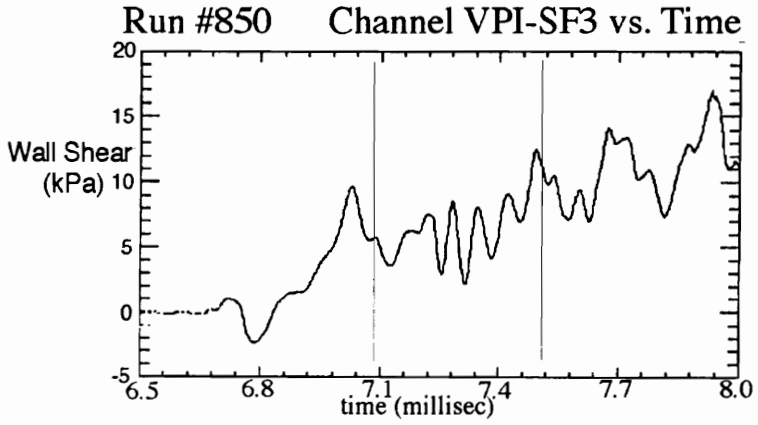

Figure 40: Combustor Wall Shear versus Time- Run 850

5.3 Second Test Entry Results and Analysis

The second series of HYPULSE skin friction tests were carried out in December 1995 and January 1996. For these tests, several gage ports were available for testing. Figure 41 shows that a total of 5 gage ports were available for instrumentation in the aft portion of the model at distances ranging from approximately 43 to 66.4 cm from the inlet section of the model. Note that the dimensions in this figure are in inches. Unfortunately, these ports were only available along the top of the model. (In the first test series the ports were in the sidewall). This meant that the gages would be in an inverted position as shown in Figure 42 so maintaining oil in the gaps was again a problem of paramount importance. It can also be seen that several heat flux sensors were tested in the upper surface of the model. The lower surface was instrumented with pressure taps only.

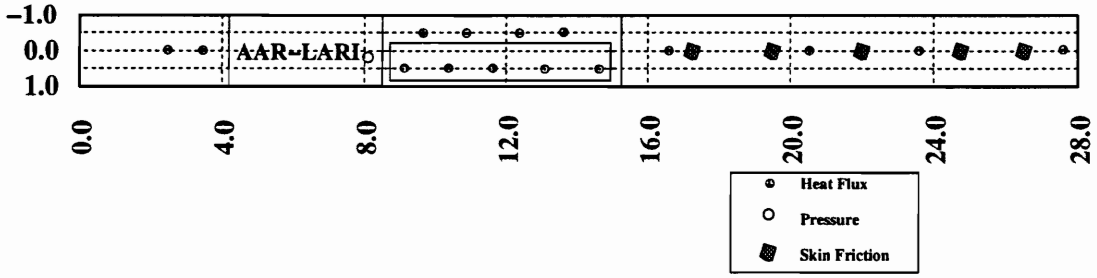

Figure 41: GASL Scramjet Model Instrumentation Port Locations

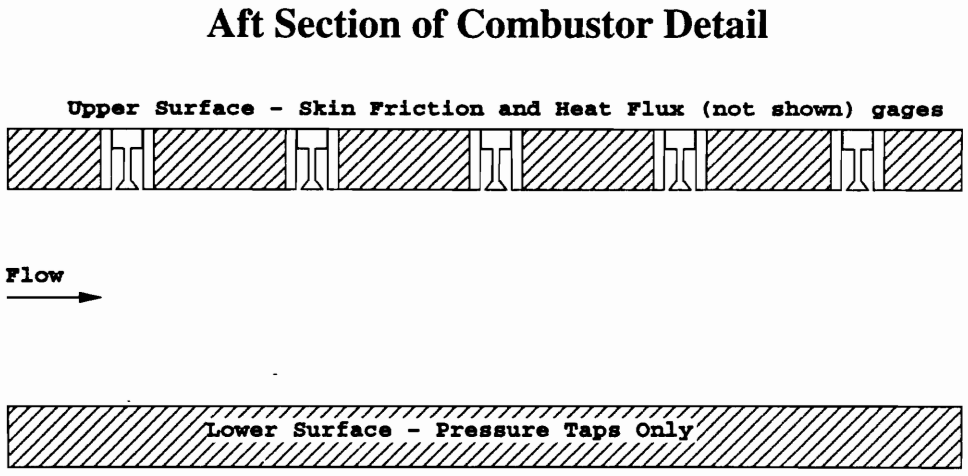

Figure 42: Cutaway view of Inverted Skin Friction Gages

Early on in the test series, it was found that the oil-filled gages were leaking. This was due to gravitational and vacuum forces drawing the oil out of the inverted gages. Due to concerns about oil dripping from the gages on the upper surface onto instrumentation on the model's lower surface, during the early runs only a pair of rubber-filled gages were used.

Later, a modified oil-filled gage with a smaller gap was developed for testing. In addition, a technique was developed by researchers at AFIT (Air Force Institute of Technology) which eliminated or sharply curtailed the oil leaking problem. So, oil-filled gages were installed during later runs.

The gages were hooked up to the Measurements Group Model 2310 signal conditioning amplifiers for excitation and amplification of the output signal. The excitation voltage was set to 0.5 Volts and the gain at 1000. The low-pass filters on the amplifiers were not used, as there was a potential for the filter to filter out the entire run.

Once again, HYPULSE was operated at the M14HP condition. The test window for runs at this condition is 400 μsec. However, this averaging period was truncated in runs A49-A51 by electrical interference from the Schlieren light source. This meant that only the first 200 μsec of data is usable. This is still adequate to obtain meaningful values.

The wall shear output for the tests are presented in the table below. The port CF1U data from runs A35, A36, and A37 was acquired with an 11kHz rubber-filled gage. The output from this gage was reduced by a factor of two corresponding to the effecting sensing head parameter for this particular gage design. Both data ports from tests A49 through A53 contained oil-filled 11 kHz gages. No gages were replaced during the test phase nor were any reoiled or otherwise removed at any time during testing. The gage ports correspond to the following axial locations in the combustor model: CF1U is approximately 17 inches downstream, CF4U approximately 24 inches, and CF5U approximately 27 inches.

GASL also reported a prior CFD analysis performed by the Hypersonics Numerical Applications Group (HNAG) at NASA Langley for this injector configuration at roughly the same combustor equivalence ratio. SHIP [47], a 3D, PNS marching

Table 6: GASL Skin Friction Data Summary

Run Number	Run Type	Gage Port	Average Shear Stress (Pa)
A35	Combustion	CF1U	2845
A36	Mixing	CF1U	775
A37	Air Tare	CF1U	1690
A49	Combustion	CF1U	1240
A49	Combustion	CF5U	2960
A50	Mixing	CF1U	1630
A50	Mixing	CF5U	790
A51	Air Tare	CF1U	2300
A51	Air Tare	CF5U	1040
A52	N2 Tare	CF1U	1870
A53	N2 Tare	CF5U	1420

code used to model fuel injection into supersonic flowfields, predicted wall shear in the aft end of the duct between 2100 and 2700 Pa for the cold fuel combustion case. Computed values for the mixing and tare cases were not reported although one would assume they would be less than the combustion case.

For the combustion tests (A35 and A49), the skin friction gages seem to yield values slightly higher than the CFD prediction. The output of the gage in port CF1U of run A49 is neglected. Considering that the measured average wall shear from this test is less than that of all the of mixing and tare data from the same skin friction gage, this is not an extreme assumption. It is believed that something unusual may have occurred in the flow at this location leading to the reduced wall shear value. From the rubber-filled gage and the oil-filled gage in port CF5U it can be seen that an uncombusted fuel/air mixture led to a reduction in wall shear to roughly 27 percent of the combustion values.

For the tests with the rubber-filled gage, the gage seems to track well with the reported heat flux in the vicinity of the gage. For combustion run A35, the measured wall shear was 2845 Pa while the local heat flux was around 3 Btu/sec/in^2. For the mixing run, A36, the measured wall shear was 775 Pa and the local heat flux was around 1 Btu/sec/in^2. For the air tare run, A37, the measured heat flux was approximately 1.5 Btu/sec/in^2 with a measured wall shear of 1690 Pa. While this

sample size is too small to develop any relationship between the heat flux and the wall shear, they do seem to mirror one another in these tests.

Some typical traces from the data are shown below. Figure 43 shows a rubber-filled gage in combustion tests. Figure 44 shows an oil-filled gage of the same design in a nitrogen gas tare run with no fuel injection or combustion.

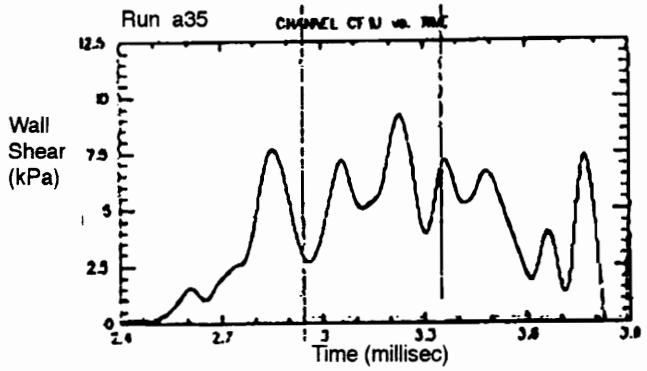

Figure 43: Wall Shear versus Time- GASL Run A35

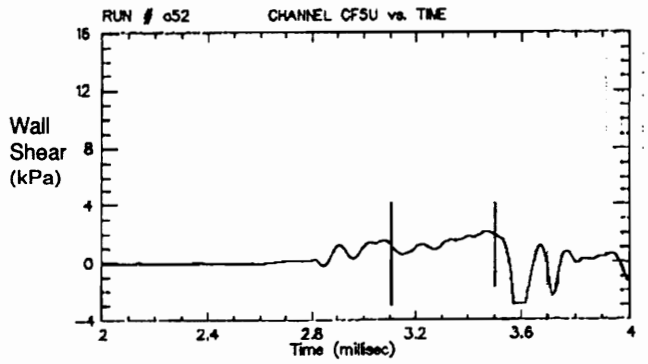

Figure 44: Wall Shear versus Time- GASL Run A52

Somewhat surprising was the large oscillations on the signal from the rubber-filled gage. One might expect that the rubber gage would serve to damp out any vibrations due to the presence of the rubber. Instead, the oil-filled gage showed less vibrational tendencies. This may be in due in part that the plastic is a viscoelastic material which can absorb a great deal of vibrational energy. Nonetheless, it is somewhat

counter-intuitive to see the rubber-filled gage have less damping than the oil-filled gage.

Shown in Figure 45, is another interesting development regarding the pressure sensitivity of the skin friction gage. The gage presented here is an Air Force Institute of Technology fabricated model. The top trace corresponds to the static pressure on the lower wall and the bottom trace to the skin friction gage signal. It can be seen that as a shock travels down the model and causes a spike in static pressure (at approximately 3.35 msec into the run), the gage responds to this flow disturbance as well. The spike is nearly four times larger than the regular output signal which causes a contamination of the wall shear trace. However, while it is now difficult to get a quantitative value for the wall shear due to the large spike in the wall shear data, the gage is definitely responding to a real property of the flow.

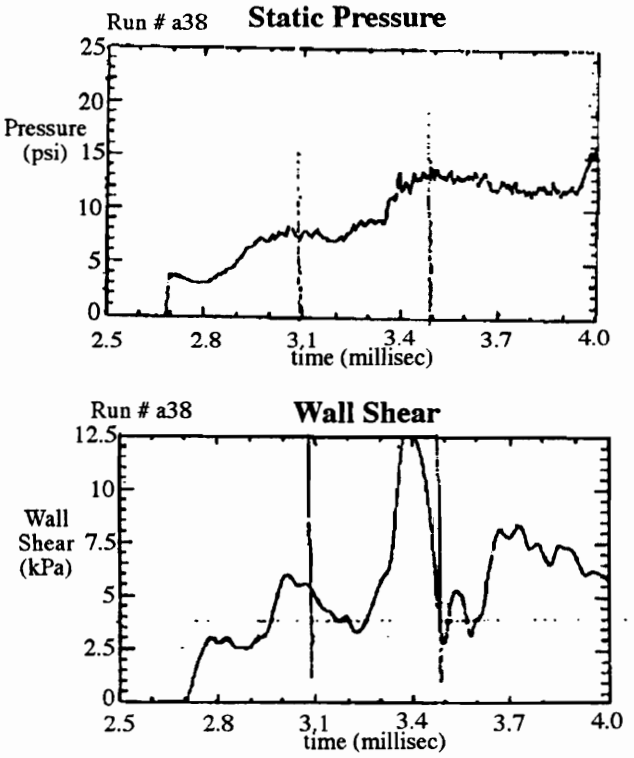

Figure 45: Spike in Gage Signal as a Response to Passing Shock

Overall, reasonable data was obtained in the second GASL test series. Agreement

between the skin friction gage and heat flux sensors was seen in runs A35-A37. Runs A49-A52 showed that the results are similar for the oil-filled and rubber-filled gages with the primary difference being a large 7 kHz oscillation on the signal of the rubber-filled gage. The response time of the gages was adequate even for the very brief test time of the HYPULSE facility. Future refinements for testing at HYPULSE would involve improving gage ruggedness and reducing any maintenance requirements. It is possible to acquire data in this facility, but support requirements make it difficult to acquire a great deal of data without a specialist on hand to tend the gages.

Chapter 6

Skin Friction Tests at Virginia Tech

A series of tests was conducted in the Virginia Tech Supersonic Tunnel. The tests were carried out at a Mach number of 2.4 and were designed to provide cold flow validation of the gage design and impulse facility results as well as an opportunity to analyze the effects of a severe pressure gradient on the sensing head.

6.1 Description of Facility and Test Procedure

A series of skin friction measurements was made in the supersonic wind tunnel at Virginia Tech. The facility is a blow-down type wind tunnel, meaning that high pressure air is stored in holding tanks upstream of the nozzle, blown down through the supersonic tunnel and then through a diffuser after which it is exhausted to the atmosphere. There are two high pressure air storage tanks with a holding capacity of 23 cubic meters. These tanks are charged by a four-stage reciprocating air compressor (Ingersoll-Rand Type HHE) which is driven by a 480 volt, 500 horsepower electric motor (Marathon Electric Company). The compressor can load the tanks to a pressure of over 40 atm.

The facility layout can be seen in Figure 46. The tunnel has various two-dimensional nozzles which can be interchanged to produce Mach 2.4, 3.0, and 4.0 flow. The Mach

2.4 nozzle was used for all of these tests. The settling chamber contains a perforated cone and several screens for flow dampening. The plenum flow conditions are reported by a pressure probe and transducer and a Type-K thermocouple.

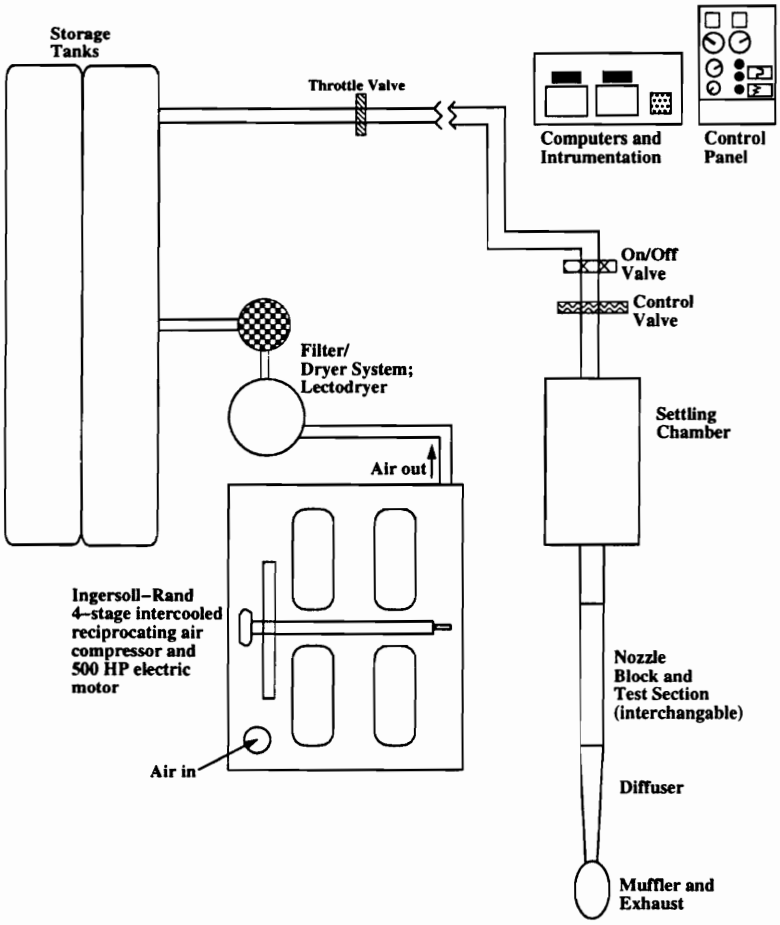

Figure 46: Virginia Tech Supersonic Tunnel Schematic

The tunnel operating and control system includes a fast-acting butterfly valve and a 30 cm diameter hydraulically actuated servo-valve for the purpose of pressure regulation. The valve is controlled by a Moog servo-amplifier with feedback from the settling chamber pressure transducer. Tunnel operation requires specifying several variables to the control system.

The tunnel operator will specify to a computer program the desired plenum pressure and run time. In addition, the user must fix the initial valve opening position

and threshold for tunnel control. The servo control system will not take over tunnel control until that threshold is met. The initial valve opening and tank pressure must be selected so that the threshold value is obtained without too large a starting spike in the plenum pressure.

The test section has a interchangeable floor piece so that various types of instrumentation can be installed in the test section. There is a provision for a sting mount on a gear and ratchet system so that models or wedges can be placed into the flow. The test section also has large doors on the side with Schlieren-quality glass for good model accessibility.

A mean flow rake is employed to obtain flow qualities through the boundary layer and in the inviscid region. The components of the rake are described in Pope [48]. It consists of a Pitot pressure probe, a cone static probe, and a vented total temperature probe. This probe was connected to a traverse so that it can be used in the boundary layer and the freestream. From examination of total pressure profile, the boundary layer thickness, δ, can be computed. From examination of total and static pressure and the total temperature and use of relations such as the Rayleigh-Pitot formula and the Taylor-McColl differential equation governing flow over an axisymmetric cone, virtually all flow conditions can be computed.

Data was acquired using an IBM PC compatible 486 computer. This computer was fitted with a pair of Metrabyte DAS-20 A/D D/A cards. The first card, at base address 300 Hex, was connected via a screw terminal adaptor to a box that allowed for the sampling of 8 differential inputs via BNC connectors. This first card was used to acquire the pressure and wall shear data. The second card, at 310 Hex, was connected to a Metrabyte EXP-16 multiplexer. This board has 16 multiplexed channels with an electronic ice point and instrumentation amplifier on the card. The second card was used to sample the temperature data.

The commercial software package, LABTECH NOTEBOOK, was used to control the DAS-20 data acquisition cards. This software has curve fits for the thermocouple data as well as allows for selectable gains to insure optimal digital resolution on each channel. It also allows for a variety of algebraic and trigonometric manipulations to be applied to the data. For these tests, the data acquisition system was manually

triggered with an acquisition period of 17 seconds at 100 Hz. Two data files were written for each test series– one with the raw outputs from the transducers and one with the calibration constants applied. In the pressure gradient tests, a 7 point moving average was applied to the skin friction data to smooth the signal.

The gages were again hooked up to signal conditioning amplifiers (Measurements Group Model 2310). The excitation voltage was 0.5 V to minimize thermal drift, and a gain of 1000 was used. The low pass filter was not used. The static pressure transducer was hooked up to the Ectron Model 515-5SG Excitation Supply and Model 562 Differential DC Amplifier with an excitation of 5 Volts and a gain of 200. The output from the Ectron amplifier was then patched into the data acquisition system. The plenum pressure transducer has its own self-contained excitation and amplification system. Both transducers were calibrated prior to testing and these calibrations were in agreement with previously obtained calibration values.

The upstream total pressure is given by the plenum pressure transducer and the wall shear is given by the skin friction gage. For a perfect gas,

$$q = \frac{\gamma}{2} p_\infty M_\infty^2 = \frac{\gamma}{2} \left\{ \frac{p_t}{(1 + \frac{\gamma-1}{2} M_\infty^2)^{\frac{\gamma}{\gamma-1}}} \right\} M_\infty^2 \tag{36}$$

with gamma (for a diatomic perfect gas = 1.4), M_∞, and p_t known, the local dynamic presure can be found. The skin friction, C_f, is simply computed from

$$C_f = \frac{\tau_w}{q} \tag{37}$$

The plenum pressure varies quite a bit over the test period. A typical run may show a spike up to 5.4 atm and then a slow decline from 4.4 to 4.1 or 3.8 atm during the rest of the test phase. For this reason, p_t data is taken over the entire run, and C_f is expressed as $C_f(t) = \frac{\tau_w(t)}{q(t)}$. The skin friction remains roughly constant as τ_w tends to follow q.

For the skin friction tests, a new tunnel floor piece was constructed. This piece allowed for up to four gages to be tested at once. As shown in Figure 47, the gage ports were positioned so that side-by-side comparisons of gage designs could be performed by putting one design in the even numbered ports and another design in the odd numbered ports. Ports 1 and 2 were at the same axial location nominally 5.715 cm

aft of the start of the floor piece, and ports 3 and 4 were nominally 20.96 cm behind the start of the floor piece. In addition, port 3 was directly behind port 1 and likewise port 4 was directly behind port 2. With this arrangement, a disturbance can be placed between the two axial locations and the effect of that disturbance on each of the gage designs can be examined.

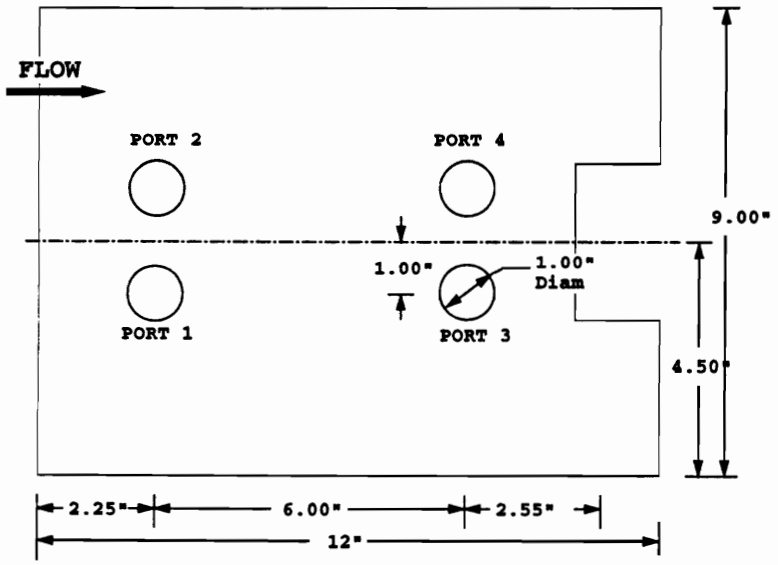

Figure 47: SST Gage Port Layout

6.2 Cold Flow Results and Analysis

A series of pre-test checkout runs were first run to insure that the gages were functioning properly in the longer testing environment. Next, a series of cold flow tests were run to generate data and compare to skin friction correlations.

These tests were conducted at Mach 2.4 with a total pressure, set in the tunnel control program, of 6.12 atm, and a total temperature of 285K and Reynolds number per meter of $4x10^7$. Output from several of these runs is shown in Table 7. This table specifies the run number, the gage identifier number, gage port corresponding to Figure 47, and the measured skin friction. The gage identifier consists of 2 values– the gage series letter followed by a number indicating which individual gage it was in

that series. The D and E series were both 10 kHz models with the D series being 10 kHz gages with the rubber gap sized by the gelim program. The B series of gages were the 3.6 kHz gages which were optimized for use in the supersonic tunnel. The gelim program was used to size the gap in all of the rubber-filled B series gages as well. Gages with an "r" at the end of their identifier indicate a rubber-filled model. For the gages optimized for the supersonic tunnel (a 3.6 kHz design), the averaging period was determined by the start and unstart of the supersonic tunnel. The 3.6 kHz gage had geometric properties that increased its strain under the low shear force present in the supersonic tunnel. The primary modifications were increasing the area of the sensing head by nearly 40% and lengthening by 45%. This new geometry results in over a 2.5-fold increase in strain produced by an equivalent shear force and also serves to keep the strain gages farther back from the thermal gradient, now a cold gradient from the expanded flow rather than a heat gradient of the combusting flow, present in these much longer duration tests. The increased strain generated per Pascal of wall shear force was required to accurately measure the low values of wall shear present in the supersonic tunnel. For the other designs, such as the "baseline" 10 kHz model, the averaging period was shortened by thermal contamination of the gage signal as measured by the modified gages with thermocouples in them. Using a gage's known calibration and the measured dynamic pressure, the skin friction value is calculated by taking the average during the test window. Again, the skin friction values here only represent the longitudinal component which should be the only component of wall shear in the supersonic tunnel for this nominally two-dimensional flow. If there was a small transverse component, the magnitude of the total skin friction would be slightly underpredicted.

A calculation of the skin friction coefficient based on the boundary layer thickness at the balance location indicates a skin friction coefficient of $C_f = 0.0017$ [19]. This is done by first finding the boundary layer thickness using pressure data. A shadowgraph could also have been used. Then, the empirical Schultz-Grunow [4] relation for the skin friction coefficient in wall-bounded incompressible turbulent boundary layers

$$C_f = 0.0456(Re_\delta)^{-0.25} \tag{38}$$

Table 7: SST Cold Flow Correlation Data

Run Number	Gage Identifier	Gage Port	Cf
96	D1r	1	.002141
98	D1r	1	.001755
99	E1	3	.001895
101	D1r	3	.001502
102	D1r	3	.001970
106	B1	1	.001795
107	B1	1	.001854
108	B1	1	.001857
108	B2r	2	.001648
109	B1	1	.001848
109	B2r	2	.001664
111	B3	2	.001640
112	B3	2	.001459
113	B3	2	.001536
114	B1	3	.001799
115	B1	3	.002022
116	E1	2	.001997
121	B1	2	.001400
122	B1	2	.001765
124	B1	1	.001682
126	B1	1	.001707
126	B3	2	.001741
127	B1	1	.001759
127	B3	2	.001672
128	B1	1	.001933
128	B3	2	.001659

is used to get an initial estimate of the skin friction. This is valid up to approximately $Re_x = 10^7$. The flow of interest is a compressible flow, so this incompressible estimate is improved with the incompressible to compressible relation of Van Driest. This comparison for a given Reynolds number is based upon experimental data and calculations [19].

The figures below show some typical supersonic tunnel skin friction traces. Notice that p_t is a function of time throughout each of the runs as it decreases slowly after an initial startup spike and that the p_t is not the same from run to run. Figure 48 shows an oil-filled 3.6 kHz gage located in the port 1. Figures 49 and 50 show a pair of 3.6 kHz gages located in the front ports at the same axial location. Gage B1 is an oil-filled model while B2 is a rubber-filled gage. The results are similar. Figure 51 shows another oil-filled 3.6 kHz gage, this time in port 2. The trace for this gage is excellent; very flat throughout the entire test time. Again, traces for runs not discussed in detail here can be seen in Appendix section B.2 starting on page 133.

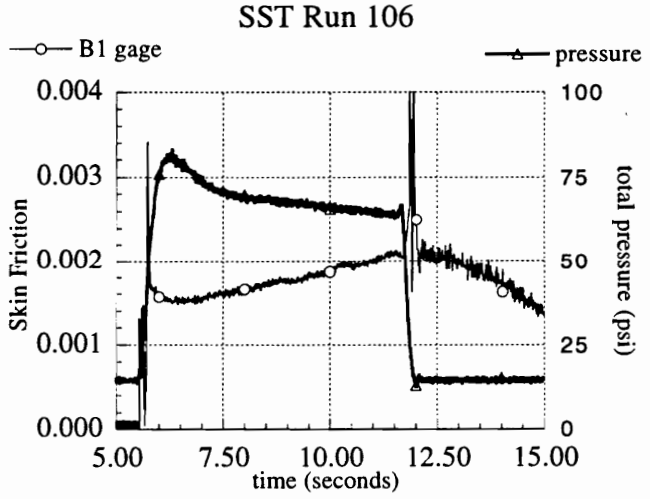

Figure 48: SST Cold Flow Test- Run 106

Figure 52 shows a characteristic temperature and plenum pressure versus time trace. It can be seen that the temperature remains constant throughout (and after) the tunnel test. The nominal 1.5 K variation in the output is due to the digital resolution of the thermocouple and amplifier combination. No change in the temperature at the beam base was seen in any of the runs in which that data was taken.

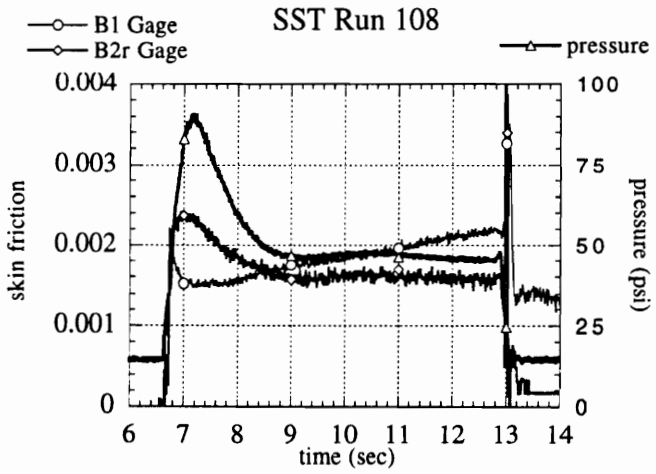

Figure 49: SST Cold Flow Test- Run 108

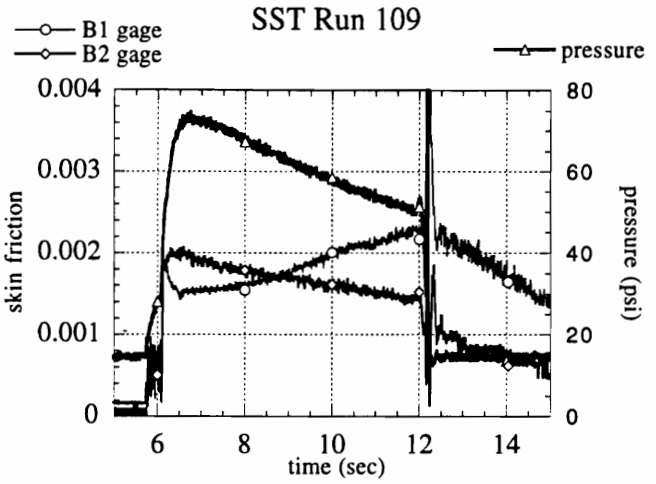

Figure 50: SST Cold Flow Test- Run 109

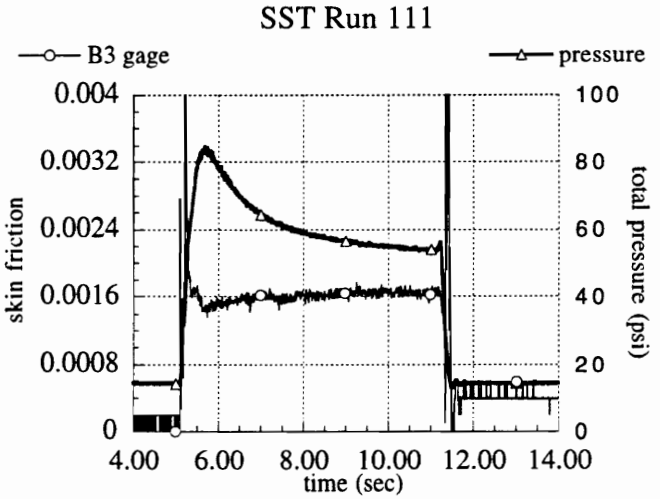

Figure 51: SST Cold Flow Test- Run 111

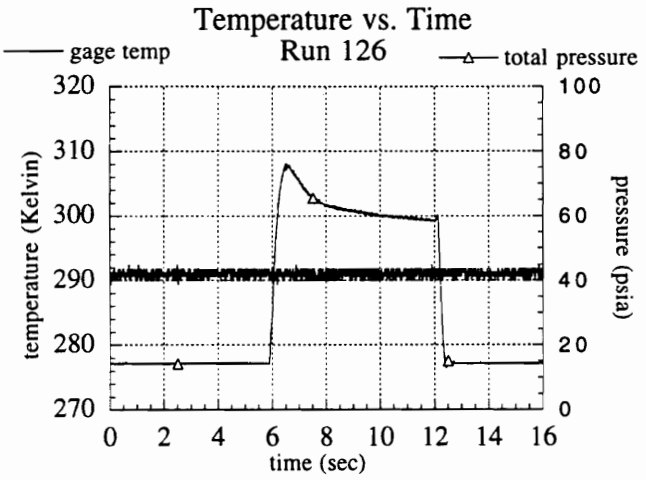

Figure 52: SST Cold Flow Temperature vs. Time

The primary sources of error in these tests were both the low shear magnitude and thermal contamination of the output signal. Both of these sources of error would impact the 10 kHz gage design much more than the 3.6 kHz design.

The low shear magnitude would be a problem for these gages due to a low amount of microstrain generated at the base of the beam. Assuming an upstream total pressure of 75 psi, the Mach 2.4 flow, and a skin friction coefficient of .0017, the local wall shear is approximately 0.03 psi or 200 Pascals. This low shear value diminishes the resolution of the skin friction value and makes the value more susceptible to other sources of error.

In addition, for gages within the same design class, the gages with the higher shear sensitivity performed better on average (i.e., if there were two gages of similar design, one with a sensitivity of 600 Pa/volt and the other of 1000 Pa/volt, the one with the sensitivity of 600 Pa/volt would often give better data). This is simply a result of the greater resolution of the higher sensitivity gage. This allows a gage to more accurately measure the small shear force. This result was seen throughout all test series.

The 10 kHz gages are also more susceptible to thermal contamination because their beam length is only two-thirds of that of the 3.6 kHZ gage. So a temperature gradient travelling down the beam has a shorter distance to travel before reaching the strain gages. By using temperature data, the test window could be conservatively estimated to prevent using thermally contaminated data in the averaging period. Thermal contamination was seldom a problem; generally it only affected gages which had been in for several runs and suffered from nearly complete oil depletion in the gap.

6.3 Shock Pressure Gradient Tests

A shock-induced pressure gradient test was devised to measure the effect of a strong pressure gradient on the sensing head. As can be seen in Figure 53, a 6° half-angle wedge was inserted in the flow to create a shock. For an inviscid compressible flow, this would result in a $\frac{p_3}{p_1}$ of 2.03, yielding a doubling in the static pressure on the

gage head but still leaving the boundary layer attached [4]. By placing this shock impingement in the center of the gage head, the effect of a pressure differential on the gage could be seen.

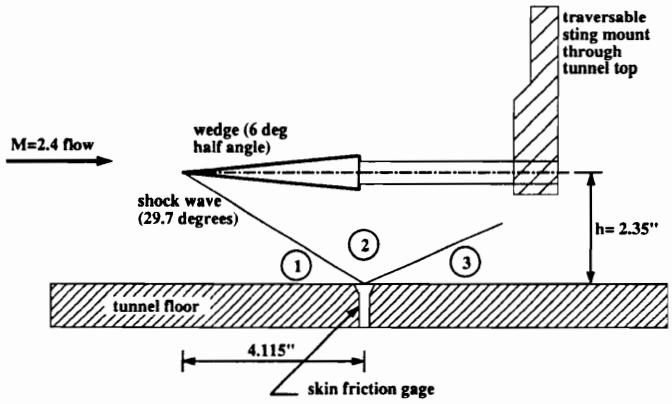

Figure 53: Shock/Boundary Layer Setup

In addition, a simple beam analysis can be carried out to determine the effect of the pressure differential. Recall, it was shown that the resulting strain at the base of the beam due to the wall shear was

$$\varepsilon = \frac{PLd}{2EI} \tag{39}$$

with P being the shear force. The effect of the pressure difference can be seen in Figure 54 below.

There will be two pressures acting on the sensing head; a p_1, in front of the shock and p_2 behind it if one assumes an ideal shock. Integrating these normal pressures over the sensing head will yield a resultant force acting on the sensing head. Assuming that the strain gages are not next to the force application, this force can then be replaced with the same force acting on the center of the beam, P, and a moment, M, which is equivalent to $(p_3 - p_1)\frac{A}{2}h$ where h is the centroid of the half of the sensor which is $\frac{4a}{3\pi}$ where a is the radius and A is the area of the sensing head. So M reduces to

$$M = 1.03 * p_1 * \frac{A}{2}\frac{2d}{3\pi} \tag{40}$$

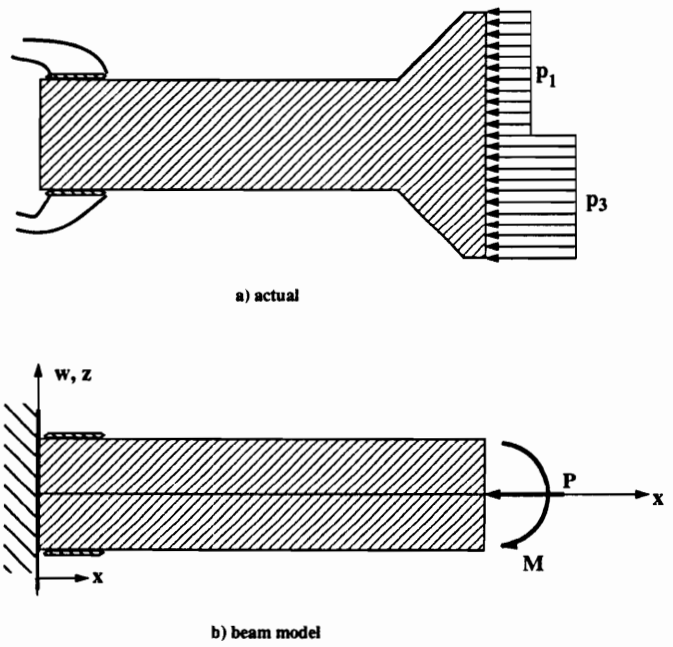

Figure 54: Pressure Difference Due to Shock Models

The governing equation for such a moment is

$$EI\frac{d^2w}{du^2} = M \tag{41}$$

For this somewhat trivial case of a cantilevered beam, where the beam does not move or rotate at the fixed end, this reduces to

$$w(x) = \frac{Mx^2}{2EI} \tag{42}$$

The strain in the x direction is

$$\varepsilon_x = \frac{du}{dx} \tag{43}$$

where $u = u_0 + \frac{dw}{dx}$ so the strain reduces to

$$\varepsilon_x = \frac{Md}{EI} \tag{44}$$

There is no change due to the pressure force as it is balanced out in each active leg of the bridge.

The next step is to compare the strain sensitivity to input due to the wall shear as in Equation 39 versus that due to the pressure gradient as in Equation 44. Using the

standard lengths and diameters of a skin friction balance, it can be shown that for a shock intersecting directly in the center of a skin friction gage, the strain difference in the 2 strain gages can be over an order of magnitude larger than that from the wall shear alone.

For these pressure gradient tests, the front of the wedge was placed 8.89 cm (3.50 in.) ahead of the center of gage ports 3 and 4. From an inviscid flow analysis, this distance would require placing the wedge 5.08 cm (2.0 in.) above the floor. In actuality, the shock tends to bend towards being normal to the floor as it enters the boundary layer, so to place the shock in the center of the gage head, the wedge must be around 6.35 cm (2.5 in.) above the tunnel floor. Each of these distances was measured by dial calipers accurate to 0.001 in. A precision square was used to assist in setting the axial location. A level was also used to insure that the wedge remained parallel to the tunnel floor throughout testing. The reported values of skin friction all are non-dimensionalized by the upstream dynamic pressure prior to the shock, rather than using the local dynamic pressure at the gage.

The first class of data involves the case where the shock hits well behind the sensing head of the gage. This is the case with the wedge at heights of 6.6 cm (2.6 in.) or greater. The data from this case is somewhat trivial as it agrees with the cold flow data and it should. The results and axial locations of these tests are shown in Table 8.

A pair of traces from the behind the gage shock tests are shown in Figures 55 and 56. Figure 55 shows a pair of oil-filled gages, while Figure 56 presents a rubber-filled gage and an oil-filled gage. Both are of the 3.6 kHz design which was constructed with a high shear sensitivity for testing in the supersonic tunnel. The scaling factor used for the rubber gage B5r is 3.0 which is very close to the geometric area ratio of the rubber plus plastic over the plastic alone (the area ratio is 3.2). The agreement between the gages is quite good.

The next set of data to be presented is that in which the shock impacts on the gage head. From the theoretical prediction, this was expected to generate an order of magnitude increase in the output signal. From the prior tests in the HYPULSE facility, it was seen that a shock wave passing over the gage resulted in around a 4

Table 8: SST Shock Behind Sensing Head Data

Run Number	Gage Number	Wedge Height (in.)	Cf
150	B3	4.50	.00260
150	B1	4.50	.00141
151	B3	4.50	.00189
151	B1	4.50	.00156
153	B3	2.90	.00155
153	B1	2.90	.00172
163	B1	2.64	.00209
157	B3	2.74	.00145
157	B1	2.74	.00154
171	B3	3.00	.00139
171	B1	3.00	.00132
172	B3	3.00	.00180
172	B1	3.00	.00135
175	B5r	3.05	.00143
175	B1	3.05	.00130
176	B1	3.05	.00143
193	B5r	2.93	.00200
193	B1	2.93	.00229
194	B5r	2.93	.00177
194	B1	2.93	.00218

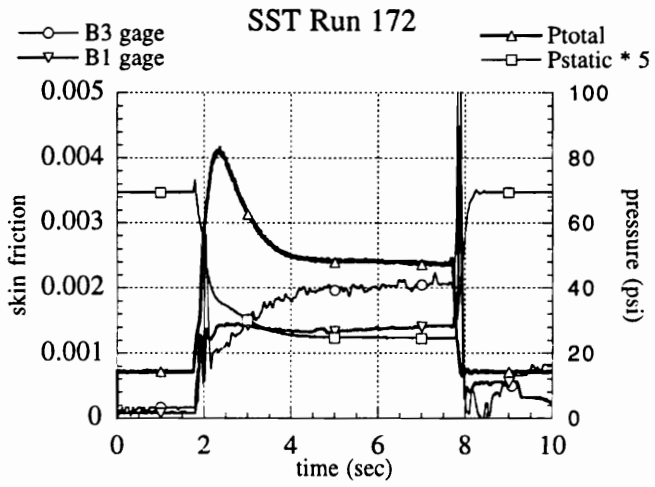

Figure 55: SST Pressure Gradient Behind Gage Test- Run 172

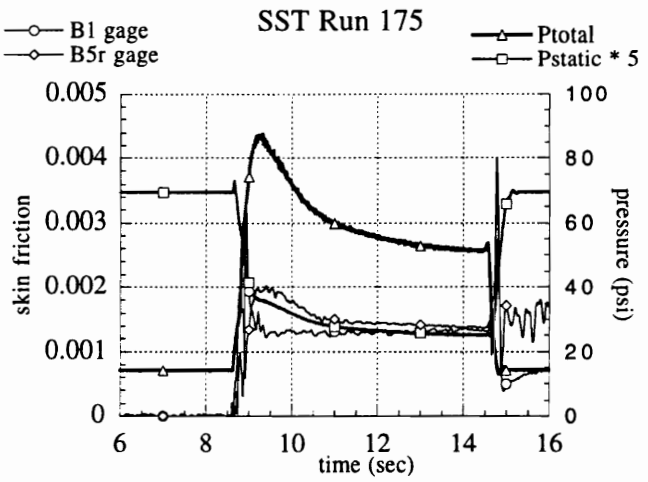

Figure 56: SST Pressure Gradient Behind Gage Test- Run 175

times increase in the output signal. It is suspected that the incompressible oil in the gap causes this decrease in pressure gradient sensitivity. Indeed, an assortment of previous researchers have used an incompressible liquid to seal the gap and reduce the errors due to a large pressure gradient on the gage head [49] [50]. The rubber is less compressible than air as well and also yields a reduction from the order of magnitude theoretical prediction.

The data for the shock impinging on the sensing head case meet the following criteria: the wedge is between 6.22 cm and 6.60 cm (2.45 and 2.60 in.) above the tunnel floor and the static pressure reading at that location was between 6.5 and 7 psia. It should be noted that the quality of the runs here varied. The signal seemed to jump around quite a bit. In some cases, this was due to a breakdown in the flow as evidenced by a sudden jump in the static pressure, but in other cases the gage signal showed a great deal of noise while the static pressure remained flat. The results are presented in the table below and then further discussed.

Figure 57 shows the data from a pair of oil-filled gages. It can be seen that the gages are already having a difficult time establishing a quantitative value as the variation from the mean value is a third or more of the total signal. Suddenly, at t=5 seconds, the supersonic flow breaks down as the static pressure jumps to around 9 psia and the wall shear decreases to nearly zero.

Table 9: SST Shock Impacting Sensing Head Data

Run Number	Gage Number	Wedge Height (in.)	Cf
160	B3	2.46	.0045
160	B1	2.46	.0035
161	B3	2.46	.0050
162	B1	2.46	.0050
173	B3	2.54	.0050
174	B3	2.54	.0060
174	B1	2.54	.0040
191	B5r	2.57	.0064
191	B1	2.57	.0030
192	B5r	2.57	.0063
192	B1	2.57	.0033

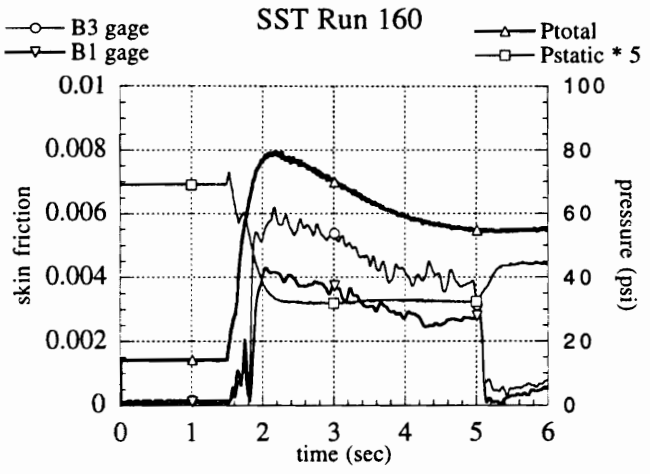

Figure 57: SST Pressure Gradient Impacting Gage Test- Run 160

Figure 58 shows the data from another run with the same pair of gages. In this run, the gages track around the .0050 skin friction value for about two seconds. After this, the gages decrease from the .0050 value to near zero although the static pressure remains constant. It is difficult at best to attempt to ascertain a quantitative value of wall shear in this sort of flow. Figure 59 shows a similar result in another run with the same pair of gages and the wedge moved downward 0.02 cm (0.008 in.) from 6.45 cm to 6.25 cm (2.54 to 2.46 in.) The skin friction data shows a temporary flatness at a given level followed by a divergence from that level with no change in static pressure, however here the gage outputs go in opposite directions. This is a somewhat unusual result but could be a result of the shock moving minutely forward on one gage and backwards on the head of the other. This could have occurred if the wedge or sting mount shifted or vibrated under the pressure load of the flow.

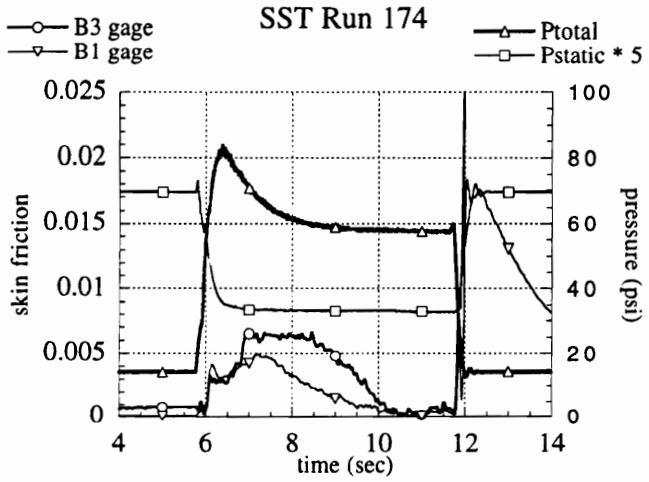

Figure 58: SST Pressure Gradient Impacting Gage Test- Run 174

Figures 60 and 61 show a comparison between a rubber and an oil-filled gage. In both runs, the rubber gage, B5r, is somewhat double-valued during the period when $p_{static} = 6.5$ psia. First it goes to a value similar to that measured by B1 and then after approximately a half second it jumps to a value of double that. This larger sensitivity to pressure gradient is not surprising. It was already mentioned that the incompressible oil in the gap can result in a reduction of the theoretically predicted gradient sensitivity. Other researchers [19] have noted a similar occurrence. Since the

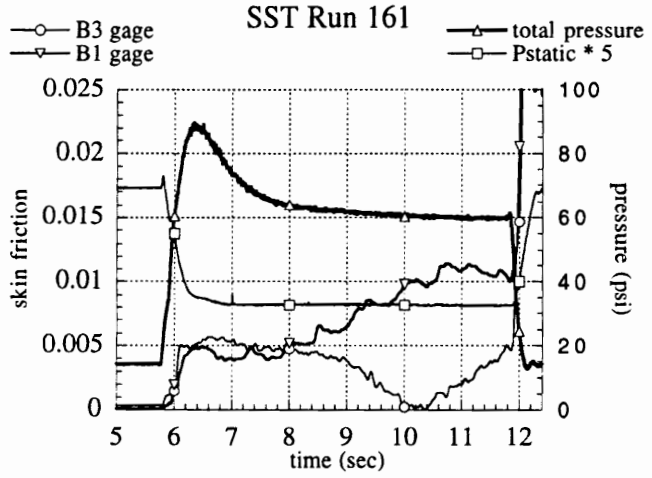

Figure 59: SST Pressure Gradient Impacting Gage Test- Run 161

rubber is more compressible than the oil and the head area exposed to the pressure difference is greater, it is not unrealistic to expect it to have a larger sensitivity. Both gages show a decline in the shear value as the flow breaks down and the static pressure jumps.

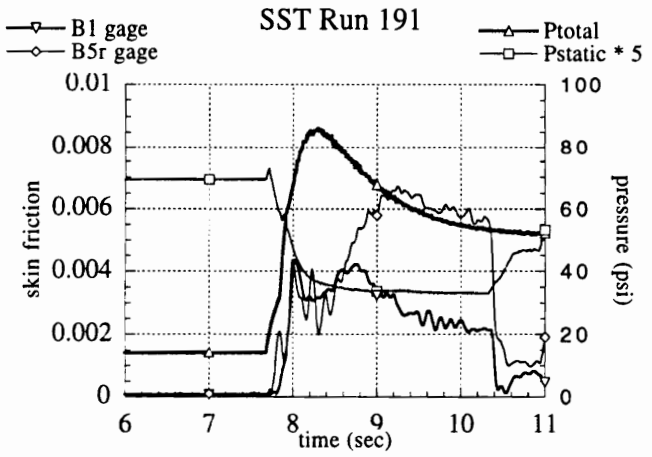

Figure 60: SST Pressure Gradient Impacting Gage Test- Run 191

The final case is when the shock impacts in front of the gages. Ideally in this situation, the static pressure should double as predicted from compressible shock relations. During testing, however, this was not always the case. Sometimes the

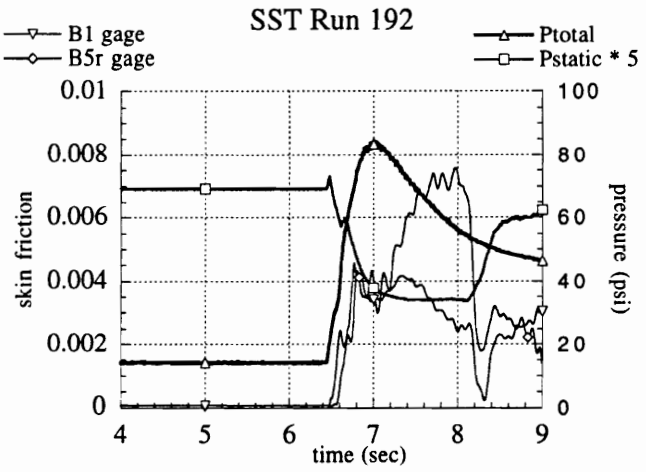

Figure 61: SST Pressure Gradient Impacting Gage Test- Run 192

doubling of p_{static} to a nominal value of 10.5 psia was seen; on other occasions, a variation of static pressure consisting of a spike up to approximately 20 psia and then a decline back to atmospheric pressure was seen when the tunnel failed to start. The differing flow conditions had a large impact on the measured wall shear. The set presented below will be for the case where the tunnel started and produced a shock reflection in front of to the gage yielding a doubling in the static pressure. In cases where the static pressure jumped from the nominal 10.5 psia value, only the time where it was at 10.5 psia will be used for the averaging period.

Figure 62 shows results from a pair of oil-filled gages. This run had the longest steady period at around 10.5 psia and the resulting values of skin friction are somewhat lower but still close to previously attained values without a shock. Figure 63 shows one of the runs with longer periods of 10.5 psi static pressure. Again, the resultant C_f is similar to what had been obtained in the unmodified flow. Figure 64 shows a trace where the static pressure went above atmospheric for two seconds before the tunnel started and attained a 10.5 psia value. This figure compares a rubber-filled gage to an oil-filled gage. Notice how the measured wall shear jumps on the rubber-filled gage trace as static pressure goes to 10.5 psi. This was seen for all four rubber-filled gage traces, whereas in the oil-filled gage runs the wall shear during the 10.5 psi window is equivalent to or less than that during the rest of the run.

Table 10: SST Shock Prior to Sensing Head Data

Run Number	Gage Number	Wedge Height (in.)	Cf
158	B3	2.375	.00139
158	B1	2.375	.00124
165	B3	2.41	.00269
166	B3	2.41	.00123
167	B1	2.41	.00150
178	B1	2.07	.00651
178	B5r	2.07	.00760
185	B1	2.20	.00245
185	B5r	2.20	.00867
195	B1	2.37	.00130
195	B5r	2.37	.00207
196	B5r	2.42	.00225

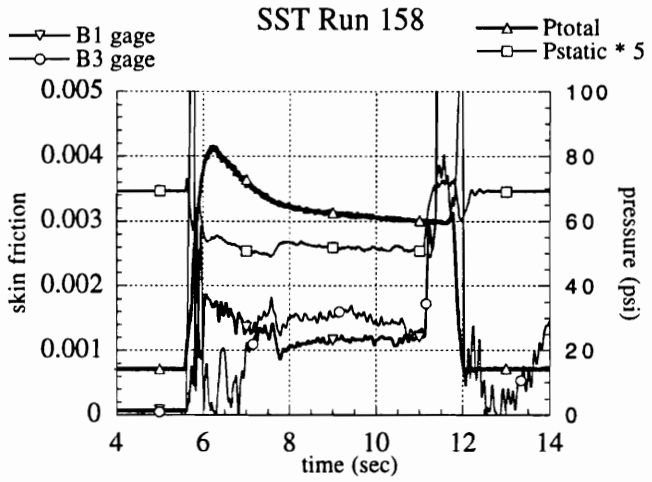

Figure 62: SST Pressure Gradient in Front of Gage Test- Run 158

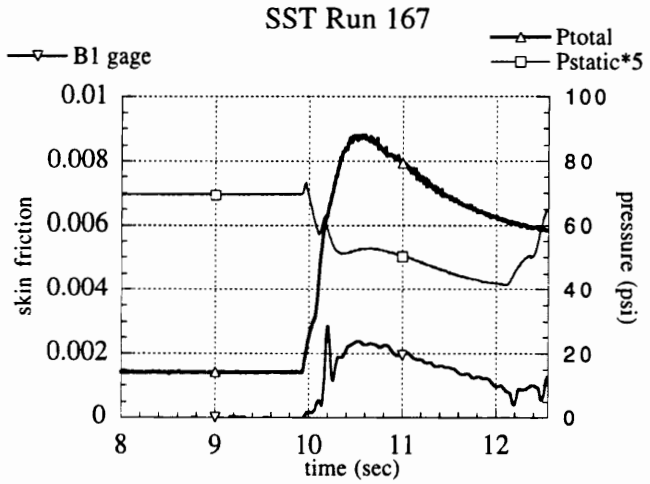

Figure 63: SST Pressure Gradient in Front of Gage Test- Run 167

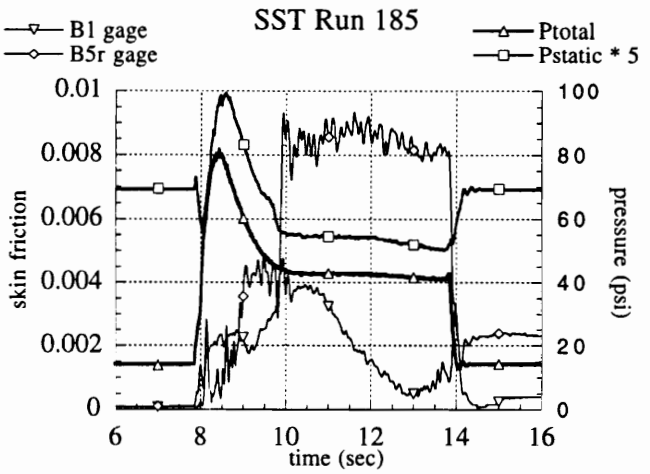

Figure 64: SST Pressure Gradient in Front of Gage Test- Run 185

The composite figure, 65, shows all of the averaged skin friction values versus wedge height for cases where the tunnel was believed to have started. For an oil-filled gage, the measured skin friction with the shock behind the gage is equivalent to the skin friction measured in flow with no shock. The oil-filled gage shows a two to three-fold increase in "average" skin friction value for the case where the shock impinges on the gage head. Average is presented in quotes, since the signal for these runs is very oscillatory. For an oil-filled gage with the shock in front of it, the average measured skin friction value was again equivalent to that measured in a flow without a shock.

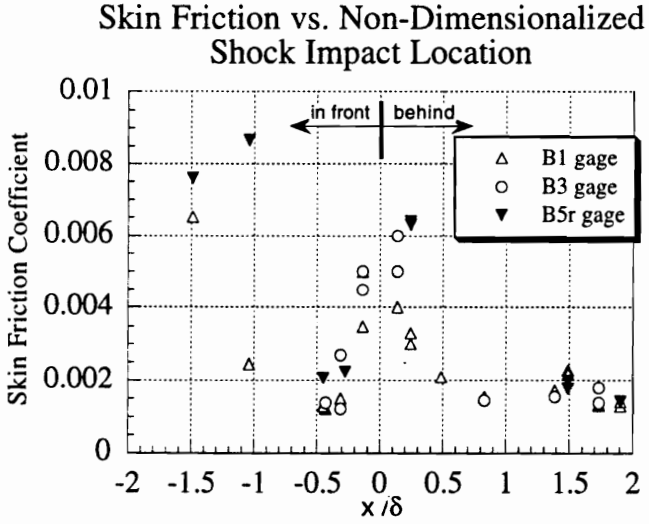

Figure 65: Shock Location versus Average Skin Friction

The results for the rubber-filled gage were somewhat different. If the shock was behind the gage, then the measured skin friction remained the same as in the case of no shock. However, for a shock impinging on the gage head, the increase in the measured value was greater than that of an equivalent oil-filled design. This is believed to be due to the compressibility of the RTV compared to the silicon oil and also due to the increased sensing head size of the plastic/rubber combination. Still the results show a similarity to the oil-filled gages. For the case of the shock reflecting prior to the gage surface, the rubber-filled gage shows some variation from the oil-filled gage. In most runs, the results are similar to the oil-filled gage although the rubber-filled gage appears to be overpredicting somewhat (as in runs 178, 195 and 196). However,

in run 185, the measured value was nearly four times that recorded by an equivalent oil-filled design. It seems reasonable to conclude that the rubber-filled gage does not respond as well as the oil-filled gage in flows with rapid variations in normal pressure. The increased size of the rubber/plastic sensing head means that the measurements are less local than those of an equivalent oil-filled gage and in the cases of a passing shock or separating and reattaching flow, the more localized measurements of the oil-filled gage do a better job of capturing what is occurring in the flow.

It is expected that the skin friction value should have decreased under the influence of the adverse pressure gradient from the shock impingement [4] [50]. As the flow experiences the adverse pressure gradient, it becomes closer to undergoing separation and the skin friction decreases. With the shock impingement causing the flow to be closer to separation, it was expected that the wall shear should decrease. Yet, the measured values showed an increase. Thus both gages show some error, with the oil-filled gages experiencing less. This error is likely due to the large effective moment due to the pressure gradient which is acting upon the sensing head and beam. By hooking up two pairs of strain gages, one on top of the other, in half-Wheatstone bridge arrangements, the difference in outputs could be calculated and the moment due to pressure gradient could be computed and subtracted from the output during data reduction.

Chapter 7

Conclusions and Recommendations

7.1 Conclusions

Wall shear (skin friction) forces in complex supersonic flows were successfully measured. A plastic cantilevered beam with semiconductor strain gages mounted to the base similar to that of Bowersox and Schetz [26] was utilized for direct measurement of wall shear in a variety of test flows. By varying the geometry of the sensing unit, this design can be adapted for a variety of test conditions. The gage design presented extended the basic gage application to impulse testing of shorter duration. Additional modifications were made to extend gage survivability and reduce time required to maintain the gages. The effect of a sharp $\frac{dp}{dx}$ was also investigated.

Results from several test series showed that accurate measurements can be made with the plastic cantilever skin friction balance. Results were obtained in scramjet model tests at the NASA Ames 16-inch Shock Tunnel facility and also at the GASL HYPULSE facility. Both of these tests showed the gage's ability to make measurements in a harsh and complicated flowfield with a very short test time. In cases where a quantitative value was not possible to determine such as a shock passing down the shock tunnel, the gage qualitatively demonstrated that it was reacting to real dynamics of the flow. Cold flow tests in the Virginia Tech supersonic tunnel confirmed that

the uncertainty in the shear measurement is approximately 10 percent.

A significant variant on the baseline oil-filled gage was designed using a 2-part silicon rubber in the gap instead. The elimination of the oil in the gap results in a large reduction in the need to support the gages between runs doing such tasks as replenishing the oil . The increased gap size used to reduce the spring stiffness of the rubber compound was found to lead to an increased sensing head size that was proportional to the ratio of the sum of the area of the rubber and plastic sensing head over the area of the plastic sensing head alone. Successful data were acquired with this design, however it was discovered that the rubber-filled gage did not perform as well as the oil-filled gage in flows with strong axial pressure gradients. This can be attributed to a number of factors. The increased sensing head size leads to less local measurements. Also, an oil-filled gage sees a diminishment of pressure gradient effects due to the incompressible nature of the silicon oil, while the rubber is a somewhat compressible substance and therefore is more affected by pressure gradients.

Several other variations on the baseline gage were tested as well. Sputtering the gage surface with a hard substance such as chromium-oxide, iridium, or titanium-oxide was found to do an excellent job of protecting the gage surface during tests with scramjet combustion models. The combination of high test temperatures and rapidly moving metallic microparticles (such as tiny fragments of the steel diaphragms which are burst to fire the shock tunnel) encounted in such facilities tended to scar the gage surface and render it unusable. The sputtering serves to combat these hostile effects and extend gage lifetime. The use of such modifications such as a stainless steel housing and hollowed out sensing beam were found to be good ideas although not nearly as effectual as the rubber-filled gap and sputtered surface variants, and the use of a reduced gap size and thermocouples to monitor gage temperatures were ideas that showed promise. Substituting Macor ceramic for the plastic sensing head was found to be a very poor idea for several reasons–it is difficult to successfully adhere a ceramic to ULTEM and Victrex and Macor's high density relative to the plastics results in a decreased natural frequency compared to an equivalent all-plastic design.

Each of the test series produced important developments. The tests at NASA Ames demonstrated the gage's ability to take good data in an impulsive facility with

a severe test environment, with correlations to the flow in the inlet found to agree with the gages' measured values. Fluctuations exhibited in the gage outputs were found to correspond to equivalent fluctuations in the facility's measured total pressure. The HYPULSE tests validated the gages' very fast time response as data were successfully acquired in a test window of well under a millisecond. The skin friction trends from these tests were found to be in agreement with the heat flux trends for tare runs, combusting runs, and runs with film cooling. A reasonable agreement between the measured wall shear values and CFD prediction for the combustion case (the only flowfield where CFD values were reported) was also seen. The measured shear values were slightly higher but this has been seen by several researchers for longer duration scramjet tests [19] [20]. No appreciable variation was seen in the average measured shear stress between the oil-filled and rubber filled-gages although the rubber-filled gages did have some 7 kHz oscillations on the output signal. A transitory spike in the output of an AFIT constructed gage was seen as a shock travelled down the model and passed over the sensing head. Although this briefly contaminated the skin friction gage signal, it showed that the gage was responding to a real property of the flow.

The tests in the Virginia Tech supersonic tunnel extended the gage's operating regime into longer-duration tests. Measured values of skin friction from cold flow tests agreed with correlations from the empirical Schultz-Grunow relation for skin friction in wall-bounded incompressible turbulent boundary layers which was improved with the incompressible to compressible relation of Van Driest. These cold flow tests also served to help ascertain the uncertainty in the skin friction measurements. The effect of a sharp adverse pressure gradient on the gage head was also investigated. It was expected that the wall shear would decrease as the adverse pressure gradient makes the flow closer to separation. However, due to the moment acting on the sensing head the measured wall shear values were found to be higher. This effect can be eliminated by using of two pairs of strain gages in half-Wheatstone bridge arrangements to calculate the moment. The effect of the moment can then be subtracted from the output during data reduction.

It should be pointed out that it would not be feasible to try to generate a "one size fits all" type of gage design. There is always a constant tradeoff between sensitivity

and natural frequency (and hence frequency response) with this gage design. Instead, a study should be conducted before each test to insure that a gage is designed with adequate response characteristics– a much different design is needed for the impulsive tests where the shear levels were an order of magnitude higher than in that in the Virginia Supersonic Tunnel but the test time was on the order of milliseconds rather than seconds. There are also additional considerations such as model geometry, physical orientation, and other flow conditions.

7.2 Recommendations

An effort should be undertaken in the area of strain gage configuration. Lengthening the beam by 2 mm would allow for an additional strain gage to be placed underneath the one on the beam and allow for the circuit to be run as a full bridge. This should increase thermal stability of the bridge circuit as well as increase the output from the bridge. The diameter of the beam would have to be increased to maintain the same natural frequency so some of the increase in output will be diminished. Likewise, the complexity of feeding eight leadwires through the beam base is a very daunting task; there is not too much room for four leadwires. Still, the full-bridge gage configuration is appealing. In flows where there was a potential for a strong adverse pressure gradient, this configuration could be converted to a pair of half-Wheatstone bridge arrangements by simply adding another Measurements Group Model 2310 signal conditioning amplifier and changing the connections to the Model 2310 units. Thus, by simply adjusting the wiring configuration, this configuration could be adjusted, while already installed in the model, to provide extra thermal or pressure gradient protection as necessary The gage surface and housing could also be modified to allow for a pressure port in the housing so that pressure data could be taken right next to the sensing head. Furthermore, the sensing head could be modified to place a small heat flux sensor on it and therefore the gage could simultaneously measure skin friction and heat flux in order to verify Reynolds Analogy in the test flow.

Additionally, there are still several areas for improvement in the rubber gage design. The driving force for the current gage design was to minimize the decrease in strain due to the stiffness of the rubber. Reducing the change in effective sensing head diameter may be a worthwhile parameter to introduce into the optimization process. It would provide for a more localized measurement of wall shear. A theoretical analysis of the "effective sensing head" for the rubber gages would provide a valuable design tool. The computational design program gelim could then be extended to include this analysis in the optimization. The manufacturing process can be changed as well. Currently, a gage must be fully constructed and then the gap is filled with rubber. After this, the gage is tested under vacuum to insure that there is no pressure sensitivity due to the rubber. Even with prudent assembly, occasionally some air bubbles are found and those gages must be discarded. A technique to more successfully eliminate air bubbles would help reduce the average successful construction time. Also in manufacturing, cooling the rubber to its brittle point ($-60°$ F) would make it easier to get a flat surface on the head as the rubber would then become machinable.

Among the more needed components to the design process is an impulsive "checkout" facility. For the first year and a half, a small shock tunnel was available for this purpose. Such a facility was a valuable tool in being able to quickly and cheaply ascertain whether or not a certain gage variation is worthwhile. Hopefully the Virginia Tech Hypersonic Tunnel can be used for such a purpose since such a facility can quickly identify poor design concepts (such as the all-Macor gage) and rapidly affirm good ideas. In a sense, such a facility serves to provide a "dynamic calibration" to complement the static calibration technique.

The last recommendation is to recognize the power of the large data set. This skin friction gage design tends to be correct more often than not. In previous tests, an unusual shear value would be obtained causing one to question the accuracy of the sensor. However, additional measurement data of other flow variables would show that the gage was measuring a true property of the flow. On other occasions, unexpected values would be repeatedly be obtained which would prove the original

theoretical model to be insufficient. The gage wasn't performing poorly; the theoretical model was. Refinement and improvement of the skin friction gage is dependent upon experience and having information at one's fingertips. No matter how much prior analysis is done, the first estimate is seldom as good as the third or fourth.

Bibliography

[1] Nitsche, W., Haberland, C., and Thunker, R., "Comparative Investigations on Friction Drag Measuring Techniques in Experimental Aerodynamics," ICAS-84-2.4.1, 14th ICAS Congress, Sept. 1984.

[2] Wooden, P. A. and Hull, G. H., "Correlation of Measured and Theoretical Heat Transfer and Skin Friction at Hypersonic Speeds Including Reynolds Analogy," AIAA Paper No. 90-5244, Oct. 1990.

[3] Putz, J., *The Devlopment of Instrumentation for the Support of Skin Friction and Heat Flux Measurements.* PhD thesis, Virginia Polytechnic Institute and State University, 1991.

[4] Schetz, J., *Boundary Layer Analysis.* Prentice-Hall, Inc., 1993. ISBN 0-13-086775-X.

[5] Rubesin, M., "A Modified Reynolds Analogy for the Compressible Turbulent Boundary Layer on a Flat Plate," NASA TN-2917, 1953.

[6] Bruno, J. R., "Balance for Measuring Skin Friction in the Presence of Heat Transfer," NOLTR 69-56, June 1969.

[7] Gador, A. Y. and Louis, J. F., "High Temperature Heat Transfer and Skin Friction Measurements in Turbulent Flows Along Highly Cooled Walls," AIAA 86-1235, AIAA/ASME 4th Joint Thermophysics and Heat Trasfer Conference, June 1986.

[8] Owen, F. and Johnson, D. A., "Separated Skin-Friction Measurements– Source of Error: An Assesment and Elimination," AIAA 80-1409, AIAA 13th Fluid and Plasma Dynamics Conference, July 1980.

[9] Bellhouse, B. J. and Schultz, D. L., "Determination of mean and dynamic skin friction, separation and transition in low- speed flow with a thin-film heated element," Journal of Fluid Mechanics, pp. 379–400, 1966.

[10] Gaudet, L. and Gell, T. G., "Use of Liquid Crystals for qualitative and quantitative 2-D studies of transition and skin friction," in *ICIASF '89 - 13th International Congress on Instrumentation in Aerospace Simulation Facilities*, vol. 43, pp. 66–81, 1989.

[11] Seto, J. A. and Hornung, H. G., "Internally Mounted Thin-Liquid-Film Skin Friction Meter Comparison with Floating Element Method and Without Pressure Gradient," AIAA 91-0060, AIAA 29th Aerospace Sciences Meeting, Jan. 1991.

[12] Seto, J. A. and Hornung, H. G., "Two-directional skin friction measurement utilizing a compact internally mounted thin-liquid-film skin friction meter," AIAA 93-0180, AIAA 31st Aerospace Sciences Meeting and Exhibit, Jan. 1993.

[13] Tanner, L. H. and Blows, L. G., "A Study of the Motion of Oil Films on Surfaces in Air Flow, with Application to the Measurement of Skin Friction," Journal of Physics E: Scientific Instruments, pp. 194–202, 1976.

[14] Monson, D. J. and Higuchi, H., "Skin Friction Measurements by a New Nonintrusive Double Laser Beam Oil Viscosity Balance Technique," AIAA 80-1373, AIAA 13th Fluid and Plasma Dynamics Conference, July 1980.

[15] O'Brien, S. A. and Christiansen, W. H., "A Technique for Short-Duration Skin-Friction Measurements," AIAA 93-2920, AIAA 24th Fluid Dynamics Conference, July 1993.

[16] Winter, K. G., "An Outline of the Techniques Available for the Measurement of Skin Friction in Turbulent Boundary Layers," Progress in Aerospace Sciences, pp. 1–57, 1977.

[17] Allen, J. M., "Improved Sensing Element for Skin-Friction Balance Measurements," AIAA Journal, vol. 18, pp. 1342–1345, Nov. 1980.

[18] Vakili, A. D., "A New Skin Friction Balance and Selected Measurements," Experiments in Fluids, pp. 401–406, 1992.

[19] Chadwick, K. M., *An Actively Cool Floating Element Skin Friction Balance for Direct Measurement in High Enthalpy Supersonic Flows.* PhD thesis, Virginia Polytechnic Institute and State University, 1992.

[20] Deturris, D. J., *A Technique for Direct Measurement of Skin Friction in Supersonic Combustion Flow.* PhD thesis, Virginia Polytechnic Institute and State University, 1992.

[21] Bogdan, L., "Instrumentation Techniques for Short-Duration Test Facilities," Tech. Rep. Calspan Report No. WTH-030, Calspan Corp., Mar. 1967.

[22] MacArthur, R. C., "Transducer for Direct Measurement of Skin Friction in a Hypersonic Shock Tunnel," Tech. Rep. Calspan Report No. 129, Calspan Corp., Aug. 1963.

[23] MacArthur, R. C., "Contoured Skin Friction Transducers," Tech. Rep. Calspan Report No. AN-2403-Y-1, Calspan Corp., Aug. 1967.

[24] Kelly, G. M., Simmons, J. M., and Paull, A., "Skin-Friction Gauge for Use in Hypervelocity Impulse Facilities," AIAA Journal, vol. 30, pp. 844–845, Mar. 1992.

[25] Bowersox, R. D., Schetz, J. A., Chadwick, K., and Deiwert, S., "Technique for Direct Measurement of Skin Friction in High Enthalpy Impulsive Scramjet Flowfields," AIAA Journal, pp. 1286–1291, July 1995.

[26] Bowersox, R. and Schetz, J., "Skin Friction Gages for High Enthalpy Impuslive Flows," AIAA 93-5079, AIAA/DGLR 5th International Aerospace Planes and Hypersonic Technologies Conference, Nov. 1993.

[27] "General Electric Corporation, LEXAN and ULTEM Properties Guide."

[28] "Westlake Plastics Corportation, Vicrex PES Properties Guide."

[29] Kulite-Semiconductor-Products, *Kulite Semiconductor Strain Gage Manual.* Leonia, NJ.

[30] Beer, F. P. and Johnston, E. R., *Mechanics of Materials.* Mc-Graw Hill, 1981.

[31] Cannon, R. H., *Dynamics of Physical Systems.* Mc-Graw Hill Book Company, 1967.

[32] Doebelin, E. O., *Measuremen Systems Application and Design Fourth Edition.* Mc-Graw Hill Book Company, 1990.

[33] "Dow Corning, Macor Machinable Glass Ceramic Properties and Technical Data."

[34] Kapania, R. and Issac, J. private communication, 1995.

[35] Deiwert, G. S., Cavolowsky, J. A., and Loomis, M. P., "Large Scale Scramjet Testing in the Ames 16-Inch Shock Tunnel," AIAA Paper No. 94-2519, June 1994.

[36] Novean, M., Schetz, J., Hazelton, D., and Bowersox, R., "Skin Friction Measurements in Short Duration High Enthalpy Flows," AIAA 95-6109, AIAA 6thi International Aerospace Planes and Hypersonics Technologies Conference, Apr. 1995.

[37] Van Driest, E. R., "The Problem of Aerodynamic Heating," Aeronautical Engineering Review, vol. 15, no. 10, pp. 26–41, 1956.

[38] White, F. M. and Christoph, G. H., "A Simple Theory for the Two-Dimensional Compressible Turbulent Boundary Layer," Journal of Basic Engineering, vol. 94, pp. 636–642, 1972.

[39] Eckert, E. R. G., "Engineering Relations for Heat Transfer and Friction in High-Velocity Laminar and Turbulent Boundary-Layer Flow Over Surfaces with Constant Pressure and Temperature," Transactions of the ASME, vol. 78, Aug. 1956.

[40] Hopkins, E. J. and Inouye, M., "An Evaluation of Theories for Predicting Turbulent Skin Friction and Heat Transfer on Flat Plates at Supersonic and Hypersonic Mach Numbers," AIAA Journal, vol. 9, pp. 993–1003, 1971.

[41] Spalding, D. B. and Chi, S. W., "The Drag of a Compressible Turbulent Boundary Layer on a Smooth Flat Plate With and Without Heat Transfer," Journal of Fluid Mechanics, vol. 18, pp. 117–143, Jan. 1964.

[42] Saada, A. S., *Elasticity: Theory and Applications.* Pergamon Press, 1974.

[43] Tamagno, J., Bakos, R., Pulsonetti, M., and Erdos, J., "Hypervelocity Real Gas Capabilities of GASL's Expansion Tube (HYPULSE) Facility," AIAA 90-1390, AIAA 16th Aerospace Ground Testing Conference, June 1990.

[44] Calleja, J. and Tamagno, J., "Calibration of HYPULSE of Hypervelocity Air Flows Corresponding to Flight Mach Numbers 13.5, 15, and 17," Tech. Rep. NASA Contractor Report 191578, General Applied Science Laboratories, Inc., Ronkonkoma, New York, Dec. 1993.

[45] Erdos, J., Calleja, J., and Tamagno, J., "Increase in the Hypervelocity Test Envelope of the HYPULSE Shock-Expansion Tube," AIAA 94-2524, AIAA 18th Aerospace Ground Testing Conference, June 1994.

[46] Calleja, J. fascimile transmission, July 1995.

[47] Markatos, N., Spalding, D., and Tatchell, D., "Combustion of Hydrogen Injected into a Supersonic Airstream (The Ship Computer Program)," Tech. Rep. NASA Contractor Report CR-2802, Fluid Mechanics and Thermal Systems, Inc., Waverly, AL, Apr. 1977.

[48] Pope, A. and Goin, K., *High Speed Wind Tunnel Testing.* Wiley, 1965.

[49] Hirt, F., Zurfluh, U., and Thomann, H., "Skin Friction Balances for Large Pressure Gradients," Experiments in Fluids, pp. 296–300, 1986.

[50] Frei, D. and Thomann, H., "Direct Measurements of Skin Friction in a Turbulent Boundary Layer with a Strong Adverse Pressure Gradient," Journal of Fluid Mechanics, pp. 79–95, 1980.

Appendix A

Source Code

Listed below are the FORTRAN program listings of programs which were utilized in the design of the skin friction gages. All programs can be easily compiled under F77 and executed.

A.1 Skin Friction Gage Design

Program sfgdm is a modified version of the original sfdg (skin friction gage design) program written by R. Bowersox. The modification is that the user can now specify an independent variable for a parametric study (i.e. vary beam length from 5mm to 6mm in increments of 0.1mm while holding all other geometric variables fixed).

```
c-------------------------------------------+
c  Program:  sfgd (Skin Friction Gauge Design) |
c  Purpose:  Estimate time response of a       |
c            cantilever beam with a end weight |
c            and end loading                   |
c-------------------------------------------+
c
      real massbeam,massend,i,par(250),parinc
      integer runnum,pcount,j,chp,text
      character*50 mat
      character*14 fout
      character*30 pp
c
      iflag = 0
      pi = 4.*atan(1.)
c
c
    1 write(*,*)
      if(iflag.eq.0) go to 11
       write(*,*) ' Use the same material ?'
       write(*,*) '  1 - yes   2 - no'
       read(*,*) imat
       if(imat.eq.1) go to 12
```

```
c
   11 continue
      iflag = 1
      write(*,*) ' MATERIAL PROPERTIES'
      write(*,*)
      write(*,*) 'Enter the name of the material'
      read(*,'(a)') mat
c
      write(*,*) 'Enter the density (kg/m**3) '
      read(*,*)rho
c
      write(*,*) 'Enter E (GPa)'
      read(*,*) ge
      e = ge*1.e9
c
   12 write(*,*) 'Enter the output filename'
      read(*,'(a)') fout
      open(1,file=fout)
c
c     setup for choosing independent variable parametric study
      write(*,*)
      write(*,*) 'Enter number of independent beam parameter'
      write(*,*)
      write(*,*) '1 -- Outer Diameter'
      write(*,*) '2 -- Inner Diameter'
      write(*,*) '3 -- Length'
      write(*,*) '4 -- Head Diameter'
      write(*,*) '5 -- Head Tip Thickness'
      write(*,*) '6 -- Head Root Thickness'
      read(*,*) chp
      write(*,*)
      write(*,*) 'Enter number of separate runs'
      read(*,*) runnum
      write(*,*) 'Enter beginning value for parameter'
      read(*,*) par(1)
      write(*,*) 'Enter ending value for parameter'
      read(*,*) par(runnum)
      parinc = (par(runnum)-par(1))/(runnum-1.0)
      do 20 pcount=2,runnum-1
  20   par(pcount) = par(1)+parinc*(pcount-1)

c
      write(*,*)
      write(*,*) ' BEAM PARAMETERS'
      write(*,*)
c
      text = 1
c
      do 300 j=1,runnum
      if (text.eq.1.and.chp.ne.1) then
      write(*,*) 'Enter the outer diameter (mm)'
       read(*,*) d
      endif
      if (chp.eq.1) then
       d = par(j)
      endif
       d = d/1000.
       r = .5*d
```

```
      if (text.eq.1.and.chp.ne.2) then
       write(*,*) 'Enter the inner diameter (mm)'
       read(*,*) di
      endif
      if (chp.eq.2) then
       di = par(j)
      endif
       di = di/1000.
       ri = 0.5*di
       area = .25*pi*(d*d-di*di)
       i = .25*pi*(r**4-ri**4)
c
      if (text.eq.1.and.chp.ne.3) then
       write(*,*) 'Enter the length (mm)'
       read(*,*) xl
      endif
      if (chp.eq.3) then
       xl = par(j)
      endif
       xl = xl/1000.
c
c     write(*,*) 'Enter the density (kg/m**3) '
c     read(*,*)rho
      massbeam = area*xl*rho
c
c     write(*,*) 'Enter E (GPa)'
c     read(*,*) ge
c     e = ge*1.e9
c

      if (text.eq.1) then
       write(*,*)
       write(*,*) ' HEAD PARAMETERS'
       write(*,*)
      endif
      if (text.eq.1.and.chp.ne.4) then
       write(*,*) 'Enter the head diameter (mm)'
       read(*,*) dhead
      endif
      if (chp.eq.4) then
       dhead = par(j)
      endif
       dhead = dhead/1000.
       ah = .25*pi*dhead*dhead
c
      if (text.eq.1.and.chp.ne.5) then
       write(*,*) 'Enter the head tip thickness (mm) '
       read(*,*) tt
      endif
      if (chp.eq.5) then
       tt = par(j)
      endif
       tt = tt/1000.
c
      if (text.eq.1.and.chp.ne.6) then
       write(*,*) 'Enter the head root thickness (mm)'
       read(*,*) tr
```

```
      endif
      if (chp.eq.6) then
       tr = par(j)
      endif
       tr = tr/1000.
      tbar = .5*(tr + tt)
      aeff = ah - .25*pi*d*d
      massend = rho*aeff*tbar
c
c  Static Response
c
      if (text.eq.1) then
       write(*,*)
       write(*,*) 'Enter the wall shear (Pa)'
       read(*,*) tauw
      endif
      f = ah*tauw
c
      sigma = f*xl*r/i
c      write(*,*) 'Max stress (MPa) = +-',sigma/1.e6
      strain = sigma/e
c      write(*,*) 'Max strain (micro) = ',strain*1.e6
      del = f*xl**3/6./e/i*2.
c      write(*,*) 'The displacement (mm) = ',del*1000.
c
c  Dynamic Response
c
c      write(*,*)
c      write(*,*) 'II.  Dynamic Response'
c      write(*,*)
c
      tau = xl**(1.5)*sqrt((massbeam+4.*massend)/e/i)/3.5*2.*pi
c      write(*,*) 'The time constant = ',tau,' sec'
      fresp = 1./tau
c      write(*,*) 'The Natural Frequency (kHz) = ',fresp/1000.
c
c  viscosity
c
       xk = 12.*e*i/xl**3
       xm = massbeam+4.*massend
       wn = sqrt(xk/xm)
       vdot = f*xl**3/e/i/6*wn
c       write(*,*) 'vdot = ',vdot
       awet = pi*d*xl+ah-pi*d*d/4.
       c = 14./awet/xl**(1.5)*sqrt(e*i*xm)
       xmu = c*del
c       write(*,*) 'The critical damping = ',xmu
c       write(*,*)
c       write(*,*)
c
c
  100 format(2x,'Miniature Beam Design (first iteration computed)'/)
      d = d*1000.
      dinch = d/25.4
      di = di*1000.
      diinch = di/25.4
      xl = xl*1000.
      xlinch = xl/25.4
```

```
      dhead = dhead*1000.
      dhinch = dhead/25.4
      tt = tt*1000.
      ttinch = tt/25.4
      tr = tr*1000.
      trinch = tr/25.4
      if (text.eq.1) then
      write(1,100)
      write(1,*)
      write(1,110) d,dinch,di,diinch,xl,xlinch,dhead,dhinch,
     $             tt,ttinch,tr,trinch
      write(*,100)
      write(*,*)
      write(*,110) d,dinch,di,diinch,xl,xlinch,dhead,dhinch,
     $             tt,ttinch,tr,trinch
  110 format(3x,'Beam Dimensions',/,
     $       4x,'Outer Diameter  = ',f6.3,' (mm) = ',f6.3,' (in)',/,
     $       4x,'Inner Diameter  = ',f6.3,' (mm) = ',f6.3,' (in)',/,
     $       4x,'Length          = ',f6.3,' (mm) = ',f6.3,' (in)',/,
     $       4x,'Head Diameter   = ',f6.3,' (mm) = ',f6.3,' (in)',/,
     $       4x,'Head Tip thick  = ',f6.3,' (mm) = ',f6.3,' (in)',/,
     $       4x,'Head Root thick = ',f6.3,' (mm) = ',f6.3,' (in)',/)
      endif
      massbeam = massbeam*1000.
      xmblbs = massbeam/453.59*1000.
      xmbmg = massbeam*1000.
      massend = massend*1000.
      xmelbs = massend/453.59*1000.
      xmemg = massend*1000.
      geksi = e/6893./1000.
      rhoeng = rho*0.06243
      if (text.eq.1) then
      write(1,120) mat,ge,geksi,rho,rhoeng,xmbmg,xmblbs,xmemg,xmelbs
      write(*,120) mat,ge,geksi,rho,rhoeng,xmbmg,xmblbs,xmemg,xmelbs
  120 format(3x,'Material Properties',/,
     $       4x,a50,/,
     $       4x,'E         = ',f7.2,' (GPa)    = ',f7.2,' (ksi)    ',/,
     $       4x,'Density   = ',f7.2,' (kg/m^3) = ',f7.2,' (lb/ft^3)',/,
     $       4x,'Mass Beam = ',f7.2,' (mgram)  = ',f7.2,' (lbs*1000)',/,
     $       4x,'Mass End  = ',f7.2,' (mgram)  = ',f7.2,' (lbs*1000)',/)
      endif
      sigksi = sigma/6893.
      sigma = sigma/1000000.
      strain = strain*1000000.
      delmil = del/2.54e-8
      del = del*1.e6
      xi = i*(1000.)**4
      xift4 = xi/416231.*1000000.
      taupsi = tauw/6893.
      if (text.eq.1) then
      write(1,130) tauw,taupsi,xi,xift4,sigma,sigksi,strain,del,delmil
      write(*,130) tauw,taupsi,xi,xift4,sigma,sigksi,strain,del,delmil
  130 format(3x,'Static Results',/,
     $       4x,'Wall Shear = ',f7.2,' (Pa)      = ',f7.2,' (psi)',/,
     $       4x,'I          = ',f7.2,' (mm^4)    = ',f7.2,' (in^4*1e6)'
     $       ,/,
     $       4x,'Max Stress = ',f7.2,' (MPa)     = ',f7.2,' (psi)'/,
     $       4x,'Max Strain = ',f7.2,' (mirco-strains)',/,
```

```
     $       4x,'Deflection = ',f7.2,' (microns) = ',f7.2,' (micro-in)'
     $       ,/)
      endif
      sg = 1.0
      oil = xmu/sg/1000.*1.e6
      if (text.eq.1) then
      write(1,140) tau*1.e6,fresp/1000.,xmu*100.,oil
      write(*,140) tau*1.e6,fresp/1000.,xmu*100.,oil
  140 format(3x,'Dynamic Results',/,
     $       4x,'Time Constant     = ',f7.2,' (micro-sec)',/,
     $       4x,'Natural Frequency = ',f7.2,' (kHz)',/,
     $       4x,'Critical Damping  = ',f7.2,' (Pa-s*100)',/,
     $       4x,'Oil Dynamic Visc (s.g. = 1.0)  = ',f7.0,' (c-s)')
      write(1,*)
      write(1,*)
      write(1,150) 'Results Table for Variation of Requested Parameter'
      write(*,*)
      write(*,*)
      write(*,150) 'Results Table for Variation of Requested Parameter'
  150 format(15x,A,/)
      if (chp.eq.1) then
       pp = '   O.D. (mm)      O.D. (in) '
      else if (chp.eq.2) then
       pp = 'Inner D. (mm)  Inner D. (in)'
      else if (chp.eq.3) then
       PP = ' Length (mm)    Length (in) '
      else if (chp.eq.4) then
       pp = ' Head D. (mm)   Head D. (in)'
      else if (chp.eq.5) then
       pp = 'Head T.T.(mm)  Head T.T.(in)'
      else if (chp.eq.6) then
       pp = 'Head R.T.(mm)  Head R.T.(in)'
      endif
      write(1,160) pp
      write(*,160) pp
  160 format(2x,A,4x'  Micro-Strain   Nat. f (kHz)     Tau (mS)')
      endif
      write(1,170) par(j), par(j)/25.4, strain, fresp/1000., tau*1.e3
      write(*,170) par(j), par(j)/25.4, strain, fresp/1000., tau*1.e3
  170 format(2x,f10.4,f15.5,f20.4,f15.4,f15.5)
      text = 0
  300 end do
      write(*,*) 'Run a new case'
      write(*,*) ' 1 - yes  2 - no'
      read(*,*) icase
      if(icase.eq.1) go to 1
c
      write(*,*)
      stop
      end
```

A.2 Rubber Gage Design

There are 2 programs that are run for the rubber filled anulus gage design. The first is fstiff which calculates the spring stiffness of the rubber from the geometry of the

beam and anulus and the Young's modulus and Poisson's ratio of the rubber.

The second program is gelim, which uses a Gaussian Elimation (hence, gelim) routine to solve for the output strain and tip displacement. The coding for these programs was done by J. Isaac.

```
      program fstiff

      implicit double precision (a-h,o-z)
      dimension a(2),b(2),ak(2)

      open (unit=1,file='fstiff.dat', status='old')
      open (unit=3,file='fstiff.out', status='unknown')
c
c     ym = Youngs modulus
c     pr=  Poisson ratio
c     a(i),b(i) = inner radius and outer radius
c
      pi=datan(1.d0)*4.0
      read(1,*)ym
      read(1,*)pr
      read(1,*)(a(i),b(i),i=1,2)

      ebar=ym/((1.0+pr)*(1.0-2.0*pr))
      do 1 i=1,2
      ak(i)=pi*ebar/4.0*((2.0*pr-1)*(5.0*a(i)**2+3.0*b(i)**2
     &      -8.0*a(i)*b(i))+ 4.0*b(i)**2*(1.0-pr**2)*
     &      dlog(b(i)/a(i)))/(a(i)-b(i))**2
1     continue

      write(3,*)'stiff1 =', ak(1)
      write(3,*)'stiff2 =', ak(2)

      end
```

```
c|-------------------------------------------------------|
c| Program GELIM.F                                       |
c|  Uses gaussian elimination to solve for beam deflection|
c|    and strain                                         |
c|                                                       |
c|PROGRAM GELIM                                          |
c| * Input                                               |
c|        E1 = modulus of beam @ base                    |
c|        E2 = modulus of beam @ head                    |
c|        d1 = diameter of beam at base (meters)         |
c|        d2 = diameter of beam at head (meters)         |
c|        al1 = length of base to head (meters)          |
c|        al2 = head thickness (meters)                  |
c|        ak1 = k1 from FSTIFF.OUT                       |
c|        ak2 = k2 from FSTIFF.OUT                       |
c|        af  = wall shear pressure (Pa)                 |
c| * Output                                              |
c|        strain (strain = meters/meters)                |
c|        tip displacement (meters)                      |
c|-------------------------------------------------------|
```

```
      parameter(n=7)
      implicit double precision (a-h,o-z)
      dimension a(n,n+1),x(n),r(n,n+1),res(n)
c
      open (unit=1,file='gelim.inp',status='old')
      open (unit=3, file='gelim.out', status='unknown')
c
c      do 10 i=1,n
c      do 10 j=1,n+1
c      read(1,*)a(i,j)
c      write(3,*)a(i,j)
c10    continue
c
      call input(a,d1,b1,g2)
c
      do 1 i=1,n-1
      if (abs(a(i,i)).le.1.e-12) then
      call pivot(a,i)
      endif
      do 2 j=i+1,n
      r(j,i)=a(j,i)/a(i,i)
      do 3 k=i,n+1
      a(j,k)=a(j,k)-r(j,i)*a(i,k)
3     continue
2     continue
1     continue
c
      x(n)=a(n,n+1)/a(n,n)
      do 4 i=n-1,1,-1
      sum=0.0
      do 5 j=i+1,n
      sum=sum+a(i,j)*x(j)
5     continue
      x(i)=(a(i,n+1)-sum)/a(i,i)
4     continue
c
c      write(3,*)' c value'
c      do 6 i=1,n
c6      write(3,*)x(i)
c
      strain=d1*b1**2*(x(1)-x(3))
      tipdisp=exp(g2)*(x(4)*dsin(g2)+x(5)*dcos(g2))+
     &        exp(-g2)*(x(6)*dsin(g2)+x(7)*dcos(g2))
      write(3,*)' strain =',strain
      write(3,*)' tipdisp =',tipdisp
c
      do 123 i=1,n
      res(i)=0.0
      do 124 j=1,n
      res(i)=res(i)+a(i,j)*x(j)
124   continue
c      write(3,*)res(i)
123   continue
c
      end
c
c
```

```
      subroutine pivot(a,i)
c
      parameter(n=7)
      implicit double precision (a-h,o-z)
      dimension a(n,n+1),temp(1,n+1)
c
      do 1 li=i+1,n
      if (a(li,i).ne.0.) then
      do 2 kl=1,n+1
      temp(1,kl)=a(i,kl)
      a(i,kl)=a(li,kl)
      a(li,kl)=temp(1,kl)
2      continue
      else
      endif
1     continue
c
      return
      end
c
c
      subroutine input(a,d1,b1,g2)
c
      parameter(n=7)
      implicit double precision (a-h,o-z)
      dimension a(n,n+1)
c
      pi=datan(1.d0)*4.0
c
      read(1,*)e1
      read(1,*)e2
      read(1,*)d1
      read(1,*)d2
      read(1,*)al1
      read(1,*)al2
      read(1,*)ak1
      read(1,*)ak2
      read(1,*)pres
c
      ai1=pi*d1**4/64.0
      ai2=pi*d2**4/64.0
      af=pres*pi*d2*d2/4.0
c
c      e1=1.
c      e2=1.
c      ai1=1.
c      ai2=1.
c      al1=0.5
c      al2=0.5
c      ak=1.
c
      b1=(ak1/(4.0*e1*ai1))**0.25
      b2=(ak2/(4.0*e2*ai2))**0.25
      g1=b1*al1
      g2=b2*al2
      br=b1/b2
      alf=e1*ai1/(e2*ai2)
      delta=-af/(b2**3*e2*ai2)
```

```
c      write(3,*)b1,b2,g1,g2
c      write(3,*)' delta =', delta
c
       a(1,1)=1.0
       a(1,2)=2.0
       a(1,3)=1.0
       a(1,4)=0.0
       a(1,5)=0.0
       a(1,6)=0.0
       a(1,7)=0.0
       a(1,8)=0.0
c
       a(2,1)=b1*exp(g1)*2.0*dcos(g1)
       a(2,2)=-b1*dsin(g1)*2.0*(exp(g1)+exp(-g1))
       a(2,3)=-b1*exp(-g1)*2.0*dcos(g1)
       a(2,4)=-2.0*b2/(alf*br)
       a(2,5)=0.0
       a(2,6)=-a(2,4)
       a(2,7)=0.0
       a(2,8)=0.0
c
       a(3,1)=exp(g1)*dsin(g1)
       a(3,2)=exp(g1)*dcos(g1)-exp(-g1)*dcos(g1)
       a(3,3)=exp(-g1)*dsin(g1)
       a(3,4)=0.0
       a(3,5)=-1.0
       a(3,6)=0.0
       a(3,7)=-1.0
       a(3,8)=0.0
c
       a(4,1)=b1*exp(g1)*(dcos(g1)+dsin(g1))
       a(4,2)=b1*exp(g1)*(dcos(g1)-dsin(g1))+b1*exp(-g1)*(dsin(g1)+
     &        dcos(g1))
       a(4,3)=b1*exp(-g1)*(dcos(g1)-dsin(g1))
       a(4,4)=-b2
       a(4,5)=-b2
       a(4,6)=-b2
       a(4,7)=b2
       a(4,8)=0.0
c
       a(5,1)=b1*exp(g1)*2.0*(dcos(g1)-dsin(g1))
       a(5,2)=b1*exp(g1)*2.0*(-dcos(g1)-dsin(g1))-
     &        b1*exp(-g1)*2.0*(dcos(g1)-dsin(g1))
       a(5,3)=b1*exp(-g1)*2.0*(dcos(g1)+dsin(g1))
       a(5,4)=-2.0*b2/(alf*br**2)
       a(5,5)=-a(5,4)
       a(5,6)=a(5,4)
       a(5,7)=a(5,4)
       a(5,8)=0.0
c
       a(6,1)=0.0
       a(6,2)=0.0
       a(6,3)=0.0
       a(6,4)=2.0*exp(g2)*dcos(g2)
       a(6,5)=-2.0*exp(g2)*dsin(g2)
       a(6,6)=-2.0*exp(-g2)*dcos(g2)
       a(6,7)=2.0*exp(-g2)*dsin(g2)
       a(6,8)=0.0
```

```
c
      a(7,1)=0.0
      a(7,2)=0.0
      a(7,3)=0.0
      a(7,4)=exp(g2)*2.0*(dcos(g2)-dsin(g2))
      a(7,5)=exp(g2)*2.0*(-dcos(g2)-dsin(g2))
      a(7,6)=exp(-g2)*2.0*(dcos(g2)+dsin(g2))
      a(7,7)=exp(-g2)*2.0*(dcos(g2)-dsin(g2))
      a(7,8)=delta
c
      return
      end
```

Appendix B

Additional Traces

B.1 NASA Ames Figures

The data traces listed in the results from the 16" Shock Tunnel tests but not directly referenced in the discussion of those results can be found below. The output of some of the gages will be negative because of the sense of the wiring, not because the wall shear is negative; an absolute value should be taken with some of the negative values.

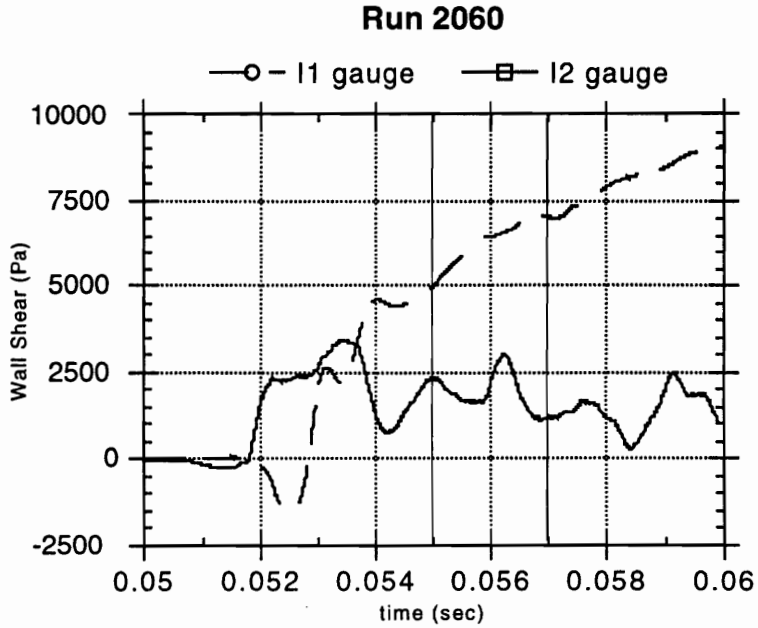

Figure 66: Wall Shear Run 2060I2

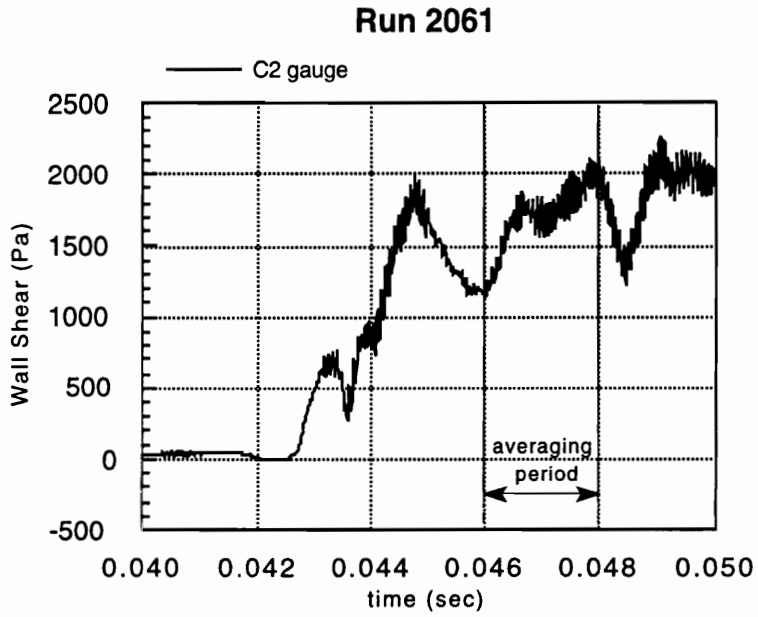

Figure 67: Wall Shear Run 2061C2

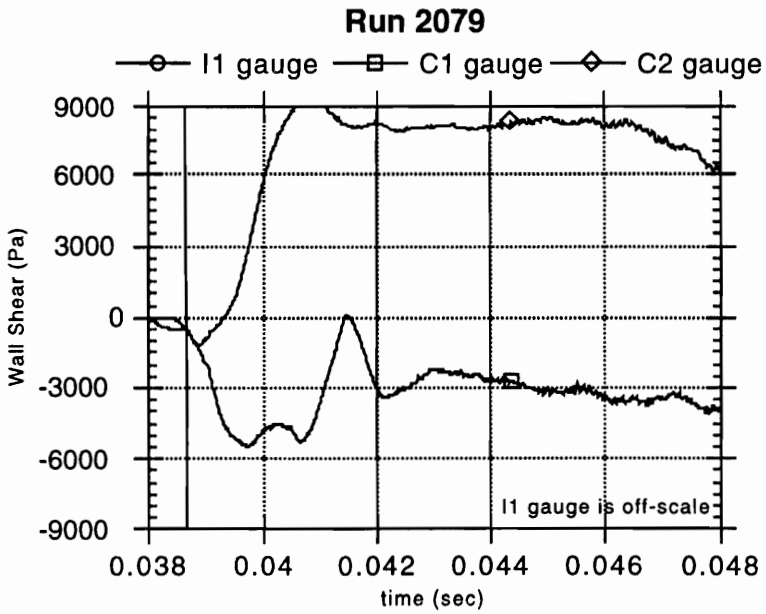

Figure 68: Wall Shear Run 2079C2

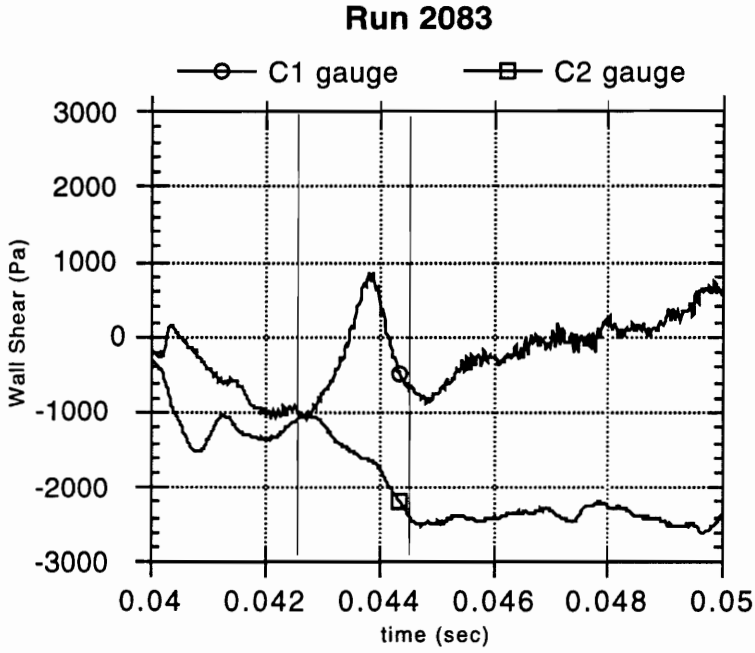

Figure 69: Wall Shear Run 2083C2

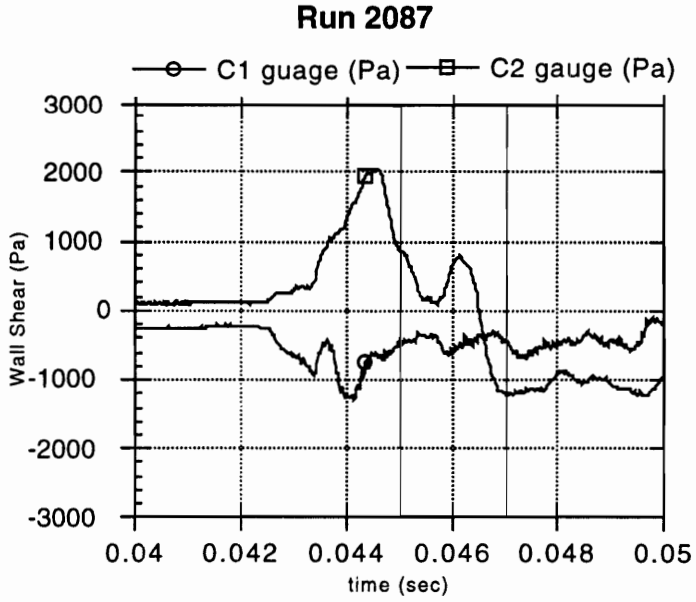

Figure 70: Wall Shear Run 2087C1

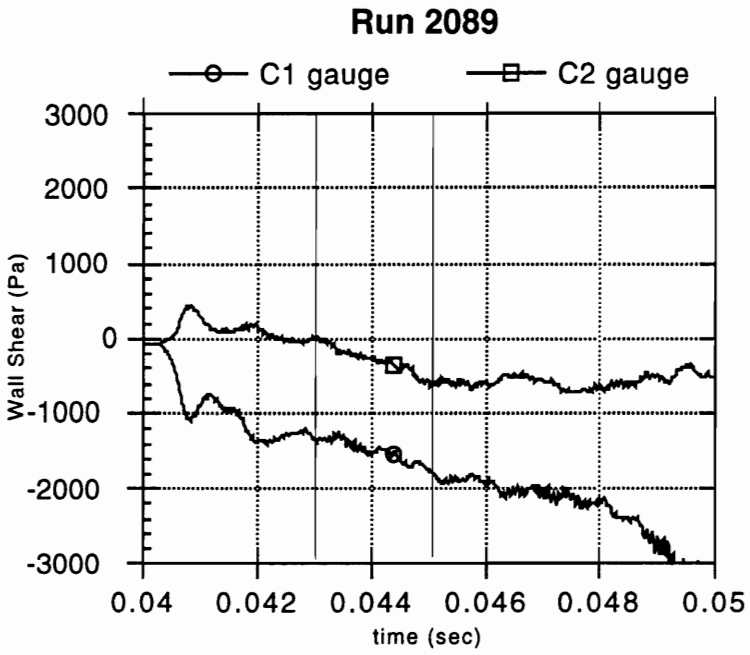

Figure 71: Wall Shear Run 2089C2

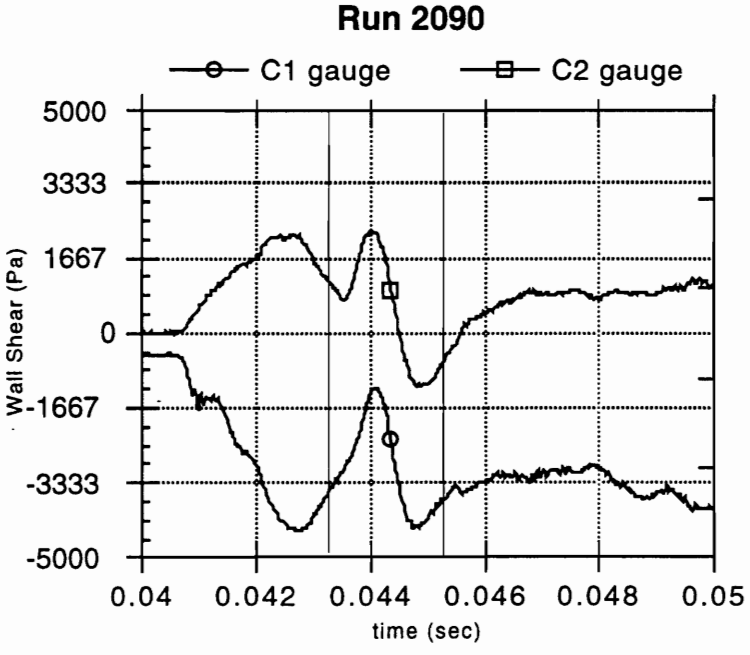

Figure 72: Wall Shear Run 2090C1

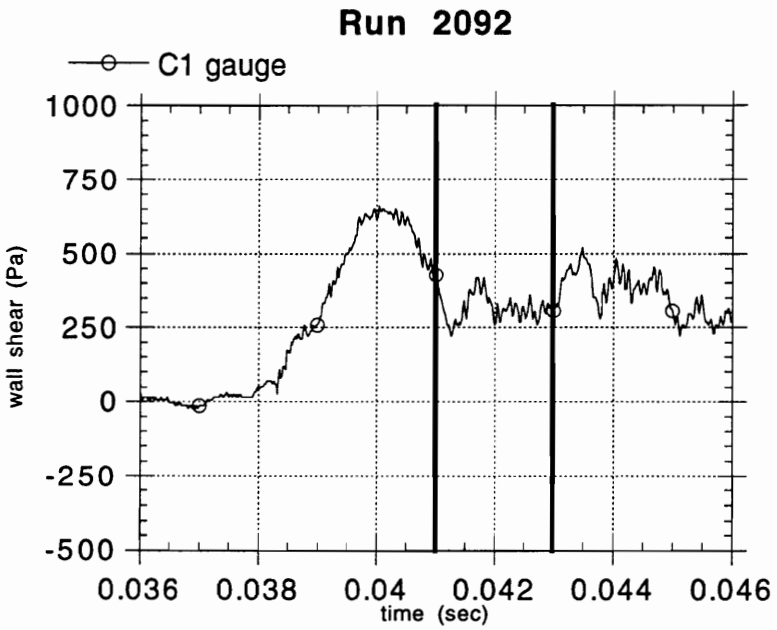

Figure 73: Wall Shear Run 2092C1

B.2 Virginia Tech SST Figures

The data traces below are additional data acquired in the supersonic tunnel and referenced but not directly discussed in the text. In addition, a figure showing the calibration constants of all the gages is included.

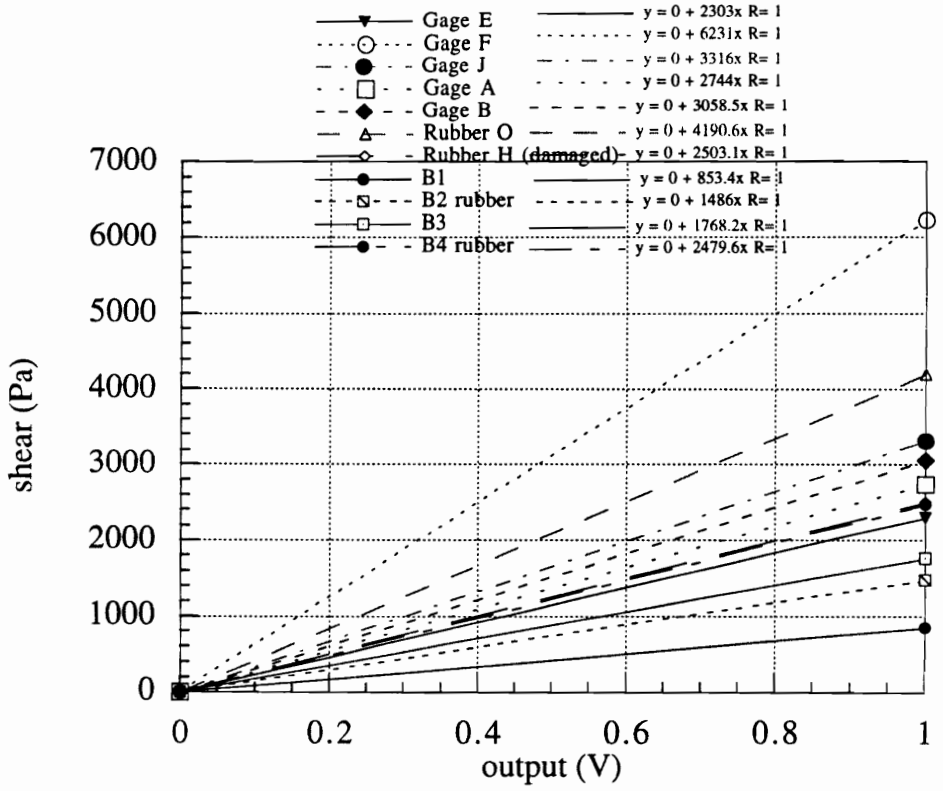

Figure 74: SST Gage Calibration Constants Plot

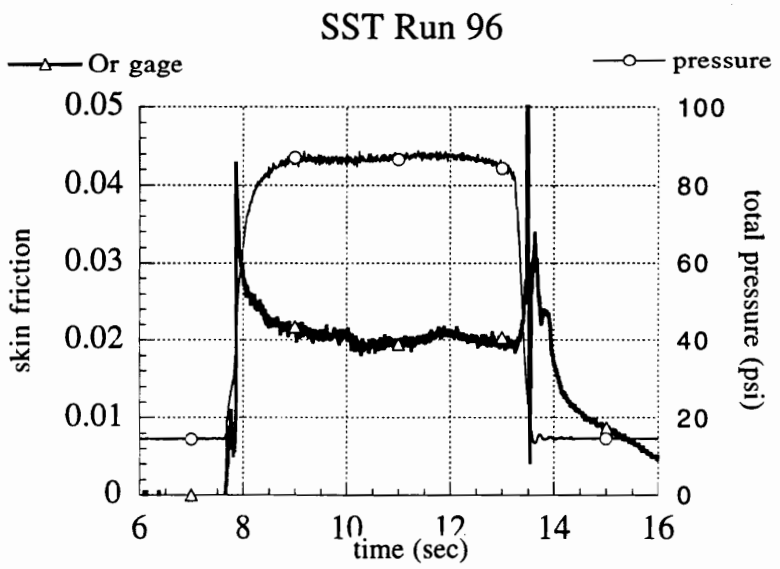

Figure 75: SST Cold Flow Test Run 96

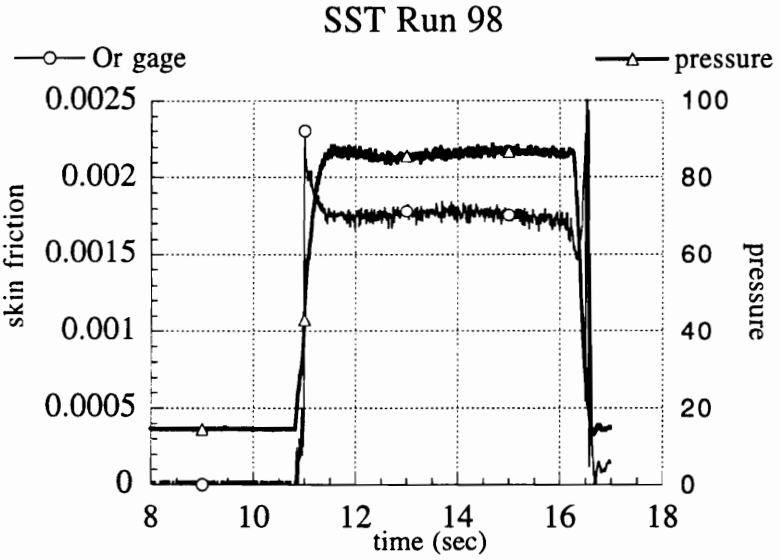

Figure 76: SST Cold Flow Test Run 98

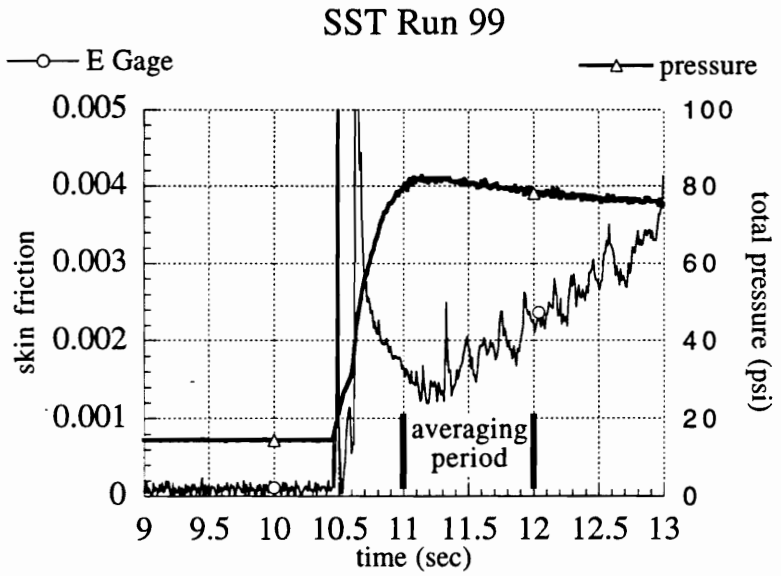

Figure 77: SST Cold Flow Test Run 99

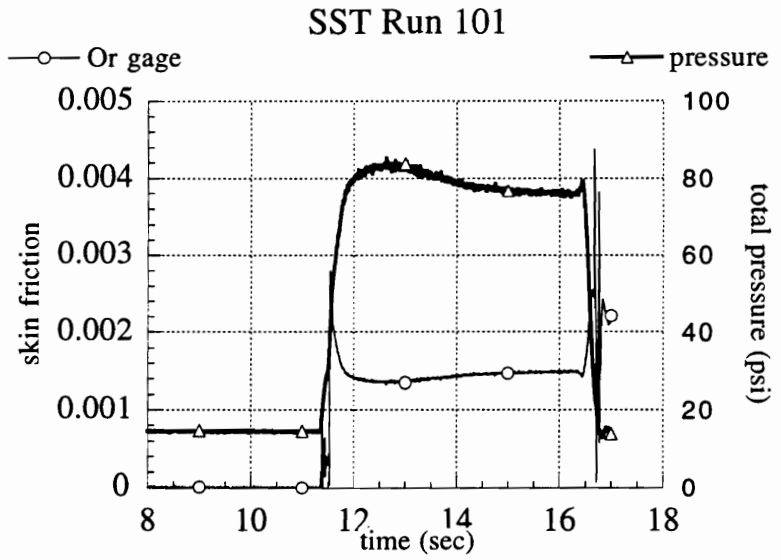

Figure 78: SST Cold Flow Test Run 101

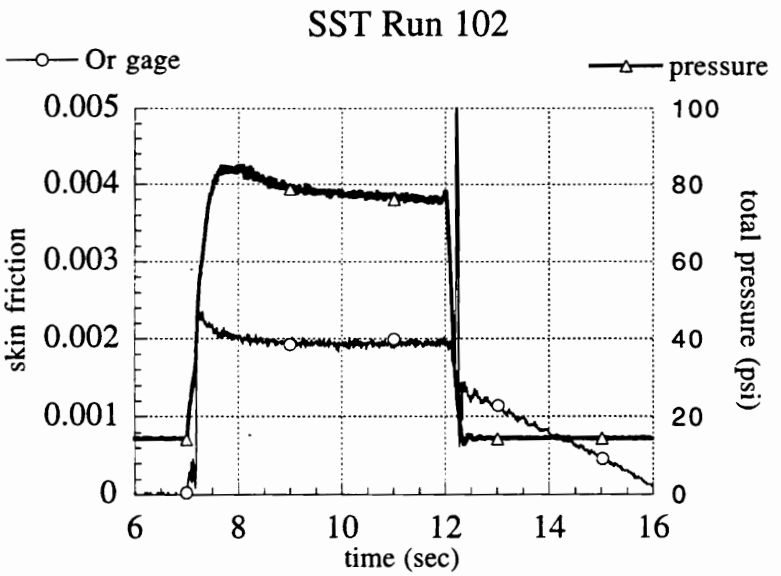

Figure 79: SST Cold Flow Test Run 102

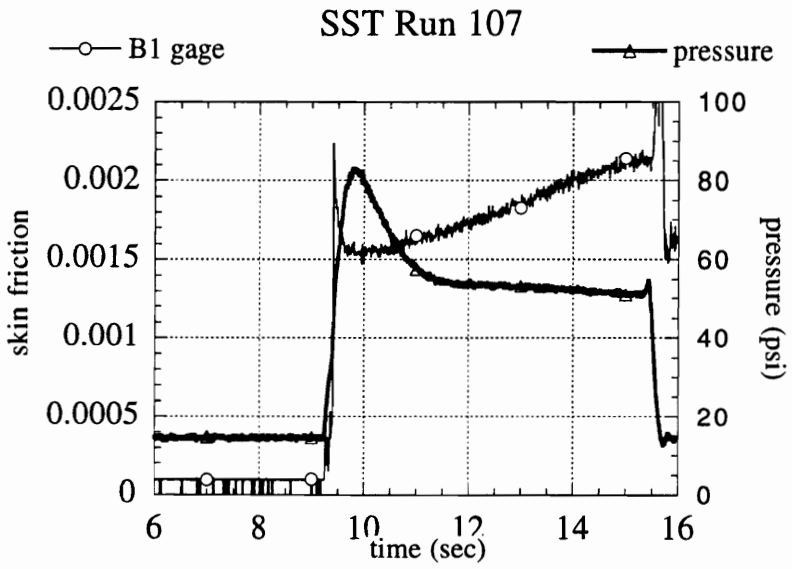

Figure 80: SST Cold Flow Test Run 107

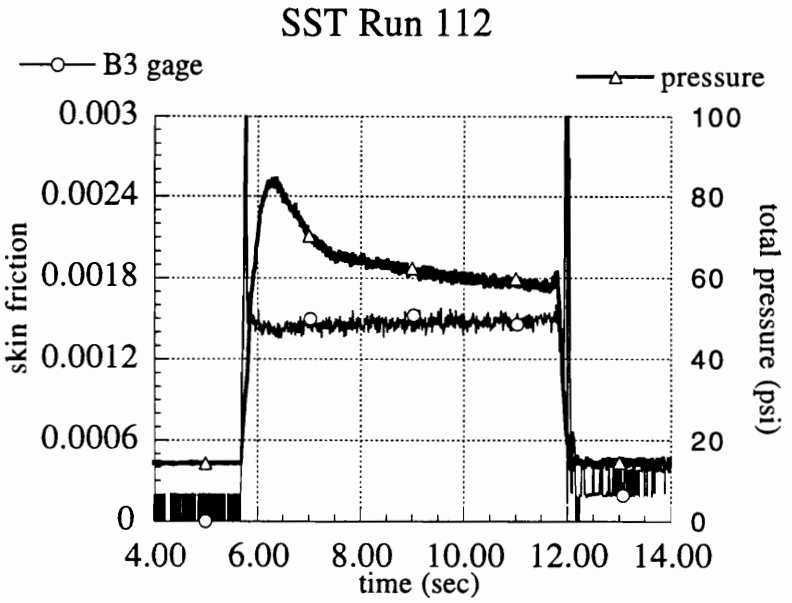

Figure 81: SST Cold Flow Test Run 112

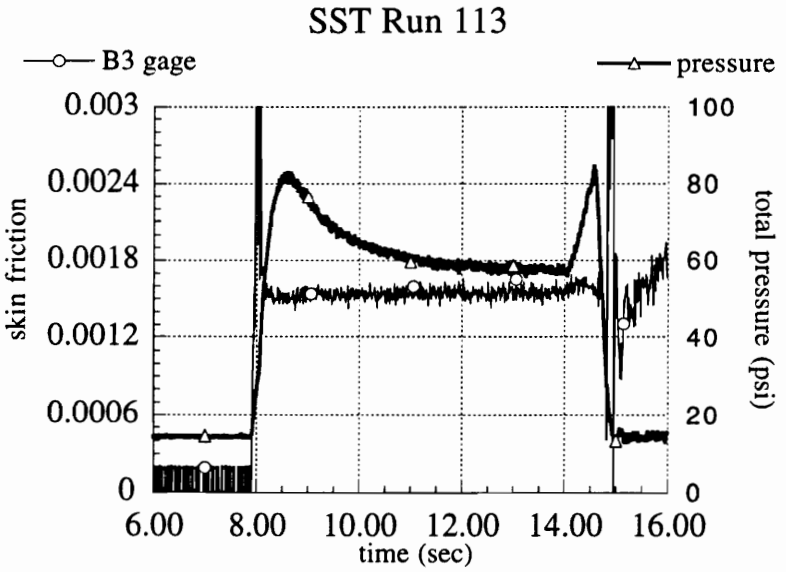

Figure 82: SST Cold Flow Test Run 113

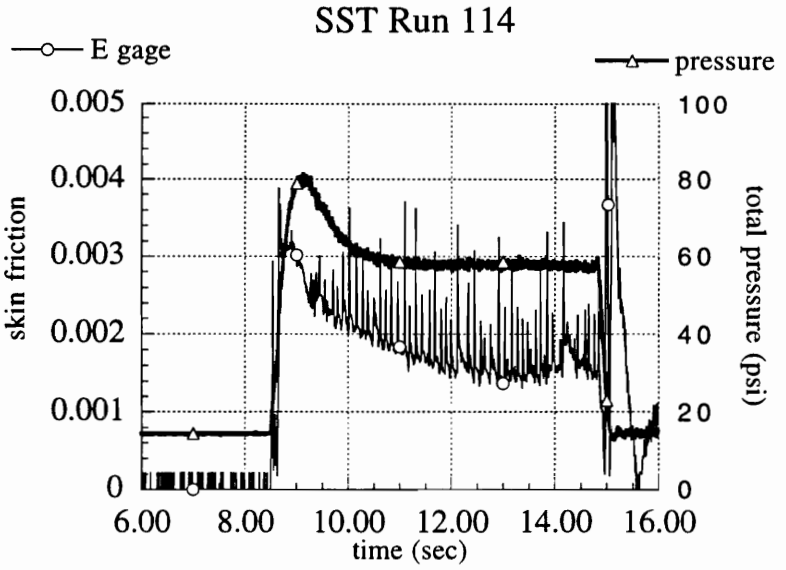

Figure 83: SST Cold Flow Test Run 114

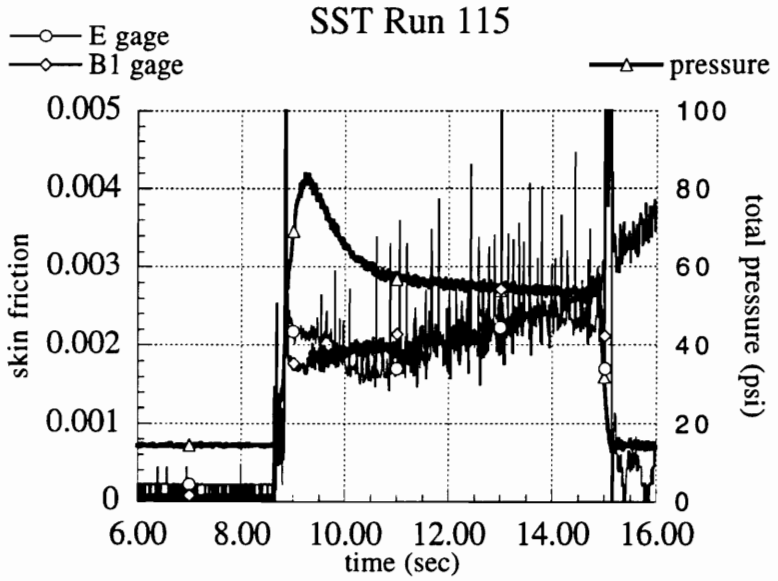

Figure 84: SST Cold Flow Test Run 115

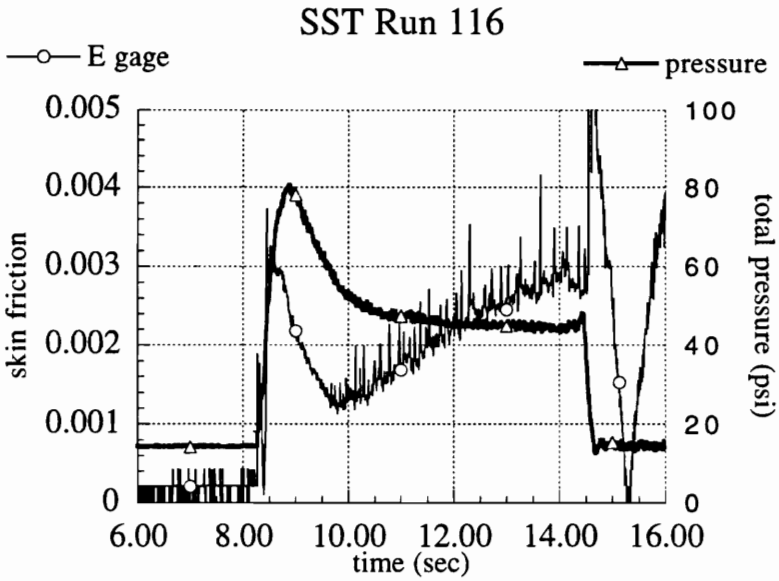

Figure 85: SST Cold Flow Test Run 116

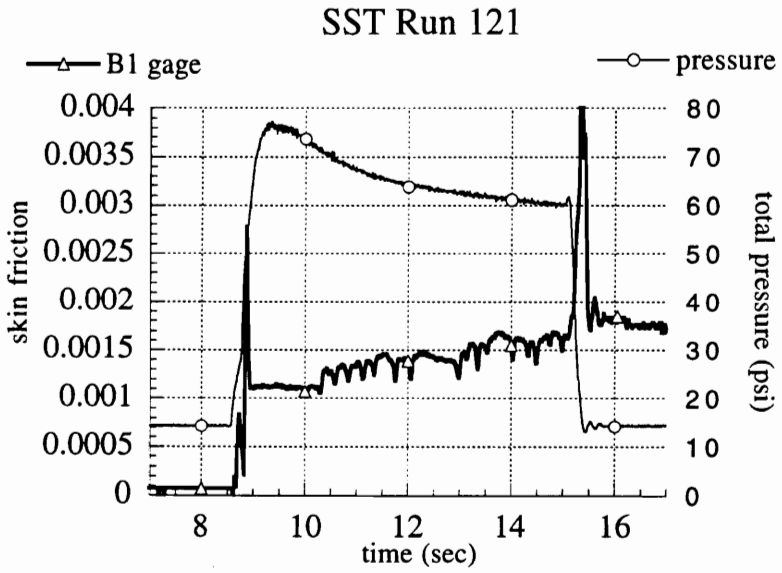

Figure 86: SST Cold Flow Test Run 121

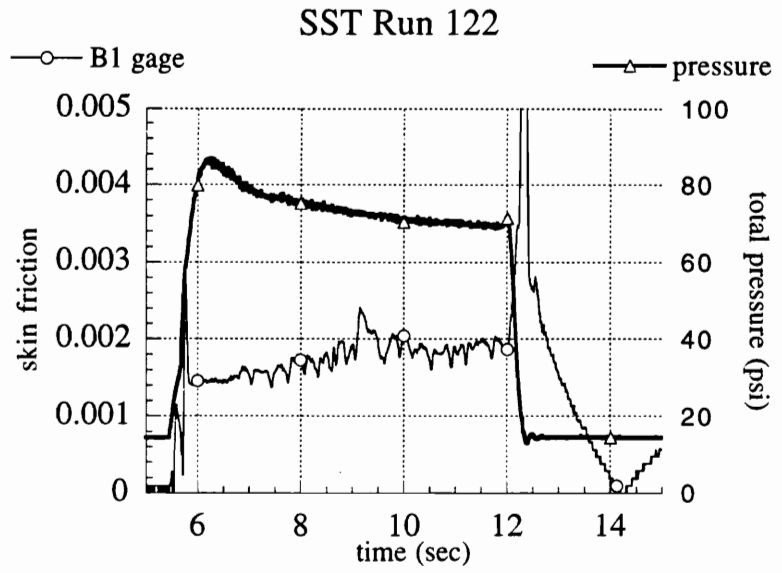

Figure 87: SST Cold Flow Test Run 122

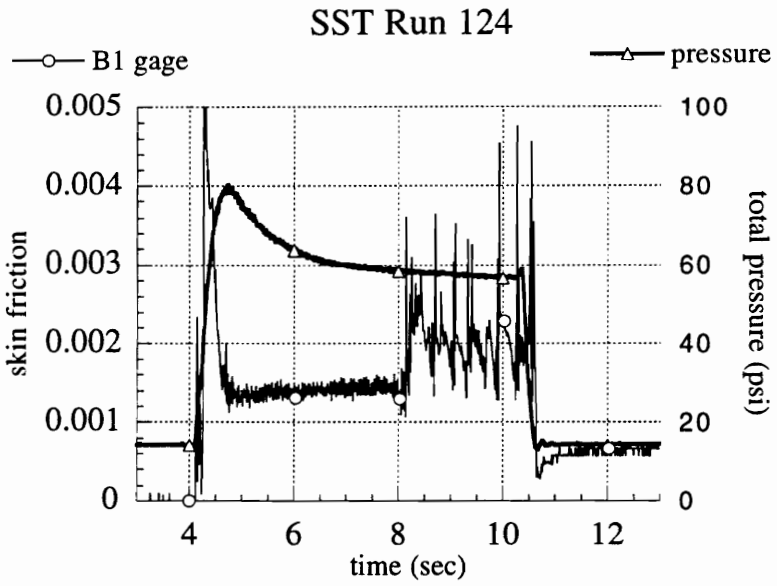

Figure 88: SST Cold Flow Test Run 124

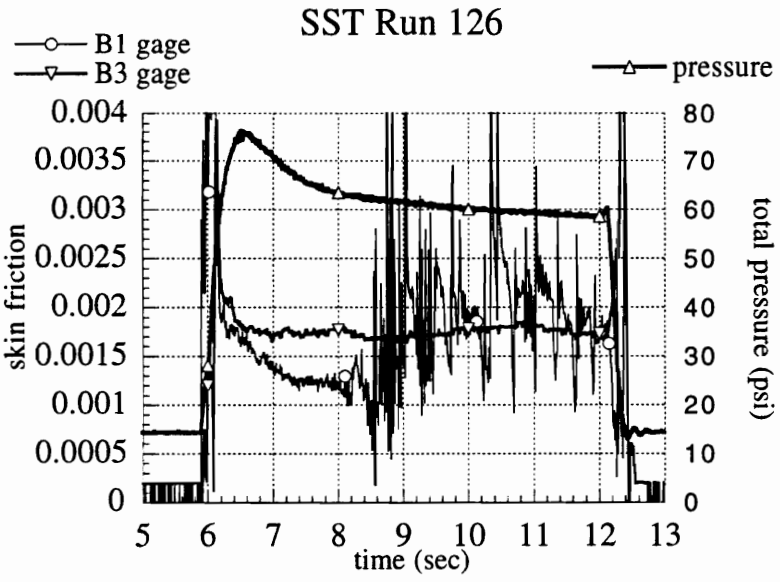

Figure 89: SST Cold Flow Test Run 126

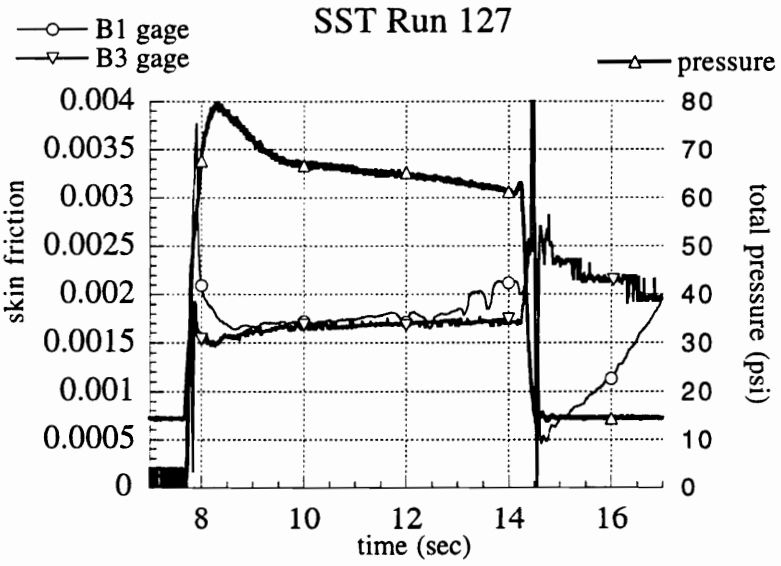

Figure 90: SST Cold Flow Test Run 127

Appendix C

Balance Drawings

Shown below are the balance drawings for the sensing part of the beam which were submitted to the shop. In the interest of making the drawings easier to dimension, the drawings are not to scale.

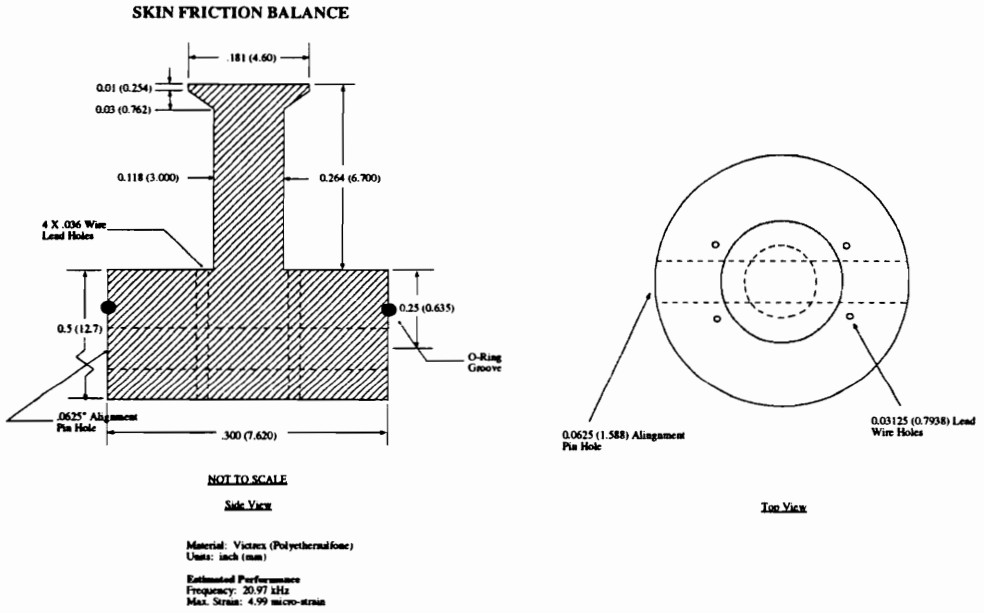

Figure 92: 20 kHz Gage Design

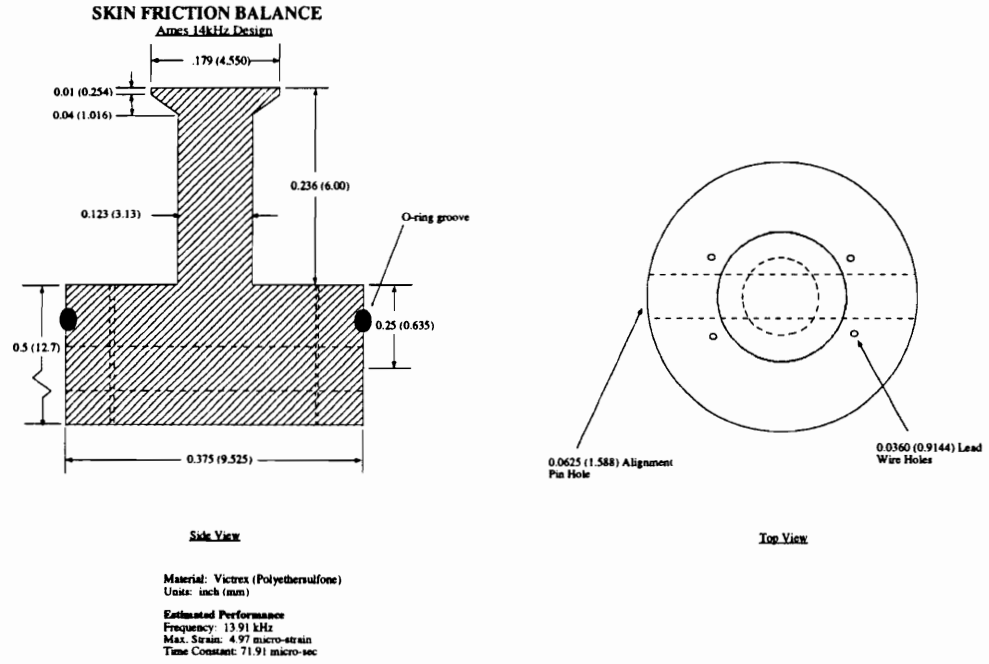

Figure 93: 14 kHz Gage Design

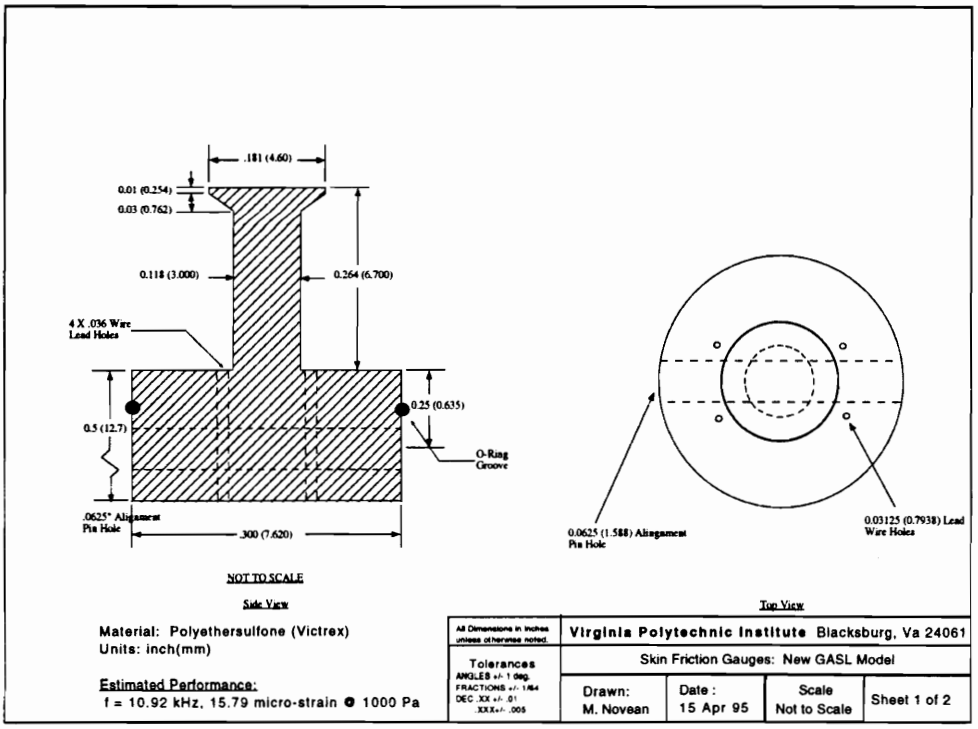

Figure 94: 11 kHz Gage Design

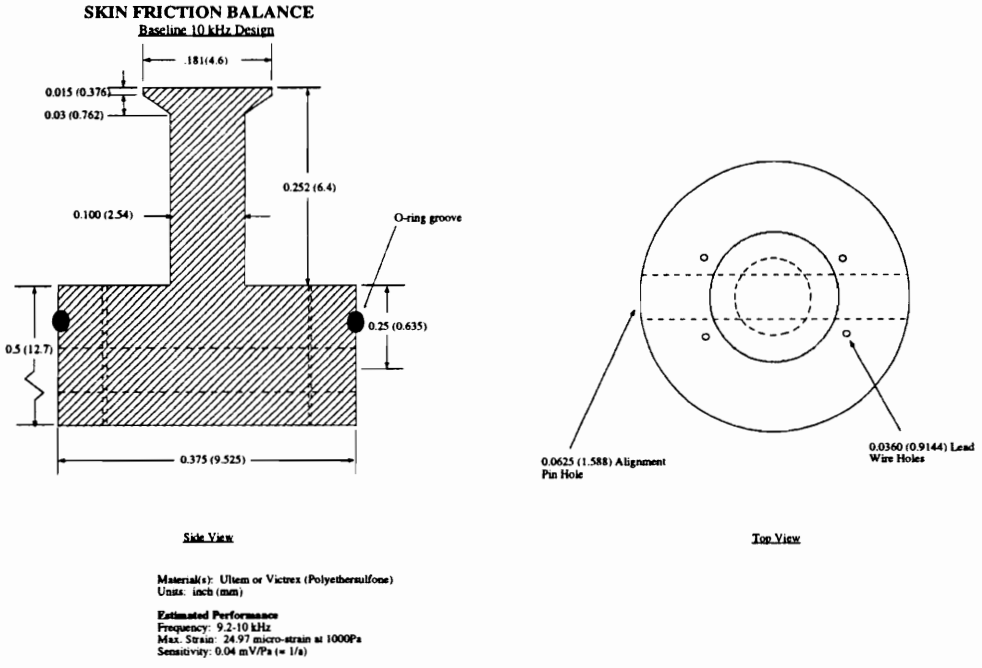

Figure 95: 10 kHz Gage Design

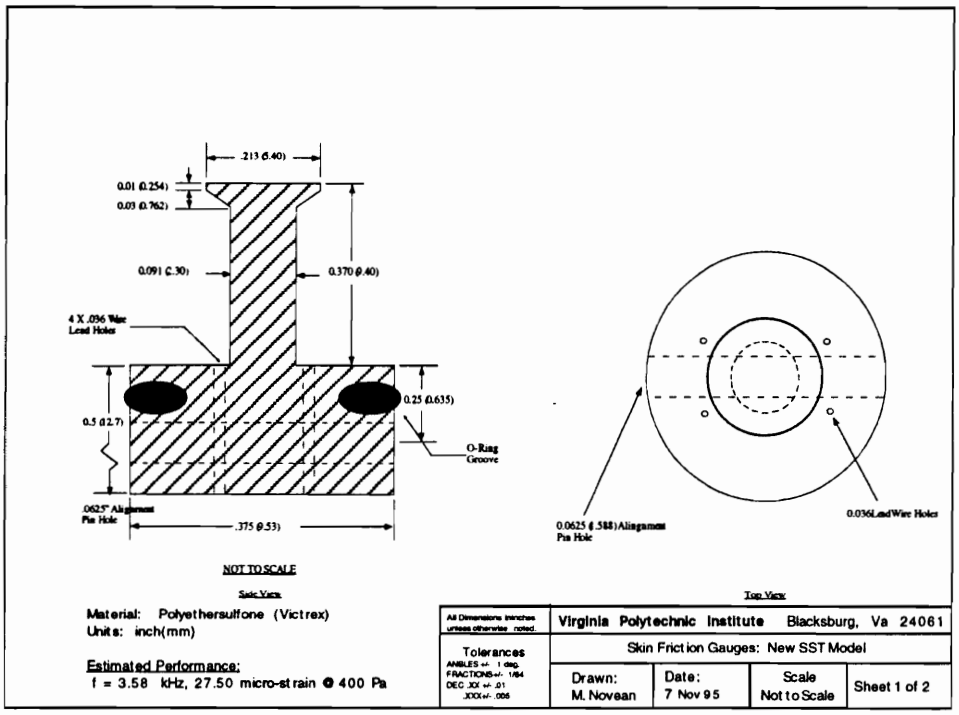

Figure 96: 3.6 kHz Gage Design

Appendix D

Uncertainty Analysis

There are several potential sources of measurement uncertainty in the skin friction measurement. Among them are calibration uncertainty, floating element errors, thermal errors, errors due to electronics, and repeatibility errors.

Calibration Uncertainty

Even starting at calibration the potential exists for possible error. The calibration requires a constant temperature to prevent drift in the bridge due to thermal effects. This can be nearly eliminated by powering up the instrumentation well prior to the tests. The 0.5 Volt excitation level is low enough that the gage will be able to transfer out any heat generated by the excitation flowing through the strain gage. By using a low excitation and having adequate time for the gage to "warm up" a steady state temperature can be reached for calibration. Thus, error due to sensor temperature changes should be below 1%. Another source of calibration uncertainty is rotation of the head from a coordinate system from where the load application axis (gravity vector) coincides with the sensing axis. This was examined experimentally. One such error is the angular rotation of the axes between vertical and the sensing axis which is coincident with the pin axis subject to manufacturing error. The gage was rotated through small angles near this axis and it was found that the variation in output was less than 1.5% for any rotation less than 10 degrees. A second potential error is the pitching of the gage so that it is not perpendicular to the load vector. By rotating through small angles, the error here was again found to be 1.5% for small rotations. Yet another source of calibration error was the potential for error in the measurement system. The meter is accurate to 3:1/2 digits so the maximum error

would be half a millivolt at 200 mV or 0.25%. Other error sources include inaccuracy due to viscoelastic effect (i.e. if you load down the gage and come back hours later, the output will be different) and human error in recording the output. These result in an inaccuracy of 1 percent.

Floating Element Errors

Such errors would involve errors due to geometric concerns. However, great care was taken to insure proper alignment of the sensing head during fabrication and testing. Errors due to gap size and protrusion could be virtually eliminated due to proper sizing. Protrusion due to thermal effects was shown to be an order of magnitude lower than what was measured by Allen to have an effect on the measurement. The only sources of uncertainty were misalignment of the gage with the flow, again calculated to be 1.5% as with calibration, and error due to pressure gradient. Errors due to pressure gradient can indeed be significant. As seen in tests in the VPI Supersonic Tunnel, they can account for a four-fold or more increase in the output signal. The disturbance will be transient for a shock passing over the sensing head but can remain essentially constant for a shock resting on the sensing head (or rubber anulus as well for a rubber-filled gage). For such a case of a steady shock resting on the gage head, the data is contaminated; therefore, if such a situation is suspected in a flow static pressure measurements or shadowgraphs are advised to see if the data should be rejected. It should also be noted that for a rubber filled gage, the sensing head refers to the area of both the plastic sensing head and the surrounding silicon rubber on the gage surface.

Thermal Error

There are two types of potential thermal errors, error due to head temperature mismatch and error due to thermal contamination of the strain gages. The error due to head temperature mismatch was analyzed with the NASA Ames data. There, for what can be considered the extreme worst case scenario, the potential error was found to be 3.6%. Actual error would almost certainly be less but this conservative value will be used. The error due to thermal contamination of the strain gages is negligible. As shown in the gage design process, by the time a temperature gradient travels down the sensing beam, the run is well over. There is the potential for thermal

contamination if the sensing gap is exposed to the oncoming hot flow. However, in the cases where this has occurred during testing, the effect has been clearly catastrophic. The output will instantaneously go full scale as the data acquisition system will be saturated. Thus, thermal contamination is a sort of binary process; either it will be negligible or it will be so damning that the data will be clearly wrong.

Other Errors

Another error source is error due to electronic components. This includes errors resulting from wires and connections, the vertical resolution of the data acquisition system, and zero drift over time. This was measured by hooking up the gage to the data acquisition system, zeroing it out prior to testing, and sampling the output at 0.5 Hz over a 3 hour period. The maximum signal drift was found to be 2.5 percent of the expected full scale. Repeatability poses a large source of uncertainty in the skin friction measurements. During static calibration, skin friction gages exhibit repeatability to less than 0.5%. However, the test regime is a dynamic flow not a static mass loading. A series of cold flow tests were conducted in the Virginia Tech Supersonic Tunnel as discussed in 6.2. From the data from runs 106 through 113, the mean skin friction value is .0017. The results showed a maximum variation of 9% from the mean value except for run 112 which has a variation of 14 % from the mean. A value of 9% was used considering that the tunnel airstream conditions vary in spite of attempts of the control system to keep conditions constant and because gages and the tunnel floor pieces were removed, refurbished, and reinstalled during testing which could have led to flow disturbances which changed the wall shear.

Overall Summary

There are several potential sources of error for skin friction gage tests. Among them are calibration uncertainty, error due to floating element misalignment, thermal error, electronics related error, repeatibility uncertainty, and error due to pressure gradient. Noise and model vibration may result in variation from a static load leevel but should not add any additional uncertainty to the measured value since these effects can be filtered and averaged in the reduction of the data. With prudent design and configuration of a gage for a particular flow, total gage uncertainty in a standard flow should be kept to under 11%. The potential for larger variations in output

certainly exist such as in the case of a shock standing on the sensing head. Whenever possible, other flow measurements should be taken to increase the confidence in the skin friction data and point out potential flow disturbances that could corrupt the data.

Vita

The author was born on November 4, 1970 in Fairfax, Virginia. He conducted his undergraduate engineering studies at Virginia Polytechnic Institute and State University. He received a Bachelor of Science in Aerospace Engineering, graduating Cum Laude in May 1992. Upon completion of his Bachelor of Science degree, he entered the graduate program at Virginia Polytechnic Institute and State University. The next three and a half years were spent in pursuit of a Doctorate in Aerospace Engineering.